

Multimodal analysis of the macaque monkey frontal lobe

Von der Medizinischen Fakultät
der Rheinisch-Westfälischen Technischen Hochschule Aachen
zur Erlangung des akademischen Grades einer Doktorin der Theoretischen Medizin
genehmigte Dissertation

vorgelegt von

mag. biol. exp.

Lucija Janković-Rapan

aus Zabok (Kroatien)

Berichter: Universitätsprofessor Dr. med. Dr. med. h.c. Karl Zilles
Universitätsprofessor Dr. med. Ferdinand Binkofski

Tag der mündlichen Prüfung: 20.01.2020

Contents

Acknowledgements	iii
Summary.....	1
Zusammenfassung.....	1
Summary	2
1 Introduction.....	3
2 Material and Methods	9
2.1 Material	9
2.2 Methods.....	9
2.2.1 Cytoarchitecture	9
2.2.2 Visualization of the 2D parcellation scheme.....	15
2.2.3 Receptorarchitecture	15
2.2.4 Statistical analysis	19
3 Results	21
3.1 2D parcellation scheme	21
3.2 Cytoarchitectonic mapping (qualitative and quantitative analysis)	23
3.2.1 Prefrontal regions	24
3.2.2 Motor regions	36
3.3 Receptorarchitectonic analysis.....	42
3.3.1 Prefrontal regions	43
3.3.2 Motor regions	59
3.4 Hierarchical cluster analysis.....	68
3.5 Principal component analysis.....	72
4 Disscusion.....	73
4.1 Comparison among different parcellation maps	73
4.2 Hierarchical organization of the frontal lobe	84
5 Conclusion	95
6 List of References.....	96
7 Abbreviations	118

Acknowledgements

Firstly, I would like to express my sincere gratitude to Professor Dr. med. Dr. med. h.c. Karl Zilles for providing me with the opportunity to conduct research in the neuroanatomy of the non-human primate brain. His research, patience, motivation and immense knowledge have been an inspiration and a great example of a successful scientific career, especially for a young scientist like me. My special thanks go also to Professor Dr. rer. soc. Ute Habel, coordinator of the IRTG 1328 Schizophrenia and Autism, for her support and the possibility to be part of an international research project. I also wish to express my gratitude to Professor Dr. med. Katrin Amunts, who through her support as head of the Institute, also made this work possible.

I would like to give special thanks to PD Dr. rer. Nat. Nicola Palomero-Gallagher, without whom my PhD journey wouldn't have been possible. Besides providing insightful comments, technical help and scientific discussions, her friendly encouragement during the whole research process, as well as during the writing of the thesis, was the most valuable support.

I would also like to express my sincere gratitude to Mrs Ursula Blohm, Mrs Renate Dohm and Mrs Brigitte Machus for their excellent technical support and help in the laboratory.

I thank my fellow colleague Dennis Stibane, with whom I shared all the bitter-sweet PhD moments, for the stimulating discussions and for all the fun and laughs we have had in the last four years. Further, I want to thank my best friend Erik Sommerlatte for the technical support, and for the continuous encouragement he provided.

Last but not least, I would like to thank my family and my boyfriend for their endless love and support.

Summary

Zusammenfassung

Ziel der vorliegenden Studie ist eine detaillierte Parzellierung des frontalen Cortex beim Makaken, die auf einem multimodalen und quantitativen Analyseansatz (kombinierte cytoarchitektonische und Multi-Rezeptoranalyse) beruht.

Das Gehirn eines adulten Rhesusaffen (*Macaca mulatta*) wurde in Paraffin eingebettet, frontal im Mikrotom geschnitten und histologisch (Zellkörperfärbung) gefärbt. Die Grenzen kortikaler Areale wurden durch eine quantitative Methode bestimmt (Messung von Änderungen des laminären Zelldichtemusters). Außerdem wurden im Frontallappen von vier männlichen adulten Makakengehirnen (*Macaca fascicularis*) mit quantitativer in vitro Rezeptorautoradiographie die regionalen und laminären Verteilungsmuster von 13 verschiedenen Rezeptoren bestimmt. In jedem Areal wurden die mittleren (gemittelt über alle kortikalen Schichten) Rezeptordichten als „Receptor fingerprints“ erfasst. Um Cluster von Arealen nach ihrem Grad an Ähnlichkeiten in ihren Fingerprints zu identifizieren wurde eine multivariate Analyse durchgeführt.

Es konnten 50 cyto- und rezeptorarchitektonische Areale identifiziert werden, von denen 16 zum motorischen Cortex, 18 zum präfrontalen Cortex, und 16 zum orbitofrontalen Cortex gehören. Die cytoarchitektonischen Grenzen wurden rezeptorarchitektonisch durch Änderungen in der Dichte und laminären Verteilung multipler Rezeptoren bestätigt. Frühere Karten des frontalen Cortex konnten partiell bestätigt werden, aber es wurde auch die Existenz einiger, bisher nicht beschriebener Areale nachgewiesen. Area 10, 8B, F7, F5 und F4 konnten weiter unterteilt werden. Das resultierende neue Parzellierungsschema wird in einer 2-D Oberflächendarstellung. Weiterhin wurden die Dichten jeder der 13 Rezeptortypen in 48 der 50 Areale gemessen. Die multivariate Analyse der so ermittelten Rezeptorfingerprints ermöglichte strukturell und funktionell relevante Cluster von Arealen zu definieren, die ähnliche neurochemische Eigenschaften teilen.

In der vorliegenden Arbeit wird daher eine detaillierte Parzellierung des Frontallappens beim Makaken vorgelegt, die auf einer multimodalen und quantitativen Analyse beruht. Die resultierende Hirnkarte stellt ein wertvolles Werkzeug für künftige Studien dar, deren Ziel es ist die komplexen Prozesse zu verstehen, die der Kognition, motorischen Funktionen, Konnektivität und Evolution des menschlichen Gehirns zugrunde liegen.

Summary

The aim of this study is to create a detailed parcellation of the macaque frontal cortex based on a multimodal and quantitative (combined cytoarchitectonic and multi-receptor analyses) approach.

The brain of an adult *Macaca mulatta* was embedded in paraffin, serially sectioned (using a microtome) in the coronal plane and stained for cell bodies. Borders of cortical areas were identified by a quantitative method based on the identification of changes in laminar cell density patterns. Quantitative *in vitro* receptor autoradiography was used to analyze the distribution patterns of 13 different transmitter receptors in the frontal lobe of four adult male *Macaca fascicularis* monkeys. For each area, mean (averaged over all cortical layers) receptor densities were visualized as a receptor fingerprint. Multivariate analyses were conducted to detect clusters of areas according to the degree of (dis)similarity of their receptor organization.

Fifty cyto- and receptorarchitectonically distinct areas were identified, of which 16 belong to the motor cortex, 18 to the prefrontal cortex, and 16 to the orbitofrontal cortex. Cytoarchitectonically identified borders were further confirmed by changes in the densities and laminar distribution patterns of multiple receptors. Some previously published parcellations could be confirmed, but also the existence of several hitherto undescribed areas was also revealed, such as a subdivision of areas 10, 8B, F7, F5 and 4. The ensuing novel parcellation scheme was presented in a 2D flat map to enable comparison with previous maps. Additionally, the density of each of the 13 receptor types was quantified in 48 of the 50 areas and multivariate analyses of the ensuing receptor fingerprints revealed structurally and functionally relevant clusters of areas which share similar neurochemical and properties.

The present study provides a detailed map of the monkey frontal lobe, based on a multimodal and quantitative approach. This map constitutes a valuable tool for future studies aiming to understand the complex processes underlying cognition, motor function,, connectivity and evolution of the human brain.

1 Introduction

Ever since Korbinian Brodmann (1909) proposed that the cerebral cortex is composed of numerous cortical areas with unique cytoarchitecture and functional properties, understanding the correlation between the regional structural and functional heterogeneity of the brain has become a major question in neuroscience (Kötter and Wanke, 2005). Although understanding the human brain is the final goal for any neuroscientific study, this is extremely challenging, not only because of the brain's complexity, but also because of ethical limitations which do not allow all the crucial material and data to be acquired directly from human brains. Thus, most of our present knowledge of brain structure, function, and behavior aspects has been obtained from animal experiments (DeFelipe, 2015). Research involving non-human primates has played a vital role in the medical progress and scientific applications in the past century, as they are closely related to humans. Although some researchers argue that results obtained from primates cannot be applied on humans due to the small but significant differences in brain connections, as long there is a limitation to access human brain material, primates will remain the best non-human model (Quigley, 2007). Macaque monkeys are currently the most widely used primate species in neurobiological research (Zang *et al.*, 2014), as multiple studies showed that the basic architectonic plan is the very similar in both primate species, human and macaque monkey, which confirmed macaque monkey as a reliable non-human primate model in neuroanatomy research (Petrides *et al.*, 2012). Furthermore, comparative studies between human and monkey brains in their cytoarchitecture and functional connectivity could identify crucial differences responsible for the structural and functional divergence of the primate brain (Molnar *et al.*, 2014) and, more important, based on data collected from monkey brain studies, could provide strong background to test fundamental hypotheses at the level of the human brain (Petrides *et al.*, 2012).

Cytoarchitectonic studies of the monkey cerebral cortex began at about the same time as those of the human cortex, facing the same problems of method and material limitations, as well as the problem of the nomenclature that did not always apply to areas with comparable architectonic features and location of areas as within the human brain parcellation scheme. Brodmann's map of the human brain from 1909 is one of the most famous parcellation schemes and many modern neuroanatomists still refer to it, however his map of the monkey (*Cercopithecus*) cortex (1905) did not accomplish the same success. Even

Brodmann himself expressed considerable uncertainty about his subdivision of the frontal cortex and noted that the numbers he used did not always refer to the homologous areas in different species. This all led to a question of reliability and the abandonment of his monkey map. Later, Walker (1940) published a new cytoarchitectonic map of the prefrontal cortex of the macaque monkey with the numerical nomenclature used by Brodmann in the human brain, although he did not compare the cytoarchitecture of the human and macaque monkey frontal lobes.

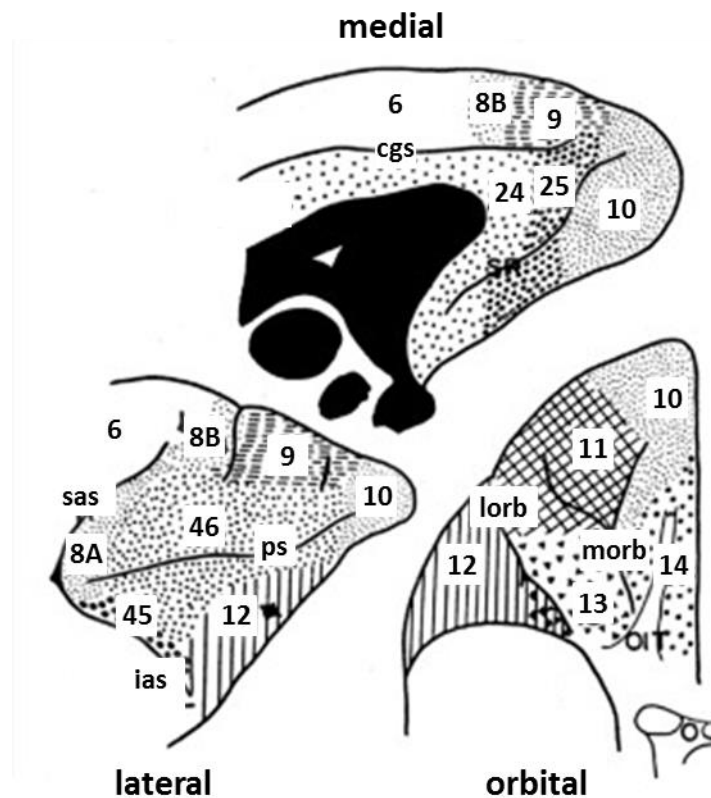
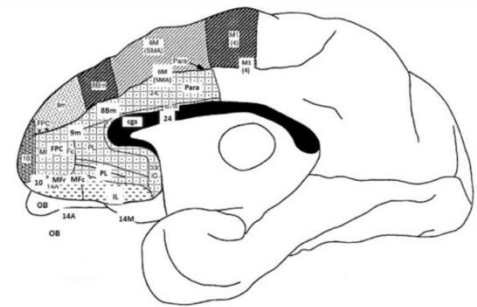
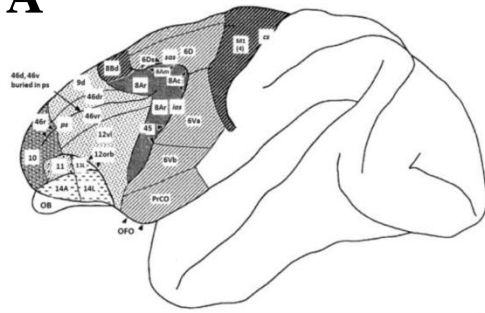
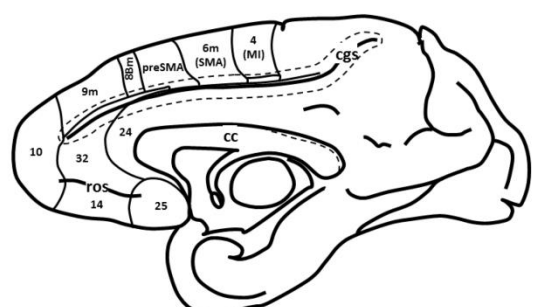
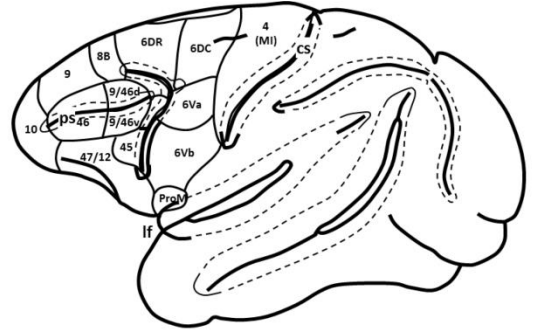
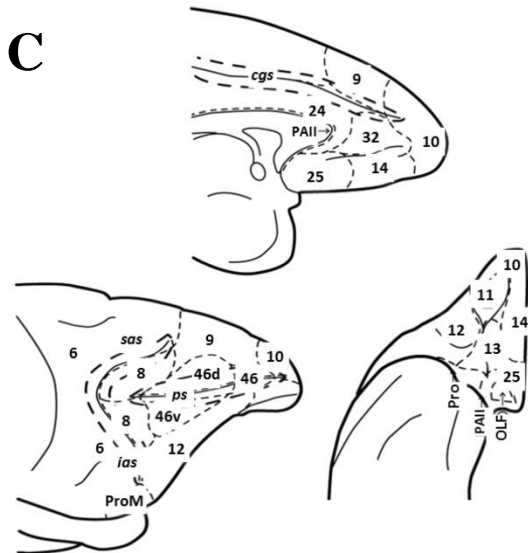
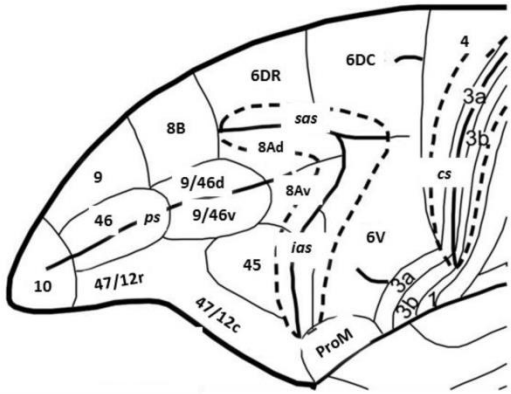


Figure 1 Walker's parcellation scheme (1940) of the monkey frontal lobe, medial, lateral and orbital overview.

Walker (1940) marked the frontopolar cortex of the monkey as area 10 and added areas 46 and 45, which were not labelled in Brodmann's map of the monkey frontal cortex. Walker's (1940) (*Fig. 1*) parcellation scheme became the basis for future microparcellation and anatomical-connectional studies (Barbas and Pandya, 1989; Petrides and Pandya, 2006; Carmichael and Price, 1994; Preuss and Goldman-Rakic, 1991, Morecraft *et al.*, 2012; Caminiti *et al.*, 2017) (*Fig. 2*) on macaque monkeys with various anterograde and retrograde tracers, and also in physiological microstimulation studies for the location of recording sites

and the analysis of the effect of different lesions within the frontal cortex on primate behavior, which was a beginning of the golden era of the experimental neuroanatomy. Various neuroanatomists focused on the microparcellation of a specific region of interest (ROI) in the monkey brain, such as mapping the motor areas (Matelli *et al.*, 1985, 1991; Barbas and Pandya, 1987) (*Fig. 2*), the orbitofrontal areas (Barbas, 2007; Carmichael and Price, 1994; Morecraft *et al.*, 1992), the dorsolateral prefrontal areas (Petrides, 2005; Preuss and Goldman-Rakic, 1991), and the ventrolateral prefrontal areas (Gerbella *et al.*, 2007; Petrides and Pandya, 2002; Preuss and Goldman-Rakic, 1991).

Although cytoarchitectonic studies provide detailed insight into the microstructural organization of the cerebral cortex, they do not provide information concerning functional aspects of the neural system. Implementing neuroimaging methods, e.g. functional magnetic resonance imaging (fMRI), positron emission tomography (PET), electroencephalography (EEG), magnetoencephalography (MEG), and, lately, functional connectivity studies, helped neuroanatomists to begin unwrapping the complex relationship of functional connectivity between different areas in the human brain. Additionally, quantitative in-vitro multi-receptor autoradiography has recently been shown to be a powerful tool to reveal important aspects of the brain's molecular and functional organization, since neurotransmitters and their receptors constitute key molecules in signal transduction (Zilles and Amunts, 2009). Furthermore, this method can also be applied to the brains of non-human species to reveal evolutionary trends at the receptor architectonical level (Zilles and Palomero-Gallagher, 2017). The heterogeneous distribution of transmitter receptors in the cerebral cortex enables the identification and characterization of principal subdivisions such as primary sensory, primary motor, and hierarchically higher sensory or multimodal areas (Palomero-Gallagher and Zilles, 2017; Zilles and Palomero-Gallagher, 2017). The cerebral cortex functions in a hierarchical manner. Progressively higher areas support functions that are more integrative. The three prefrontal regions, i.e. medial, lateral and orbital, together with (pre)motor areas, have strong reciprocal connections with other brain structures, both cortical and subcortical, constituting the highest level of cortical hierarchy responsible for the behavioral analysis and execution of actions (Fuster, 2002). Executive functions allow higher mammals, such as primates, to select actions based on internal plans and motivations, rather than impulsively responding to possibly harmful environmental stimulus. Despite the important role of this region in regulating behavior, it is still not understood how different frontal areas functionally cooperate (Koechlin and Summerfield, 2007).

A**B****C****D**

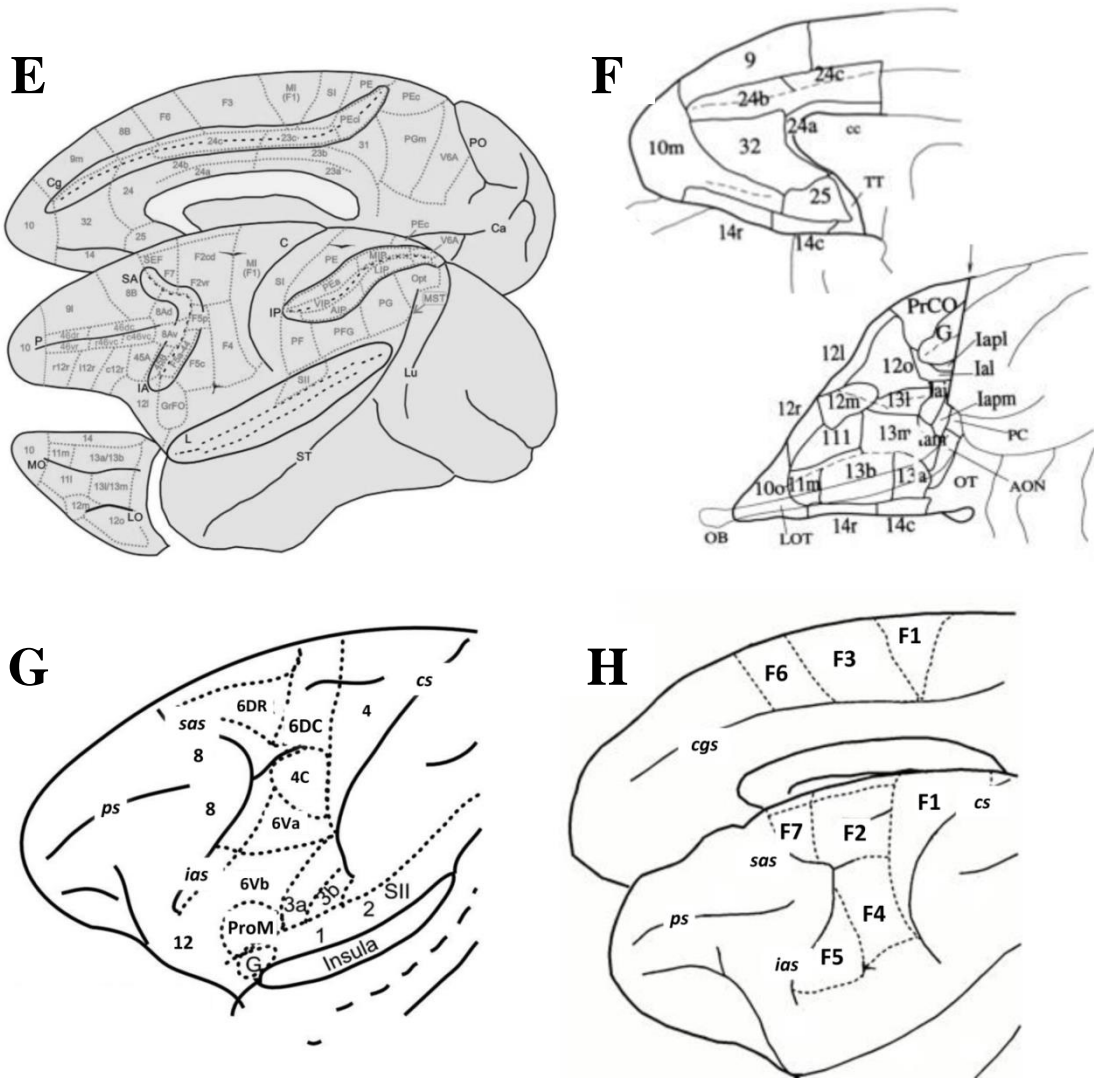


Figure 2 Distinct parcellation maps of the monkey frontal lobe or of a particular ROI in the frontal region. a) Preuss and Goldman-Rakic (1991), display the whole frontal lobe; b) Morecraft et al. (2012), display the whole frontal lobe; c) Petrides and Pandya (2006), display the whole frontal lobe; d) Barbas and Pandya (1989), display the prefrontal region; e) Caminiti et al. (2017), display the whole frontal and parietal lobe, f) Carmichael and Price (1994), display the orbito-medial prefrontal region; g) Barbas and Pandya (1987), display the motor region; h) Matelli et al. (1985, 1991), display the motor region.

Aim of the project

The aim of the present study is an independent cytoarchitectonic evaluation of previous subdivisions in the macaque frontal cortex using a multimodal approach. The project is twofold:

1) Mapping of frontal areas, i.e. prefrontal cortex and (pre)motor region, in the adult macaque monkey brain using quantitative cytoarchitectonic and multi-receptor analyses (the

distribution patterns of 13 different transmitter receptor binding sites in defined cortical areas) to provide a solid non-human model with which to better understand the complexity and evolution of the healthy primate brain. The quantitative balance between the different receptor types in each area (“receptor fingerprint”) is an indicator of the receptor organization underlying the regionally specific functions (Palomero-Gallagher *et al.*, 2009; Zilles *et al.*, 2002).

2) Conduct *hierarchical cluster analysis* to detect grouping of defined areas according to the degree of similarity of their multi-receptor architecture. In the hierarchical cluster analysis, a set of cortical areas is grouped into clusters in such a way that areas in the same cluster are similar with respect to their receptor-architecture, and more different from areas in other clusters (Palomero-Gallagher *et al.*, 2009).

The emphasis of the research is on areas in the frontal lobe, with the exception of the cingulate cortex as a part of the limbic system, to reveal the relationship between cytoarchitecture (which highlights the microstructural heterogeneity) and neurotransmitter receptor distributions (which emphasize the molecular aspects of signal processing) in the healthy nonhuman primate brain with the aim to create an atlas to be used in future studies applying the macaque monkey as a model for the human brain. Studies like this show that architectonic methods have become more objective and reliable during last decades through the use of multivariate statistical tools for analyzing and describing new cytoarchitectonic areas and subareas allowing to test differences among distinct areas for their significance (Amunts and Zilles, 2001). Since the area-specific balance of different receptors (“receptor fingerprint”) is linked to distinct functional properties of the each area, applying a hierarchical cluster analysis that is based on the receptor fingerprints, highlights primary neuronal connections of a functionally significant grouping of cortical areas along the cortex (Zilles and Amunts, 2009; Zilles and Palomero, 2017), indicating that grouped areas belong to the same neural network. This approach is an independent and reliable way for introducing new parcellation maps, providing an additional information of functional networks and precisely defined anatomical structures (Zilles and Amunts, 2009). Thus, studies like this are crucial to review previous cortical subdivisions and to objectively identify a unique parcellation scheme that will serve as a fundamental tool for the analysis of functional imaging data and thus lead to a better understanding of the complex relationship between microstructure, function and molecular organization of the neural system.

2 Material and Methods

2.1 Material

The brain of an adult macaque monkey (*Macaca mulatta*; brain ID: DP1) obtained as a gift from Professor Deepak N. Pandya was used for cytoarchitectonic analysis. The monkey was deeply anesthetized with sodium pentobarbital, transcardially perfused with cold saline followed by 10% buffered formalin and stored in a buffered formalin solution until further processing. The brains of three adult male macaques (*Macaca fascicularis*; 6±1 years of age) were obtained from Covance Laboratories (Münster, Germany) for receptor architectonical experiments. Monkeys were sacrificed by means of a lethal intravenous injection of sodium pentobarbital. The brains were immediately removed from the skull together with meninges and blood vessels, since removing them could damage cortical layer I. Due to the delicate nature of the receptor proteins, only unfixed, deep frozen tissue can be used for receptor autoradiography (Herkenham *et al.*, 1990; Zilles *et al.*, 2002). Brains were separated into hemispheres and cerebellum with brainstem and then each hemisphere was further divided into an anterior and a posterior slab at the height of the most caudal portion of the central sulcus. In the present study, only the left hemispheres were examined. The slabs were placed flat on an aluminum plate to avoid any further deformation and slowly immersed in N-methylbutane (isopentane) at -40°C, where they were left for 10 - 15 minutes, after which they were stored in air-tight plastic bags at -80°C until sectioning. Animal care was provided in accordance with the NIH Guide for Care and Use of Laboratory Animals and the European local Committees, and complied with the European Communities Council Directive.

2.2 Methods

2.2.1 Cytoarchitecture

After a dehydration step in ascending graded alcohols (70% to 100% propanol) followed by chloroform, the brain of the monkey processed for cytoarchitectonic analysis was embedded in paraffin and serially sectioned in the coronal plane with a large-scale microtome, resulting in 3305 20-µm-thick whole-brain sections. Every fifth section was mounted on gelatin coated slides. The paraffin was removed and sections rehydrated by two washing steps (each of 10 minutes) with Xem-200 („Xylol-Ersatz-Medium“, Vogel, Diatec Labortechnik GmbH) followed by graded washes in alcohol (10 minutes each in 100%, 96%

and 70% propanol) and a final rinse in pure water. Sections were then stained for the visualization of cell bodies with a modified silver method (Merker, 1983; Palomero-Gallagher *et al.*, 2008) that provides a high contrast between cell bodies and neuropil. Sections were first pretreated for 4 hours with 4% formic acid diluted in distilled water, then left overnight in a solution of 10% formic acid/30% peroxide diluted in distilled water. Before immersing sections twice for 5 minutes each in 1% acetic acid, it was important to wash them carefully under running water and to rinse them in distilled water. After being placed in a physical developer under constant movement, sections become grayish in approximately 10 minutes, but the developing step sometimes took longer and it was necessary to observe sections under the microscope until cell bodies were dark gray/black. The developer was prepared immediately before use by mixing three stock solutions (*Tab. 1*) in a specific order: first 30 ml of stock solution B, and then 70 ml of stock solution C are slowly added to 100 ml of stock solution A under constant stirring. To stop the developing process, stained sections were washed in 1% acetic acid for two 5-minute periods and finally fixed for 5 minutes in a T-Max fixative (Kodak; 2 parts of T-Max and 7 parts of distilled water). Finally, sections were dehydrated in ascending graded alcohols (70%, 96% and 100%) for 5 minutes in each dilution, followed by two 5 minutes immersions in Xylene before coverslipping with DePex mounting medium.

Table 1 Composition of stock solutions used for the silver cell-body staining.

Stock solution A		
1000	ml	distilled water
50	g	anhydrous sodium carbonate (Sigma-Aldrich)
Stock solution B		
1000	ml	distilled water
2	g	ammonium nitrate (Merck)
2	g	silver nitrate (Merck)
10	g	tungstosilicic acid hydrate (Fluka)
Stock solution C		
1000	ml	distilled water
2	g	ammonium nitrate
2	g	silver nitrate
10	g	tungstosilicic acid hydrate
7.3	ml	37% formaldehyde solution (Merck)

Observer-dependent mapping procedure (qualitative cytoarchitectonic analysis).

Classical cytoarchitectonic studies of the macaque frontal cortex (Walker, 1940; Carmichael and Price, 1994; Petrides, 2005; Preuss and Goldman-Rakic, 1991; Rizzolatti and

Luppino, 2001) were based on the visual, microscopical inspection of histological sections and identification of the laminar distribution pattern of neurons which is characteristic of a cortical area and which is different from the laminar pattern of the neighboring ones. In general, the layers of the neocortex are defined based on packing density of neural cell bodies, the proportion and spatial organization of different neuronal cell types, as well as cell sizes and shapes. Important features in cytoarchitectonic mapping are (i) the absolute thickness of cortical layers, (ii) the proportionate thickness of a layer relative to the other cortical layers and to the total cortical depth, (iii) the presence of clearly recognizable laminar borders and vertical columns, (iv) the packing density and size of neuronal cell bodies, (v) the homogenous or clustered distribution of cell bodies throughout the layers, and (vi) the presence of special cell types such as Betz cells (Betz, 1874), which are unique to Brodmann's area 4 (primary motor cortex) and cannot be found in any other cortical area, or of distinctive laminar differentiations such as the subdivision of the internal granular layer (layer IV) of the primary visual cortex (BA 17) into three sublayers, of which sublayer IV_b corresponds to the macroscopically visible Gennari stripe (Gennari, 1782).

In a first step, previously published cytoarchitectonic criteria (e.g., Walker, 1940; Petrides and Pandya, 1994; Preuss and Goldman-Rakic, 1991, Rizzolatti *et al.*, 1998; Carmichael and Price, 1994; Morecraft, 2004, Zilles *et al.*, 2002) were applied to analyze the macaque prefrontal cortex by pure qualitative and visual inspection. However, since existing maps differ in terms of number, localization and shape of cortical areas, in the present study the validity of observer-dependent observations were then confirmed with a quantitative and statistically testable approach to cytoarchitectonic analysis (Schleicher and Zilles, 1990; Schleicher *et al.*, 1999, 2000, 2005; Zilles *et al.*, 2002).

Observer-independent mapping procedure (quantitative cytoarchitectonic analysis).

The most important feature of cortical architecture is the organization of cell bodies into layers oriented parallel to the cortical surface. Areal borders are located at the transition of the laminar pattern of one area to that of the neighboring area, assuming that each area has a unique, specific laminar pattern. The quantitative approach relies on the most basic stereological parameter, the volume density of cell bodies, to quantify the laminar pattern characteristic of a cortical area. This parameter has a long tradition in quantitative neurobiology and is defined as the volume fraction of a phase (i.e. the neuronal cell bodies) in

relation to the reference volume. A first quantitative application to cortical microstructure using the “gray cell coefficient” was described by Haug (1956), who extended a previous concept of von Economo and Koskinas (1925). Volume density offers several advantages (Schleicher *et al.*, 1986). One of these advantages is that estimates of volume density are not affected by variations of staining intensity. In addition, it is independent on the degree of anisotropy (deviation from directional randomness in three dimensions; Weibel, 1979). These are major requirements for stereological analysis of the cerebral cortex, which takes place in histological specimens with varying staining intensity and in a highly anisotropic structure. Light microscopical estimates of the volume density of neurons from relatively thick histological sections are biased due to overestimation caused by projection (Reed and Howard, 1998). Using TV-based image analyzers (for a first application see Adhami, 1973), volume densities of neurons are further biased by the contribution of non-neuronal elements like glia and endothelial cells, which cannot be reliably identified using automated image analyzing procedures in silver (or Nissl) stained sections. Both effects were studied by Wree *et al.* (1982). According to their findings in various brain regions and cortical areas, the areal fraction of cell bodies as measured with an image analyzer is highly correlated with the volume density of neurons, since the density of endothelial and glial cells does not vary significantly throughout the cortical layers, and therefore represents a relatively constant, additive contribution to the volume density of neurons. This volume density of neurons measured as an areal fraction of all stained cellular profiles in square measuring fields of 20–30 μm was defined as grey level index (GLI; $0 \leq \text{GLI} \leq 100\%$; Schleicher and Zilles, 1990). This procedure requires the digitization of histological sections, computation of GLI images, extraction of GLI profiles and their statistical analysis for identification of cortical borders.

Digitization of histological sections and generation of GLI images. To gather data for quantitative cytoarchitectonic studies it was necessary to first digitize the visually identified regions of interest (ROI) at microscopic resolution. Each ROI was automatically scanned with a light microscope (Axioplan 2 imaging, ZEISS, Germany) equipped with a motor-operated stage controlled by the KS400[®] and Axiovision (Zeiss, Germany) image analyzing systems applying a 6.3 x 1.25 objective (Planapo[®], Zeiss, Germany), and a CCD camera (Axiocam MRm, ZEISS, Germany) producing frames of 524 x 524 μm in size, 512 x 512-pixel spatial resolution, and eight-bit grey resolution. Digitalized images have an in-plane resolution of 1 μm per pixel and allow the calculation of the GLI using the KS400-system and in-house scripts in MatLab (The MathWorks, Inc., Natick, MA). The GLI is

defined as the volume density of neurons measured as an areal fraction of all stained cellular forms in square measuring fields of 20-30 μm . This measuring field size was chosen because it ensured a representation of the total cortical width by not less than 64 pixels. This guarantees that none of the six cortical layers will be sampled with substantially less than ten pixels, which is the minimum requirement for object size in image analysis (Hougardy, 1975). The fraction of cell bodies is determined in a binary image generated by adaptive thresholding (Castleman, 1979). In this application, the thresholding uses the local gray value differences between the background (neuropil) and darker stained cell bodies and modified the changes in background staining within each image. This way the GLI is not affected by local changes in staining intensity within and between sections. For each area examined here, GLI images were generated from three neighboring sections.

Extraction of GLI profiles. GLI profiles were extracted by measuring the changes in grey values along traverses defined perpendicular to the cortex in the GLI images. Specifically, two lines were interactively defined, an outer contour (OC) along the border between layers I and II and an inner contour (IC) following the border between layer VI and the white matter using the edit-tool of the image analyzer toolbox in MatLab. Then, equidistant traverses were calculated between both contour lines based on a physical model of electric field lines (Jones *et al.*, 2000) and the grey values along these traverses were measured to create GLI profiles of each ROI. A GLI profile can be parametrized, i.e. presented as a frequency distribution, to quantitatively describe the laminar distribution of the volume fraction of the cell bodies (Dixon *et al.*, 1988; Schleicher *et al.*, 2009; Zilles *et al.*, 2002): *many.o* as the mean GLI across cortical layers; *max.o* as the mean cortical depth and indicates the x- coordinate of the center of gravity of the area beneath the profile curve; *std.o* the standard deviation, *skew.o* the skewness, and *kurt.o* the kurtosis of the frequency distribution. Following five parameters (*many.d*, *max.d*, *std.d*, *skew.d*, *kurt.d*) were extracted from the absolute value of the differential quotient of the same profile, where the differential quotient is an approximation of the first derivative of the profile and quantifies its local incline. Furthermore, the length of each profile was normalized using linear interpolation to a cortical thickness of 100% (0% = border between layers I and II; 100% = border to white matter). Thus, these ten parameters constitute a feature vector of each profile and can be standardized using different scales to set equal weight to each of the values used for multivariate analyses (Zilles *et al.*, 2002).

Observer-independent definition of areal borders. The Mahalanobis distance (MD; Mahalanobis *et al.*, 1949) was used to quantify differences in the shape of two profiles (Schleicher and Zilles, 1990; Schleicher *et al.*, 1999, 2000, 2005; Zilles *et al.*, 2002). Hereby, the MD is defined as the absolute distance between the two centroids of the two 10-dimensional clusters (one dimension for each parameter in the feature vector describing a profile), and is influenced by the degree of dispersion within each cluster. Thus, the MD decreases with increasing cluster dispersion, even if the distance between the centroids remains constant (Mahalanobis *et al.*, 1949). In the Results chapter we will show only newly defined borders, i.e. hitherto not previously described subdivisions within areas 10, 8B, F5, F7 and 4. To detect the position of a border, 8 to 32 adjacent profiles were grouped into blocks and the MD between immediately adjacent blocks was calculated. Then both blocks were shifted along the cortical ribbon by the distance of one profile, and the MD was also determined at this position. Distances were calculated by this sliding window procedure between all pairs of neighboring cortical sectors and all block sizes, and resulting MD values were plotted as a function of the sector's position. Each ROI was analyzed repetitively with the same set of profiles, but with systematically increasing block sizes because distance functions depend on the spatial resolution of the analyzing procedure, which is defined by the width of the cortical sectors (i.e., by the number of profiles in each block). If two blocks belong to the same area, MD values are expected to be small, since their laminar pattern is similar. However, maxima of distance functions were accepted as architectonically relevant borders only after they had been confirmed as statistically significant by applying Hotelling's T^2 test for each value of the MD (Bartels, 1981). This is a major advantage of the MD, and this test was applied in combination with a Bonferroni adjustment of the P-values for multiple comparisons (Schleicher and Zilles, 1990; Schleicher *et al.*, 1999, 2000, 2005; Zilles *et al.*, 2002). Maxima which were found to be significant ($P < 0.05$) revealed local changes in cortical architecture if they were not affected by another significant maximum within a block size. Main maxima identified with numerous block sizes in one histological section were biologically evaluated by comparison with corresponding maxima in three consecutive sections to exclude biologically meaningless maxima which may be caused by artifacts (e.g. ruptures, folds) or local discontinues in microstructure due to blood vessels or untypical cell clusters.

2.2.2 Visualization of the 2D parcellation scheme

The microstructural parcellation of the cerebral cortex has been a challenge for generations of neuroanatomists, along with the problem of how to present the parcellation of the cerebral cortex in a 2D brain scheme which displays potential areas within sulci, since this part of the brain includes approximately two thirds of the cortical surface (Zilles *et al.*, 1988). Instead of using only a general brain scheme, a 2D framework (Fig. 3) was created based on the macroanatomical landscape of the brain processed for the visualization of cell bodies (brain ID: DP1). The position of sulci and dimples of every 40th section from brain DP1 were transferred to a simple geometrical pattern by means of Adobe Illustrator CS6, thus creating a “scaffold” on which the position of cytoarchitectonic borders could be traced relative to the macroscopical landmarks while depicting areas located within sulci. Each area was labeled with a specific color. Areas from neighboring sections were connected, creating a continuous shape of each area. Although very simple, this ‘individual’ approach to create a 2D parcellation scheme shows some general advantages: (i) visualization of areas and borders inside of sulci, (ii) interhemispheric differences were not ignored, (iii) comparable with other ‘individual’ parcellation maps, without interfering with intersubject variability, (iv) provides information about brain cutting angle.

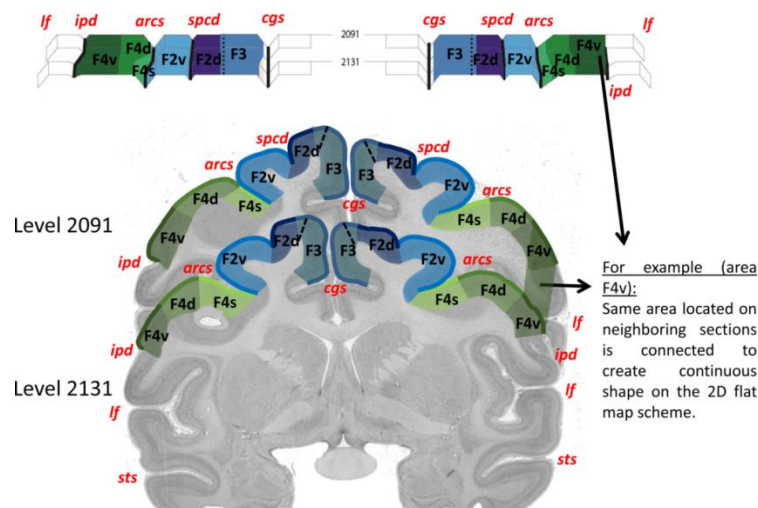


Figure 3 Example of how the 2D parcellation scheme was created. Macroanatomical landscape of two serial sections (levels 2091 and 2131) transferred into the flat geometrical “scaffold”; arcs – arcuate sulcus, lf – lateral fissure, sts – superior temporal sulcus, cgs – cingulate sulcus.

2.2.3 Receptorarchitecture

Neurotransmitters and their receptors are essential molecules of brain function, and can be visualized with various methods. Quantitative *in vitro* receptor autoradiography enables visualization of the binding sites of native receptors expressed on the cell membrane

of neurons and glia cells. Furthermore, it can be applied to a very large number of sections, e.g. sections through entire human or monkey hemispheres, and offers the possibility of precise quantification, with a high specificity of the radioactively labelled ligand binding to receptor types (Schleicher and Zilles, 1988; Zilles *et al.*, 2002, 1988; Palomero-Gallagher and Zilles, 2018). Tritiated ligands were used, since this isotope is more stable and permits a better spatial resolution compared with other isotopes such as ^{125}I and ^{14}C . Finally, analysis of multi-receptor density distribution patterns throughout the cerebral cortex provides an independent approach to validate the distinction between areas or subareas defined during cytoarchitectonic mapping by identifying the unique neurochemical features and creating a 'receptor fingerprint' based on receptorarchitecture.

Binding experiments. The unfixed frozen slabs were coronally sectioned in a cryostat (section thickness 20 μm) at -20°C , and sections were thaw-mounted on gelatin-coated glass slides. Sections were air dried and then stored overnight in air-tight plastic bags at -20°C . Serial sections were used for the visualization of receptors for glutamate (AMPA, kainate, NMDA), gamma-aminobutyric acid - GABA (GABA_A , GABA_B , GABA_A associated benzodiazepine binding sites-BZ), acetylcholine (M_1 , M_2 , M_3), noradrenalin (α_1 , α_2) and serotonin ($5\text{HT}_{1\text{A}}$, 5HT_2), or were processed for silver cell body staining (Merker, 1983). Before beginning of the binding process, sections were placed on the work bench to slowly reach room temperature without opening the air-tight bags. The binding procedure was carried out following previously published protocols (Zilles *et al.*, 2002; Palomero-Gallagher *et al.*, 2009; see *Tab. 2*), which require three steps: a preincubation, a main incubation and a rinsing step. During the preincubation sections are rehydrated and endogenous ligands that could block the binding sites are removed. In the main incubation, sections were incubated in a buffer solution with tritiated ligand to identify total binding of each ligand type. In parallel experiments, neighboring sections were incubated in another buffer solution containing the tritiated ligand with a receptor type-specific displacer in a 1000-fold higher concentration to visualize non-specific binding of the

Table 2 *In-vitro* receptor autoradiography binding protocols.

Transmitter	Receptor	Ligand (nM)	Property	Displacer	Incubation buffer	Pre-incubation	Main incubation	Final rinsing
Glutamate	AMPA	[³ H]-AMPA -10	Agonist	Quisqualate (10 µM)	50 mM Tris-acetate (pH 7.2) [+ 100 mM KSCN]*	3x10 min, 4°C	45 min, 4°C	1) 4x4 sec 2) Acetone/glutaraldehyde (100 ml + 2,5 ml), 2x2 sec, 4°C
		[³ H]-MK-801 -3.3		(+)-MK-801 (100 µM)				1) 2x5 min, 4°C 2) Distilled water, 1x22°C
	NMDA	[³ H]-Kainate -9.4	Antagonist	SYM 2081 (100 µM)	50 mM Tris-acetate (pH 7.2) [+ 30 µM glycine + 50 µM spermidine]*	15 min, 4°C	60 min, 22°C	1) 3x4 sec 2) Acetone/glutaraldehyde (100 ml + 2,5 ml), 2x2 sec, 22°C
	Kainate		Agonist					1) 3x3 sec, 4°C 2) Distilled water, 1x22°C
GABA	GABA _A	[³ H]-Muscimol -7.7	Agonist	GABA (10 µM)	50 mM Tris-citrate (pH 7.0)	3x5 min, 4°C	40 min, 4°C	1) 3x2 sec, 4°C 2) Distilled water, 1x22°C
		[³ H]-CGP 54626 -2		CGP 55845 (100 µM)				1) 2x1 min, 4°C 2) Distilled water, 1x22°C
	Benzodiazepine binding site	[³ H]-Flumazenil -1	Antagonist	Clonazepam (2 µM)	170 mM Tris-HCl (pH 7.4)	15 min, 4°C	60 min, 4°C	1) 2x1 min, 4°C 2) Distilled water, 1x22°C
		[³ H]-Pirenzepine -1		Pirenzepine (2 µM)				1) 2x2 min, 4°C 2) Distilled water, 1x22°C
Acetylcholine	M ₁	[³ H]-Oxotremorine-M (1.7)	Agonist	Carbacol (10 µM)	20 mM HEPES-Tris (pH 7.5) + 10 mM MgCl ₂ + 300 nM Pirenzepine	20 min, 22°C	60 min, 22°C	1) 2x5 min, 4°C 2) distilled water, 1 x 22°C
	M ₂	[³ H]-4-DAMP -1	Antagonist	Atropine sulfate (10 mM)				1) 2x5 min, 4°C 2) Distilled water, 1x22°C
	M ₃	[³ H]-Prazosin -0.2	Antagonist	Phentolamine Mesylate (10 µM)	50 mM Na/K-phosphate buffer (pH 7.4)	15 min, 22°C	60 min, 22°C	1) 5 min, 4°C 2) Distilled water, 1x22°C
		[³ H]-UK 14,304 (0,64)		Phentolamine Mesylate (10 µM)				1) 5 min, 4°C 2) Distilled water, 1x22°C
Serotonin	5-HT _{1A}	[³ H]-8-OH-DPAT -1	Agonist	5-Hydroxy-tryptamine (1 µM)	170 mM Tris-HCl (pH 7.4) [+ 4 mM CaCl ₂ + 0.01% ascorbate]*	30 min, 22°C	60 min, 22°C	1) 5 min, 4°C 2) Distilled water, 3x22°C
	5-HT ₂	[³ H]-Ketanserin -1.14	Antagonist	Mianserin (10 µM)				1) 2x10 min, 4°C 2) Distilled water, 3x22°C

same ligand. Specific binding ability for each ligand is defined by the difference between total and non-specific binding. In this study, non-specific binding was less than 5% of the total binding site. Through the rinsing step, the binding process was stopped; free ligand and buffer salts were removed. The radioactively labelled sections were then air-dried and co-exposed with plastic tritium-standards, calibrated for protein density and with known increasing concentrations of radioactivity, against β radiation-sensitive films for 4-18 weeks depending on the analyzed ligand (Hyperfilm®, Amersham).

Image acquisition. After films were developed, the measurement of binding site concentrations in the autoradiographs was carried out by densitometric analysis (Zilles *et al.*, 2002). Autoradiographs were digitized with an image analysis system consisting of a source of homogenous light and a CCD-camera (Axiocam MRm, Zeiss, Germany) with an S-Orthoplanar 60-mm macro lens (Zeiss, Germany) corrected for geometric distortions, connected to the image acquisition and processing system Axiovision (Zeiss, Germany). Spatial resolution of the resulting images was 3000x4000 pixels; 8-bit gray value resolution). For details of calibration, see Zilles *et al.* (2002). Since the gray values of the digitized autoradiographs code for concentrations of radioactivity, a scaling (i.e. a linearization of the digitized autoradiographs) had to be performed in which the gray values were transformed into fmol binding sites/mg protein. This process required two steps and was carried out with in house developed Matlab (The MathWorks, Inc. Natick, MA) scripts. First, the gray value images of the plastic tritium-standards were used to compute the calibration curve, which defines the non-linear relationship between gray values and concentrations of radioactivity. Radioactivity concentration R was then converted to binding site concentration C_b in fmol/mg protein using following equation 1:

$$C_b = \frac{R}{E \cdot B \cdot W_b \cdot S_a} \cdot \frac{K_D + L}{L} \quad (1)$$

where E is the efficiency of the scintillation counter used to determine the amount of radioactivity in the incubation buffer (depends on the actual counter), B is the number of decays per unit of time and radioactivity (Ci/min), W_b the protein weight of a standard (mg), S_a the specific activity of the ligand (Ci/mmol), K_D the dissociation constant of the ligand (nM), and L the free concentration of the ligand during incubation (nM). The result was a linearized image in which the gray value of each pixel in the autoradiograph is converted into

a binding site concentration in fmol/mg protein. For details see Zilles *et al.* (2002), and Palomero-Gallagher and Zilles (2018). Pseudo-color coding of autoradiographs was applied solely for visualization purposes, by means of linear contrast enhancement, which preserves the scaling between gray values and receptor concentrations. A specter of eleven colors to equally spaced density ranges was used, assigning red color for highest and black for lowest receptor concentration levels.

Measurement of binding site concentrations. Measurement of receptor binding sites was performed by computing the surface below receptor profiles, which were extracted from the linearized autoradiographs using in house developed scripts for Matlab (The MathWorks, Inc. Natick, MA) in a manner analog to the procedure described above for GLI profiles. For receptor profiles the outer contour line was defined following the pial surface, and not the border between layers I and II. Thus, for each of the three hemispheres examined, mean densities (i.e., averaged over all cortical layers) of each of the 13 different receptors in 48 of the 50 cytoarchitectonically defined areas were calculated. It was not possible to measure densities in areas 13a and 14c due to technical limitations associated with the cutting angle of the coronal sections. The precise sampling for the measurements of each microscopically defined area was verified by comparing autoradiographs with the adjacent sections which had been processed for the visualization of cell bodies. For each of the examined areas, the mean densities of all receptors averaged over all three hemispheres in that area were then visualized simultaneously as “receptor fingerprints”, i.e., as polar coordinate plots which reveal the specific balance of different receptor types within a cytoarchitectonic entity (Zilles *et al.*, 2002).

2.2.4 Statistical analysis

The receptor fingerprints of each area were treated as a feature vector characterizing that area and used to carry out hierarchical clustering and principal component analyses, which enable grouping of areas based on similarities in their receptor architecture (Palomero-Gallagher *et al.*, 2009). Before carrying out multivariate statistical tests, receptor densities were normalized by computation of z-scores, since this approach maintains the relative differences in receptor densities among areas. Thus, the mean density of a given receptor across all examined areas was subtracted from the mean density of that receptor in a given area and divided this value by the standard deviation of that receptor over all areas. This

approach is crucial, because the values of absolute receptor densities vary between receptors and by normalizing those values, each receptor contributes with equal significance to the statistical analyses. Without normalization, receptors with high absolute density values would dominate the calculation of the Euclidean distance between areas, or of the principal component analysis, and would cancel the multivariate approach in the present analysis. For the hierarchical cluster analysis, the Euclidean distance was applied as a measure of (dis)similarities between receptor fingerprints, since it accounts for differences in the size and shape of the fingerprints. The Ward linkage algorithm was chosen as the linkage method because, in combination with the Euclidean distances, it yielded a higher cophenetic correlation coefficient than any other combination of alternative linkage methods and measurements of (dis)similarity. The cophenetic correlation coefficient quantifies how well the dendrogram represents the true, multidimensional distances within the input data. The k-means clustering identified 8 as the highest acceptable number of clusters.

3 Results

3.1 2D parcellation scheme

Fig. 4 and *5* show the 2D parcellation scheme of 50 areas defined in the frontal lobe of the macaque monkey brain processed for cytoarchitecture (ID DP1). The frontal lobe can be subdivided into two parts: an anterior part, known as the prefrontal cortex (PFC), and a posterior part, which is separated by the central sulcus (*cs*) from the parietal lobe, and includes areas involved in movement, i.e., the motor cortex (MC) and the premotor cortex (preMC). The PFC is separated from the motor areas by the well-defined arcuate sulcus (*arcs*), which branches dorsally into the superior arcuate sulcus (*sas*) and ventrally into the inferior arcuate sulcus (*ias*), thus forming a letter Y on the dorso-lateral surface of the hemisphere. On the ventro-lateral side, the PFC is limited caudally by the lateral fissure (*lf*), which represents the border with temporal areas. Medially, the PFC is separated by the cingulate sulcus (*cgs*) from the limbic cortex. A further significant feature on the lateral aspect of the PFC in the macaque monkey brain is the well-defined principal sulcus (*ps*), which caudally ends within the arcuate sulcus (*Fig. 4*). The ventral surface is characterized by a variable orbital sulcal complex which is, in the brain studied here, constituted by two parallel, sagittally oriented sulcii in the left hemisphere, while in the right hemisphere these sulcii are connected forming a letter H (*Fig. 5*). Other prominent macroanatomical features, though not as deep as sulcii, are dimples, e.g. the superior precentral dimple (*spcd*) in the dorsal part of the motor cortex, the anterior dimple (*aspd*) in its rostral part, and more caudally, the posterior dimple (*pspd*) in the dorsal PFC. Ventral to the *ps* the inferior principal dimple (*ipd*) was recognizable only in the right hemisphere. Lateral areas inside and around the sulcus principalis as well orbital and ventrolateral areas represent mostly granular neocortex, with a well-developed internal granular layer IV, although few areas, e.g. areas 13 (13m, 13l, 13b), 14r, 12r and 12o have a thin, discontinuous layer IV and are thus characterized as being dysgranular. Furthermore, layer IV is surrounded by the pyramids of layers III and V, that in some areas show a characteristic gradual increase in size, with the largest cells being close to layer IV, as for example in areas 9 and 8B. The motor region is composed of agranular cortex (lacks a layer IV, but has a well recognizable outer granular layer II) with prominent pyramidal cells in layers III and V. Another gradient of pyramid size can be observed in the motor region along anterior-posterior direction, as pyramids in layer V

become larger toward the posterior frontal areas. The most caudal area of the frontal lobe, i.e. the primary motor cortex (area 4), is characterized by huge pyramids in layer V, called Betz cells (Betz, 1874).

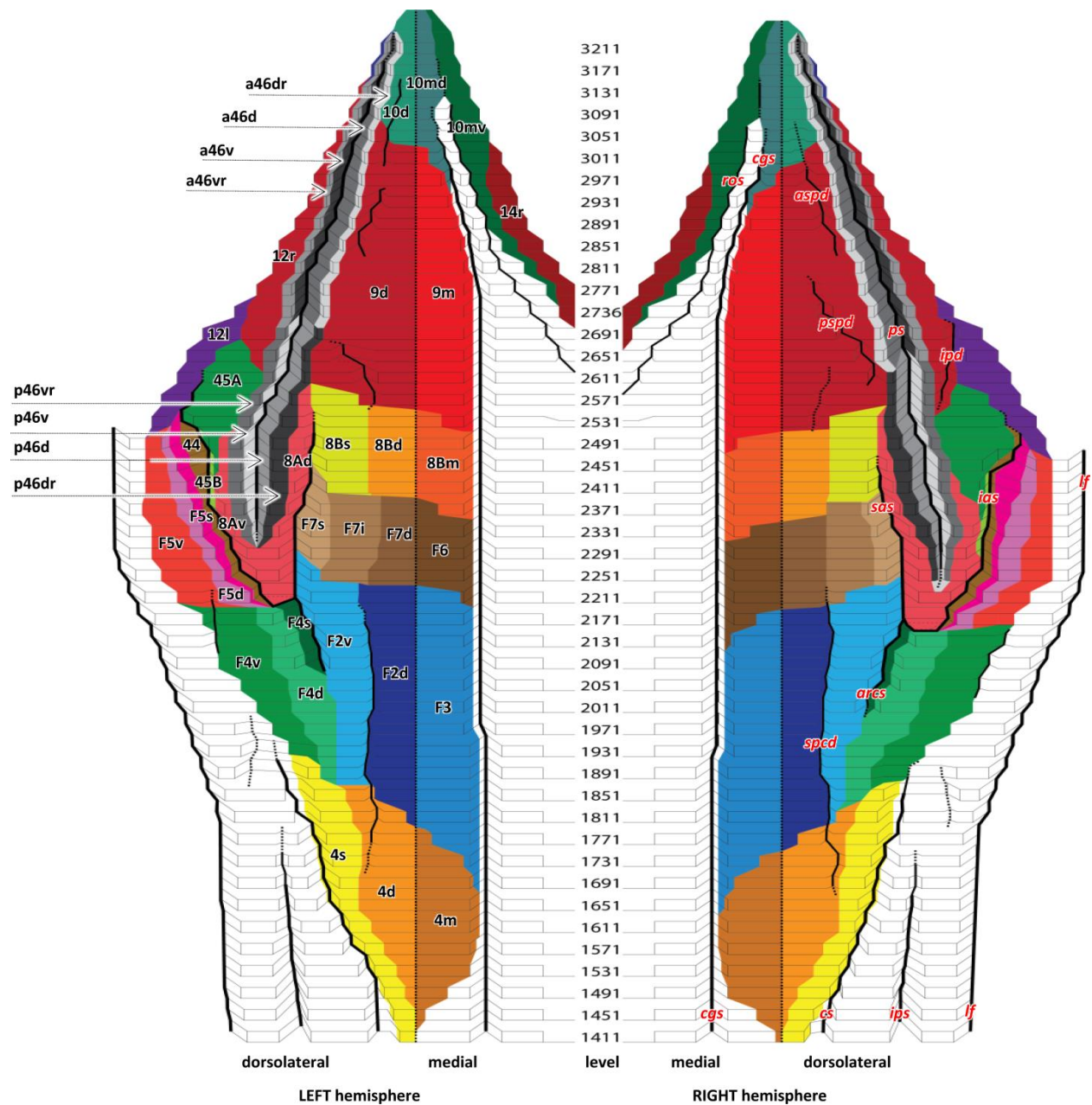


Figure 4 2D flat map depicting all identified areas on the medial and dorsolateral cortical surfaces (total of 39 subareas). Microanatomical features are marked on the right hemisphere, i.e. *ps* – principal sulcus, *sas* – superior arcuate branch, *ias* – inferior arcuate branch, *arcs* – arcuate sulcus, *lf* – lateral fissure, *sts* – superior temporal sulcus, *cgs* – cingulate sulcus, *ros* – rostral sulcus, *aspd* – anterior (superior) principal dimple, *pspd* – posterior (superior) principal dimple, *ipd* – inferior principal dimple, *spcd* – superior precentral dimple, *ips* – inferior parietal sulcus. Black dashed line marks midline. Section numbers indicated between the hemispheres.

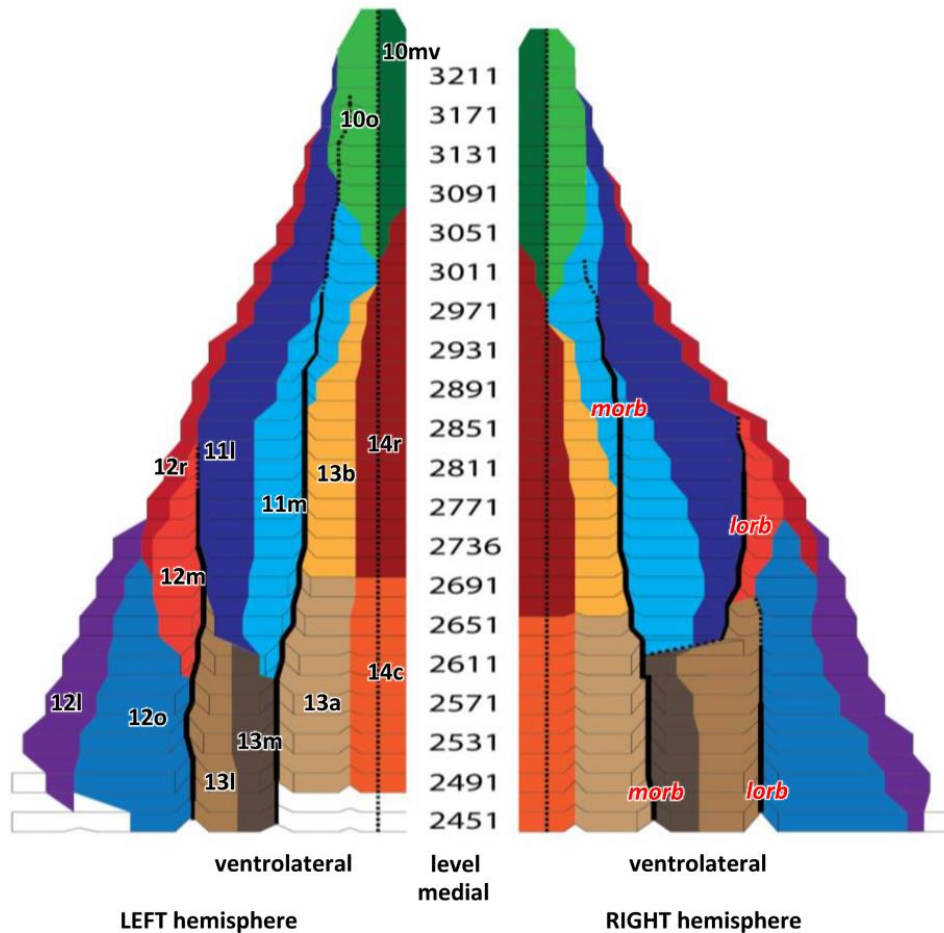


Figure 5 2D flat map depicting all identified areas on the medial and orbital cortical surfaces (total of 14 subareas). Microanatomical features were marked on the right hemisphere, *morb* – medial orbital sulcus, *lorb* – lateral orbital sulcus. Black dashed line marks midline. Section numbers indicated between the hemispheres.

3.2 Cytoarchitectonic mapping (qualitative and quantitative analysis)

Cytoarchitectonic analysis is based on the identification of cortical areas by visual inspection of every 20th coronal histological section of the macaque brain (ID DP1) and criteria described in the literature, followed by the observer-independent confirmation of borders between areas. Nomenclature and starting point of the present analysis were the following studies:

- Parcellation scheme of motor areas (i.e., primary motor cortex, areas F2, F3, F4, F5, F6 and F7) was based on studies of Brodmann (1909; primary motor cortex, area 4) and Matelli *et al.* (1985, 1991), though incorporating more recent modifications (Rizzolatti and Luppino, 2001; Schlag and Schlag-Rey, 1987; Matelli *et al.*, 1998; Belmalih *et al.*, 2009).

- Analysis of the orbital cortex, including ventro-lateral areas (i.e., areas 11, 12, 13 and 14), was based on the parcellation scheme proposed by Charmichael and Price (1994).
- Remaining areas of the frontal lobe (i.e., areas 10, 9, 8B, 8A, 46, 45) were studied based on Walker's (1940) original parcellation scheme, although integrating the more recent descriptions, e.g. of Preuss and Goldamn-Rakic (1991), Petrides and Pandya (1999, 2002, 2006), Bruce *et al.* (1985), Morecraft *et al.* (2012), Caminiti *et al.* (2017).

3.2.1 Prefrontal regions

Fronto-polar region (subdivisions of Walker's area 10; Fig. 6; Fig. 7). Four different subareas were identified within the fronto-polar region: 10d (dorsal), 10md (mediodorsal), 10mv (medioventral) and 10o (orbital). Area 10d is located on the dorsolateral surface of the frontal pole, areas 10mv and 10md on its medial surface, and 10o on its most ventral aspect, occupying the rostral portion of the ventromedial gyrus. The cortex in all subdivisions of area 10 is granular, with a very well-developed layer IV, but with slight differences in its thickness between defined subareas. Area 10d has wider and more densely packed layers II and IV than area 10md, with small-sized pyramidal cells in layers III and V, and a more blurred border between layers V and VI. Medial areas 10md and 10mv show a thinner layer IV and less prominent border between layers II and III due to the lower cell packing density of layer II, which in 10md is slightly better recognizable than in the neighboring area 10mv. Both areas show horizontal columns in layer IV, but only in 10md can the same columnar organization also be seen in layers III and V. Layer III is more dense in 10md than in 10mv, but layer V is less packed with pyramids, which makes the border between layers V and VI clearer in 10md than in 10mv. Area 10o can be distinguished from 10mv by its more prominent layer II and wider layer IV (Fig. 6). These newly identified borders within the fronto-polar region 10 were also confirmed by the observer-independent analysis, as shown in the Fig. 7.

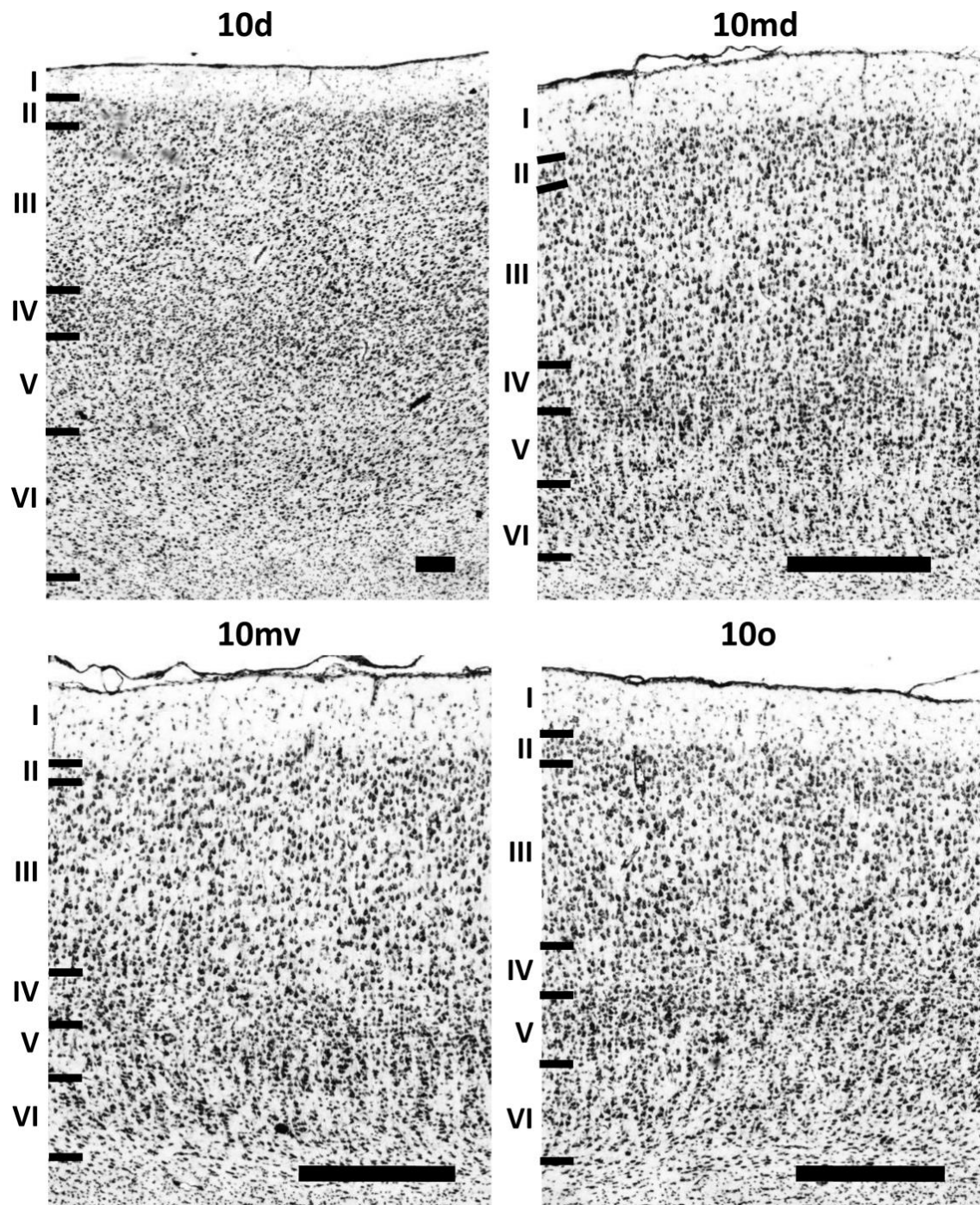


Figure 6 Visualization of the cortical layers in subdivisions of Walker's (1940) area 10; 10d (dorsal), 10md (dorso-medial), 10mv (ventro-medial), 10o (orbital). Roman numerals indicate cortical layers. Scale bar 1 mm.

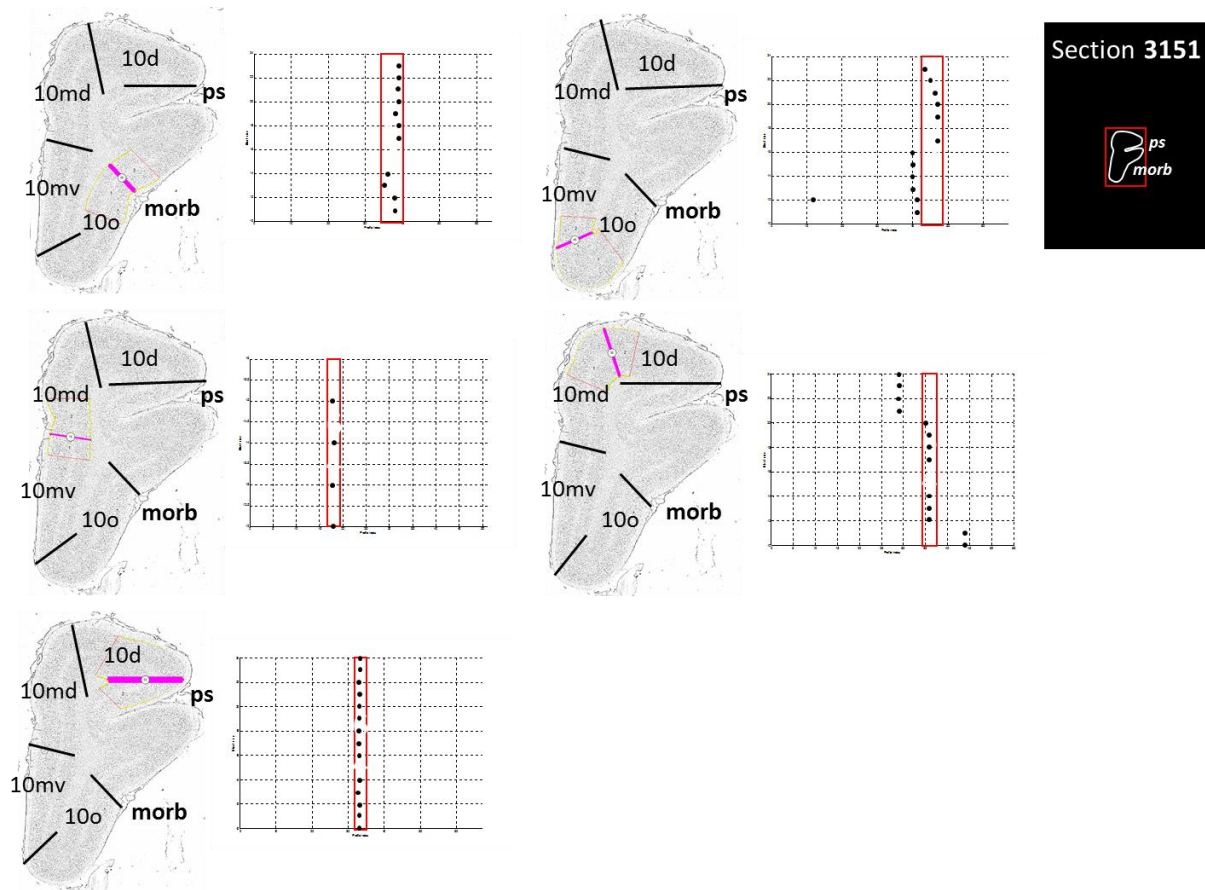


Figure 7 Positions of significant maxima in the Mahalanobis distance functions (abscissa) plotted against blocksize b (ordinate). The location of the significant maxima does not depend on the blocksize, but remains stable over large block size intervals and confirms the cytoarchitectonic subdivisions of Walker's (1940) area 10, 10d (dorsal), 10md (dorso-medial), 10mv (ventro-medial), 10o (orbital) identified by visual inspection; *ps* – principal sulcus, *morb* – medial orbital sulcus.

Orbitofrontal region (subdivision of Walker's area 14, Fig. 8; Walker's area 13, Fig. 9; Walker's area 11, Fig. 10).

Subdivisions of area 14 (14r and 14c), located on the ventromedial gyrus and of area 13 (13b and 13a), found on the medial wall of the medial orbital sulcus (*morb*), show rostro-caudal differences as described by Charnichael and Price (1994). Areas 14r (rostral) and 14c (caudal) differ by the appearance of their layer IV; area 14r is dygranular, whereas area 14c is agranular (Fig. 8). Thus, areas 14r and 14c can be easily distinguished from neighboring areas 10mv, 13b and 13a, located on the medial side of the hemisphere. 10o has recognizable granular layers II and IV, as well as bigger pyramids in layer V than in 14r. On the other hand, 13b has horizontal columnar organization only in layer V, whereas same pattern can be recognized in layers IV and V in 14r. 14c does not have continuous layer V like areas 13b and 13a.

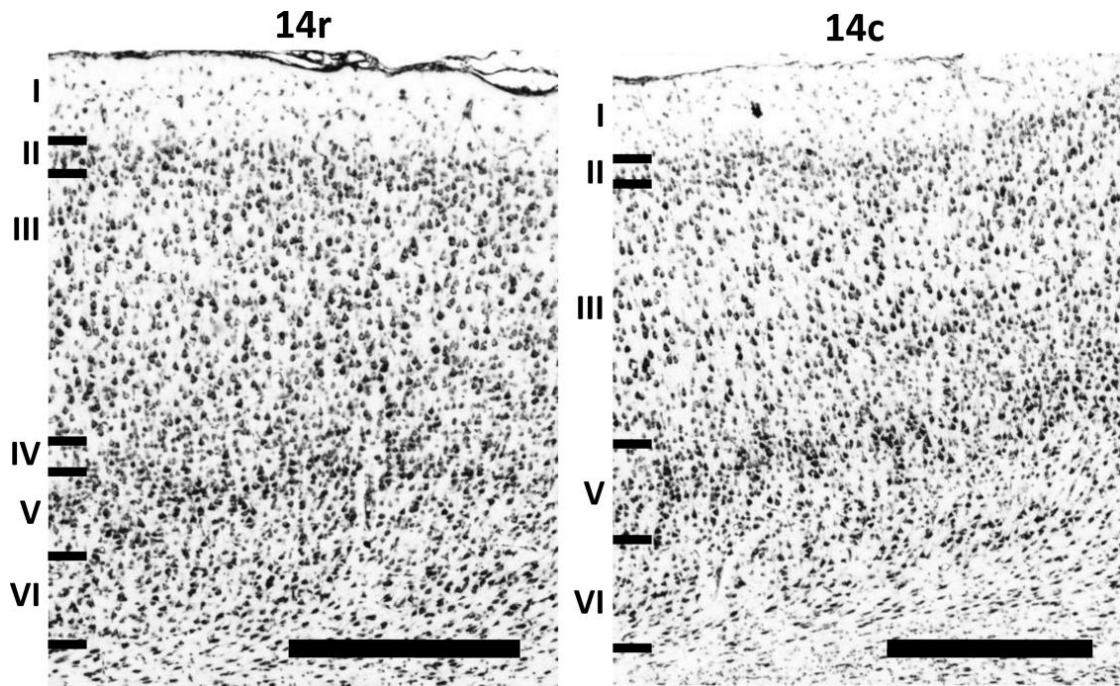


Figure 8 Visualization of the cortical layers in subdivisions of Walker's area 14; 14r (rostral), 14c (caudal). Roman numerals indicate cortical layers. Scale bar 1 mm.

Areas 13m and 13l are part of the dysgranular cortex rostral to the agranular insular region. Area 13l has more prominent pyramidal cells in the lower part of layer III, and a weakly subdivided layer V, whereas a subdivision of layer V is not visible in area 13m. Area 13b can be distinguished by its strong horizontal organizational pattern in layer V, as well as by its weak, discontinued layer IV, from caudally neighboring agranular area 13a. Area 13a has a sublaminate layer V with densely stained pyramids in the V_a sublamina (*Fig. 9*).

Rostral to areas 13m and 13l, is granular cortex encompassing areas 11m and 11l. Characteristic of these areas is the clear sublamination of layer V, which distinguishes them from surrounding areas 13b, 13m and 10o. The main difference among the subdivisions of area 11 is the pattern of cells in sublaminae V_a and V_b , which are continuous in area 11m and broken into aggregates of cells in area 11l. Moreover, 11m has bigger pyramids in the lower part of the layer III, whereas in 11l cells are similar size through layer III (*Fig. 10*).

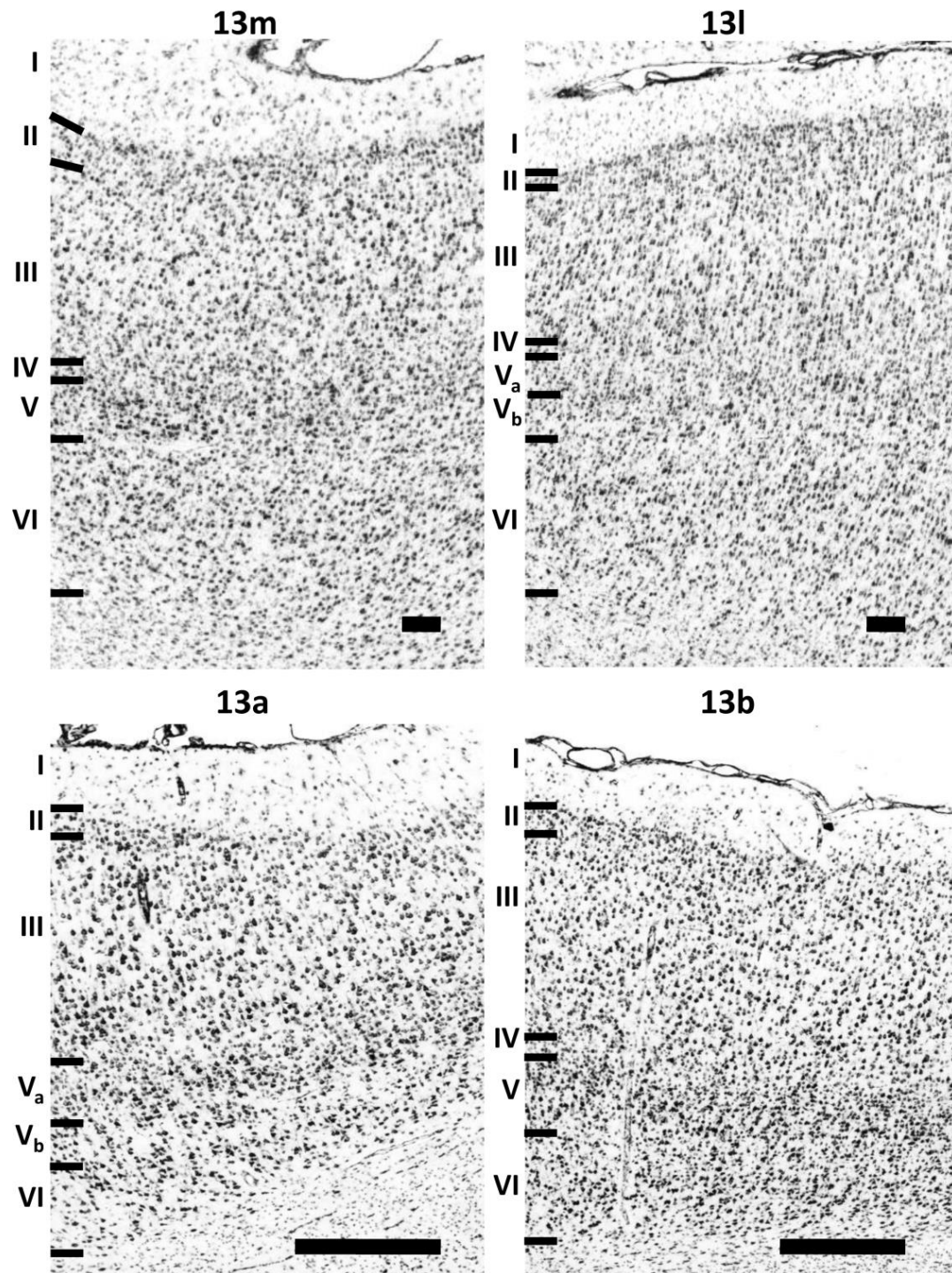


Figure 9 Visualization of the cortical layers in subdivisions of Walker's area 13; 13m (medial), 13l (lateral), 13a (caudal), 13b (rostral). Roman numerals indicate cortical layers. Scale bar 1mm.

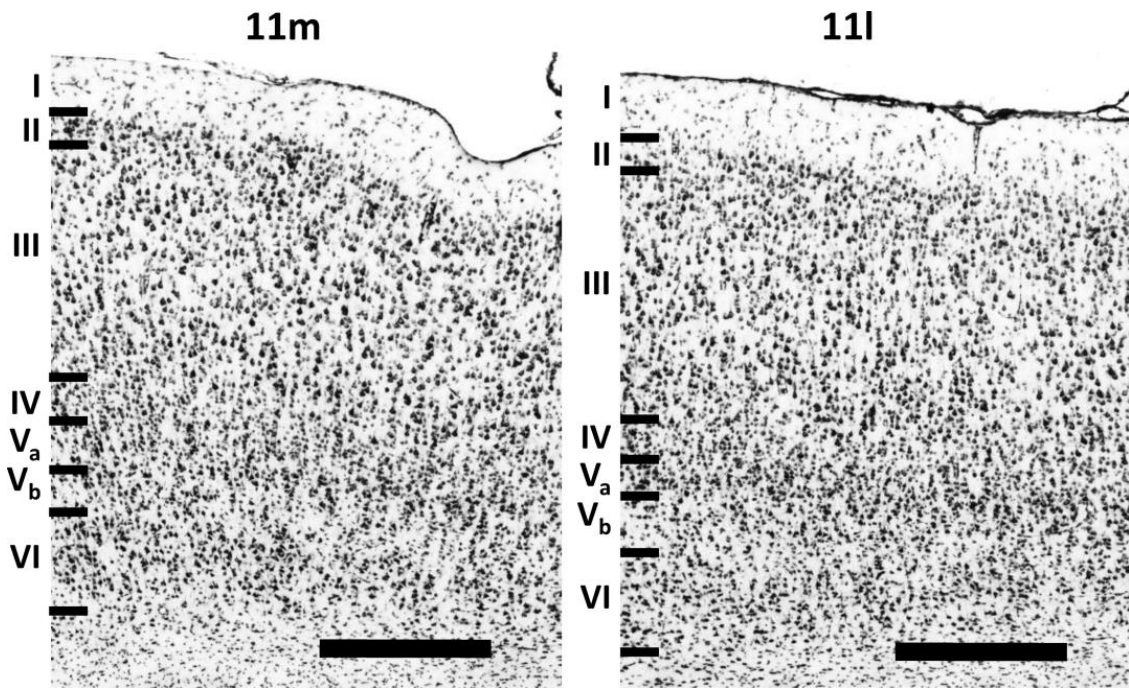


Figure 10 Visualization of the cortical layers in subdivisions of Walker's area 11; 11m (medial), 11l (lateral). Roman numerals indicate cortical layers. Scale bar 1 mm.

Ventrolateral (rostral) region (subdivision of Walker's area 12, Fig. 11). In the present study we could confirm the parcellation scheme by Charnichael and Price (1994), which subdivides Walker's area 12 into four different areas: 12r (rostral), 12m (medial), 12o (orbital), 12l (lateral). Areas are distinguished by the degree of granularity of layer IV, and the size and distribution pattern of the pyramids in layers III and V. The most rostral area on the medioventral surface of the PFC, 12r, is a dysgranular cortex with characteristic vertical striations of pyramidal cells in layers III and V. Unlike medially neighboring area 11l, there is no subdivision of layer V. Area 12m, located within the lateral orbital sulcus (*lorb*), has a bipartite layer V and a well-developed layer IV. This feature distinguishes 12m from surrounding areas 12r, 13l and 12o. The compact and darkly stained sublayer V_a in 12m is much more prominent than in caudally neighboring area 13l. Area 12o, located on the ventral surface medially from 12l on the caudal medioventral convexity, has a thin and weakly stained layer IV, and no obvious sublamination in layer V. Area 12l is granular cortex with clear subdivisions in layer V. Pyramids in lower part of the layer III are smaller than the medium- to large-size pyramidal cells in dorsally neighboring area 45A (Fig. 11).

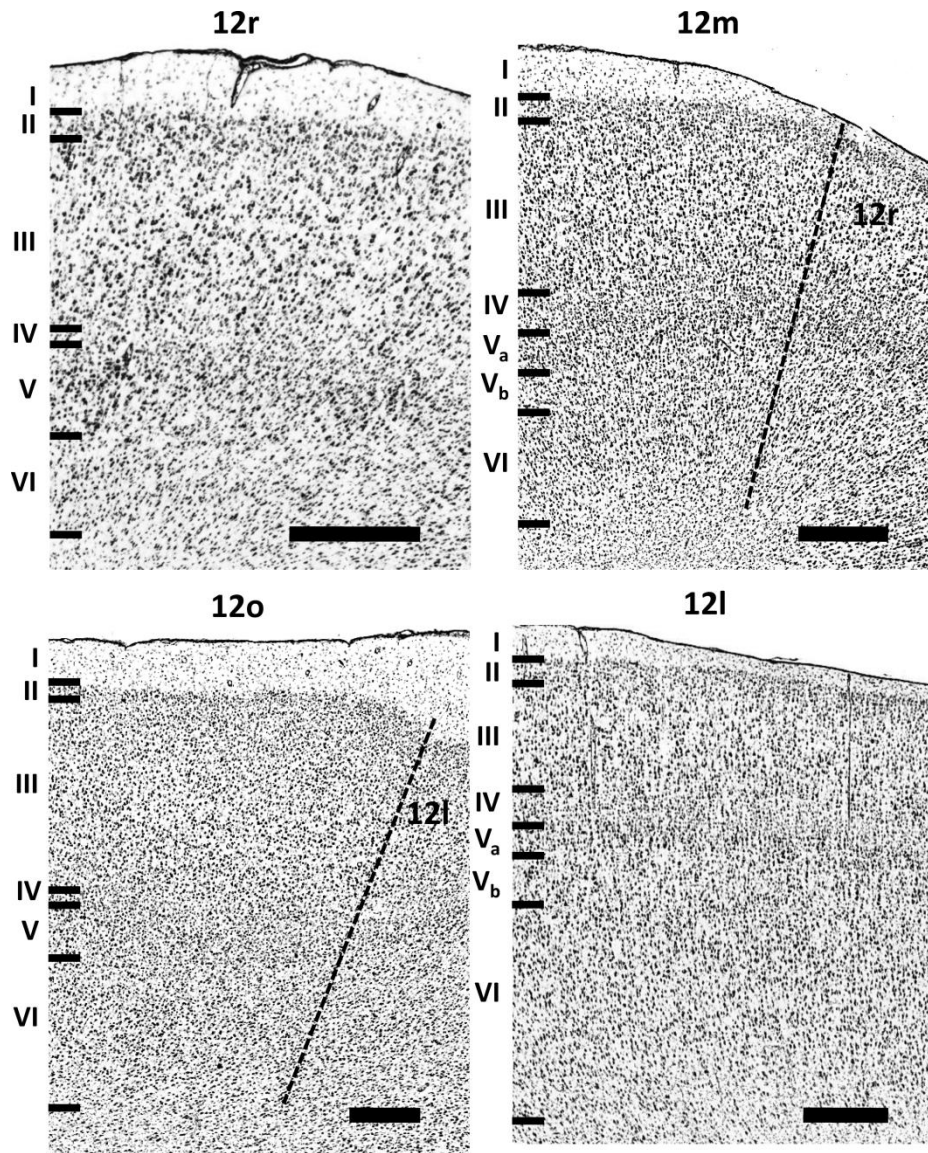


Figure 11 Visualization of the cortical layers in subdivisions of Walker's area 12; 12r (rostral), 12m (medial), 12o (orbital), 12l (lateral). Roman numerals indicate cortical layers. Scale bar 1 mm.

Medial and dorsal (rostral) region (subdivisions of Walker's area 9, Fig. 12). The present analysis confirms previous subdivision of Walker's area 9 into two subareas (Preuss and Goldman-Rakic, 1991; Petrides and Pandya, 1994, 2002; Caminiti *et al.*, 2017): 9m (medial) and 9d (dorsal). Both areas are characterized by the low packing density and width of layer III, and the subdivision of layer V, which distinguishes both subdivisions from neighboring areas. Subdivision of layer V into a prominent V_a, with large pyramidal cells closer to the well-defined layer IV, and a V_b, with a low cell packing density, clearly separates it from layer VI. Area 9m occupies the medial part of the PFC, and is located between areas 10md rostrally and 8Bm caudally. Area 9d is limited rostrally by area 10d and

caudally by areas 8Bd and 8Bs on the dorsal surface and by area a46dr on the dorso-lateral aspect of the hemisphere. The most recognizable feature of area 9d, that is not visible in area 9m, is the gradual increase in size of the pyramids in layer III (largest cells are closer to the layer IV) (*Fig. 12*).

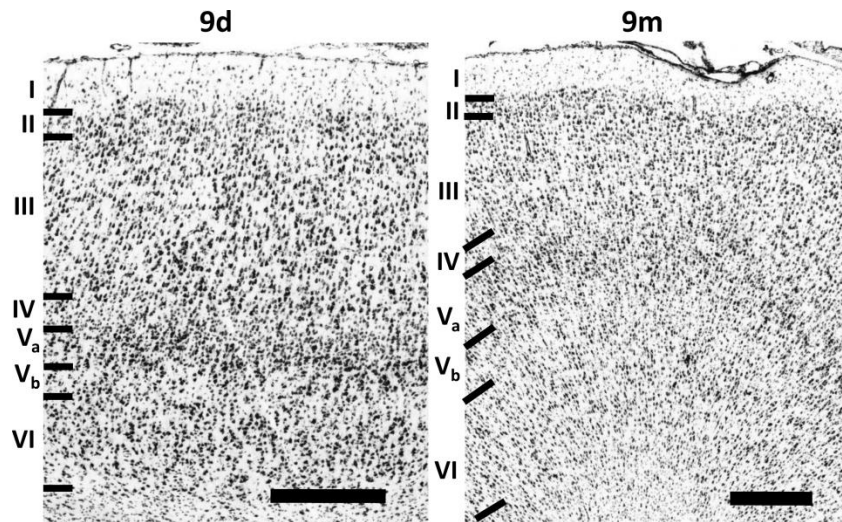


Figure 12 Visualization of the cortical layers in subdivisions of Walker's area 9; 9d (dorsal), 9m (medial). Roman numerals indicate cortical layers. Scale bar 1 mm.

Dorsolateral region within the principal sulcus (subdivision of Walker's area 46, anterior areas, *Fig. 13*, and posterior areas, *Fig. 14*). A new parcellation scheme of the dorsolateral granular subdivisions of area 46 within the *ps* is presented here. Areas on the anterior portion (*Fig. 13*) of the *ps* are labelled as a46dr (dorsorostral), a46d (dorsal), a46v (ventral), a46vr (ventrorostral) and, on the posterior portion (*Fig. 14*), p46dr (dorsorostral), p46d (dorsal), p46v (ventral), p46vr (ventrorostral). Although the cytoarchitecture of both regions is very similar, differences can be recognized in the cell body size of pyramids in layers III and V, which are medium to large in anterior areas, and smaller in posterior areas, particularly in p46d and p46v. Whereas in p46dr and p46vr medium- to large-sized pyramids in layers III and V_a are recognizable. This rostro-caudal subdivision along the *ps* is further confirmed by differences in neurotransmitter receptor densities (see below). Dorsal subdivisions of area 46 have a wider and more prominent granular layer II than the ventral areas, which, on the other hand, have more a prominent layer IV, and larger cells in layers V and VI. Areas located around the fundus of the *ps*, i.e. areas a46d, a46v, p46d, and p46v, have clear border between layer VI and the white matter, unlike the areas located on the superficial portion of the sulcus, i.e. a46dr, a46vr, p46dr, and p46vr. Differences between

ventral areas a46v/ p46v and a46vr/p46vr can be recognized by a prominent vertical columnar organization of cells in layer IV and deep layer III of a46vr/p46vr, whereas in a46v/p46v similar columnar pattern is visible only in layer IV. Unlike a46d/p46d, the border between layers V and VI is hardly visible in a46dr/p46dr (*Fig. 13 and 14*).

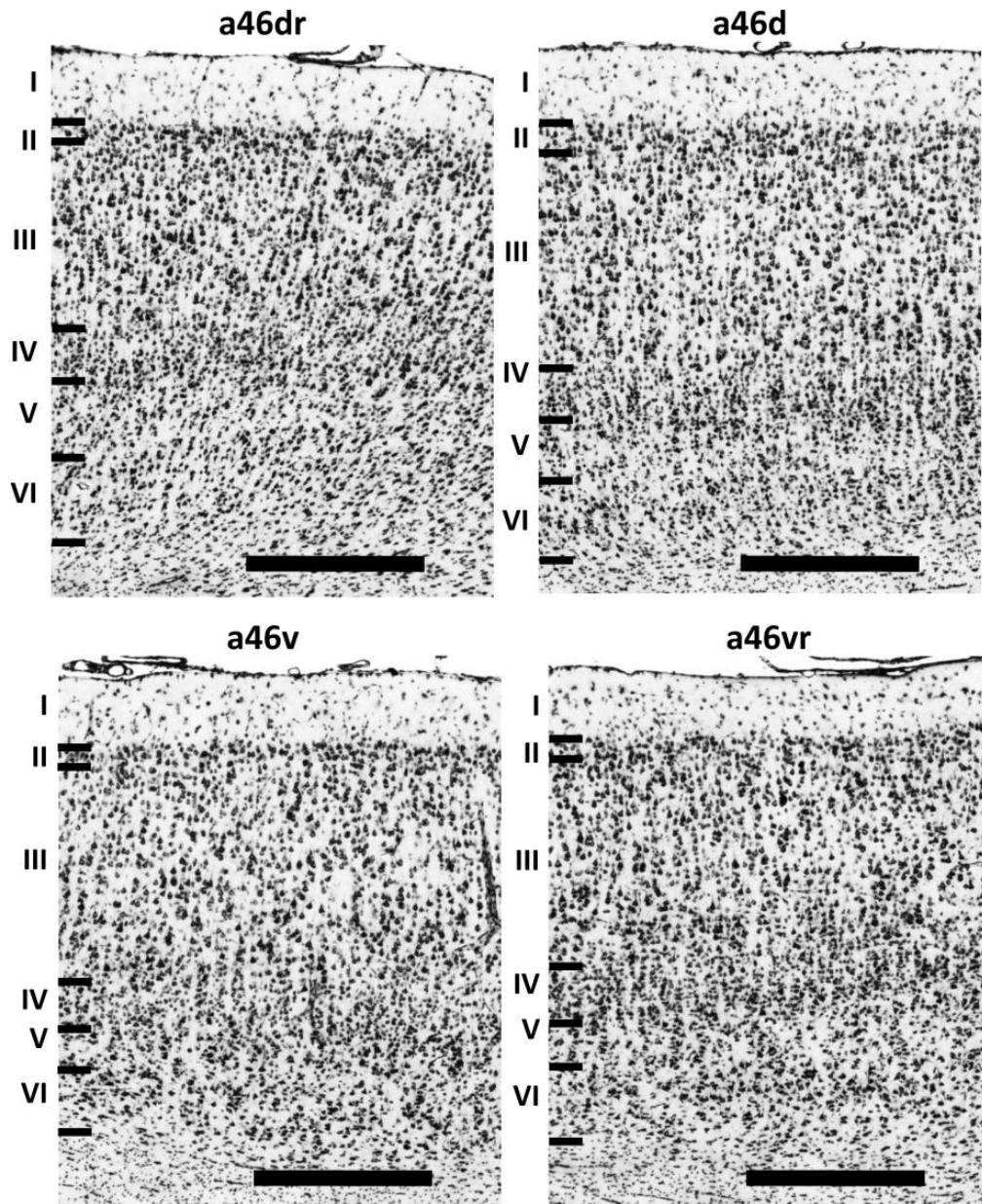


Figure 13 Visualization of the cortical layers in subdivisions of Walker's area 46; anterior areas, a46dr (dorsorostral), a46d (dorsal), a46v (ventral), a46vr (ventrostral). Roman numerals indicate cortical layers. Scale bar 1 mm.

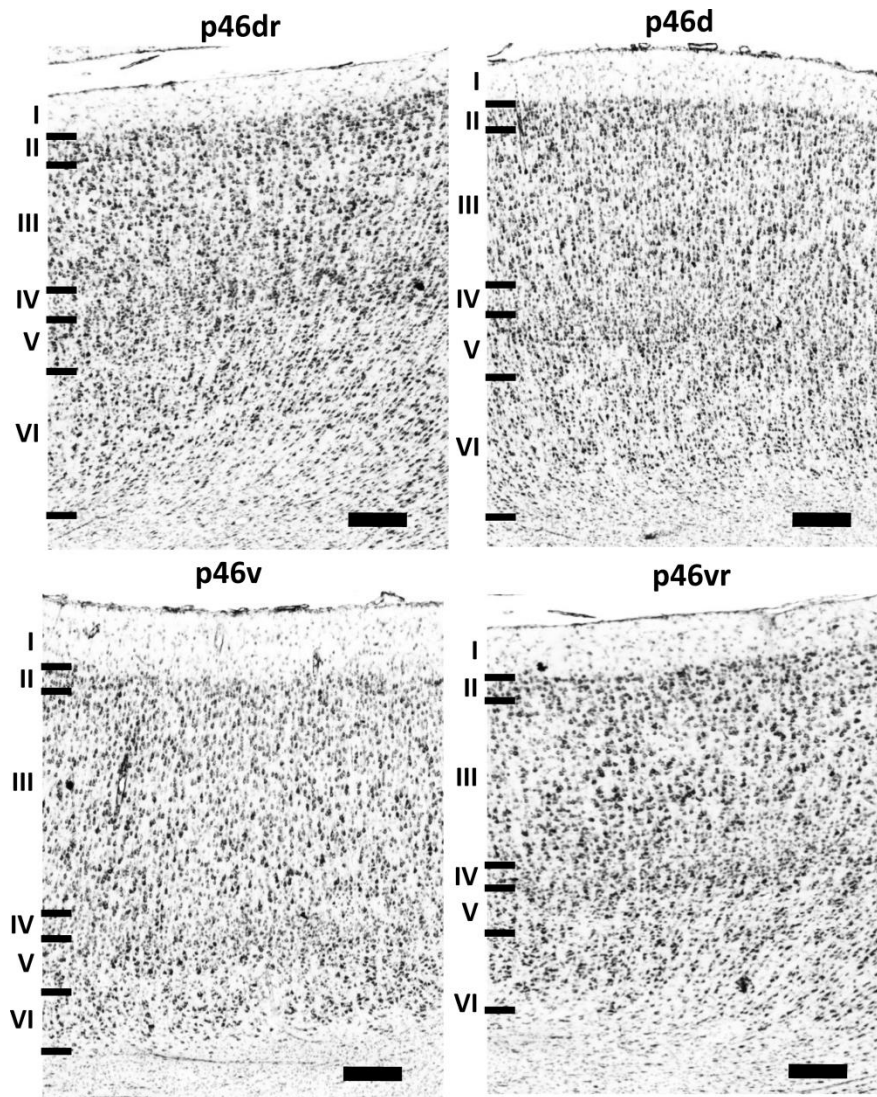


Figure 14 Visualization of the cortical layers in subdivisions of Walker's area 46; posterior areas, p46dr (dorsorostral), p46d (dorsal), p46v (ventral), p46vr (ventrorostral). Roman numerals indicate cortical layers. Scale bar 1 mm.

Medial and dorsolateral (caudal) region (subdivision of Walker's areas 8B and 8A, Fig. 15 and Fig. 16). The most posterior part of the PFC is occupied by subdivisions of Walker's (1940) areas 8A and 8B, which represent a transitional zone between granular cortex of the PFC and agranular cortex of the motor areas. Area 8A is located on the dorsal wall of the superior branch of the arcuate sulcus in the macaque. The present analysis of this area resulted in the confirmation of previous subdivisions (Bruce *et al.*, 1985; Petrides and Pandya, 2006), i.e. 8Av (ventral) and 8Ad (dorsal), as well as in the identification of new subareas, i.e. 8Bm (medial), 8Bd (dorsal) and area 8Bs (sulcal). 8Bm is part of the medial posterior portion of the PFC, bordering caudally with medial premotor area F6 and rostrally with prefrontal medial area 9m. Area 8Bd is found on the dorsal surface of the hemisphere

rostral to the *sas*, and 8Bs is located on the dorsal wall of the *sas*. Subdivisions of area 8B are dysgranular, whereas subdivisions of area 8A constitute the granular part of the frontal eye field region, located within both arcuate sulcus branches and surrounding the posterior part of area 46 located inside the *ps*. Area 8Bm is weakly laminated, with small-sized pyramids in layers III and V. A thin layer IV is

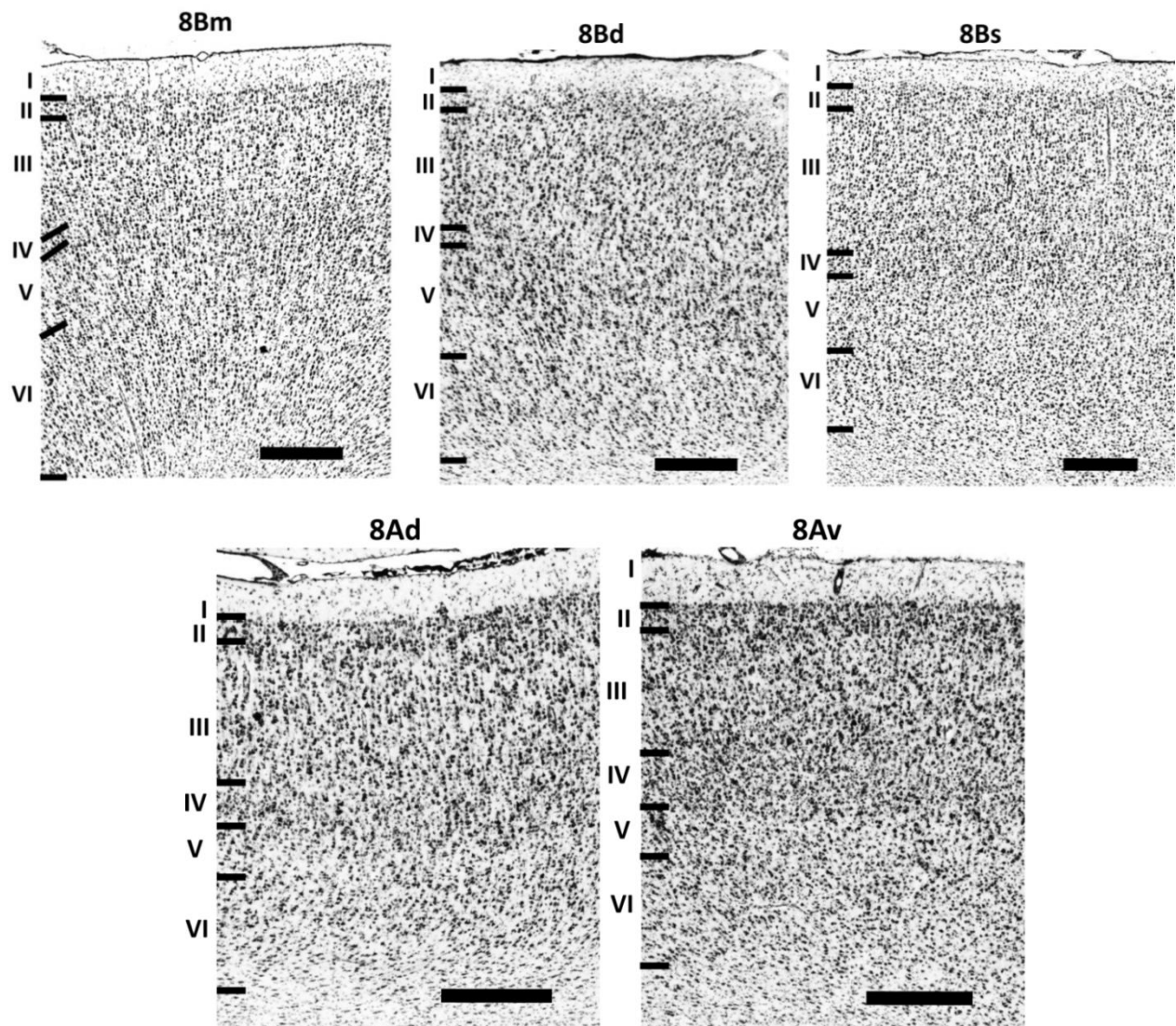


Figure 15 Visualization of the cortical layers in subdivisions of Walker's area 8B; 8Bm (medial), 8Bd (dorsal), area 8Bs (sulcal), and Walker's area 8A; 8Av (ventral) and 8Ad (dorsal). Roman numerals indicate cortical layers. Scale bar 1mm.

hidden behind scattered pyramidal cells of the layer V, which creates a prominent stripe that cannot be visualized in neighboring area F6. In area 8Bd layer II is more dense and prominent than in 8Bs. The pyramids in layers III and V of 8Bd increase from medium to large sizes, which is not characteristic of surrounding areas 8Bm and 8Bs, that share similar

cytoarchitectonic traits. The main difference between them is that 8Bs displays a few scattered medium-size pyramids in layer V (*Fig. 15*). New subdivisions of area 8B are confirmed by observer-independent analysis, as shown in the *Fig. 16*. Area 8Ad is located on the ventral wall of the *sas*. Areas 8Ad and 8Av have a clear laminar structure, with a well-developed layer IV, which is especially wide and dense in 8Av. They are also characterized by a high cell packing density in superficial layers II and III. 8Ad has medium-sized pyramids in layer III, while 8Av has numerous small-sized pyramids, with large ones scattered equally through its layer III (*Fig. 15*).

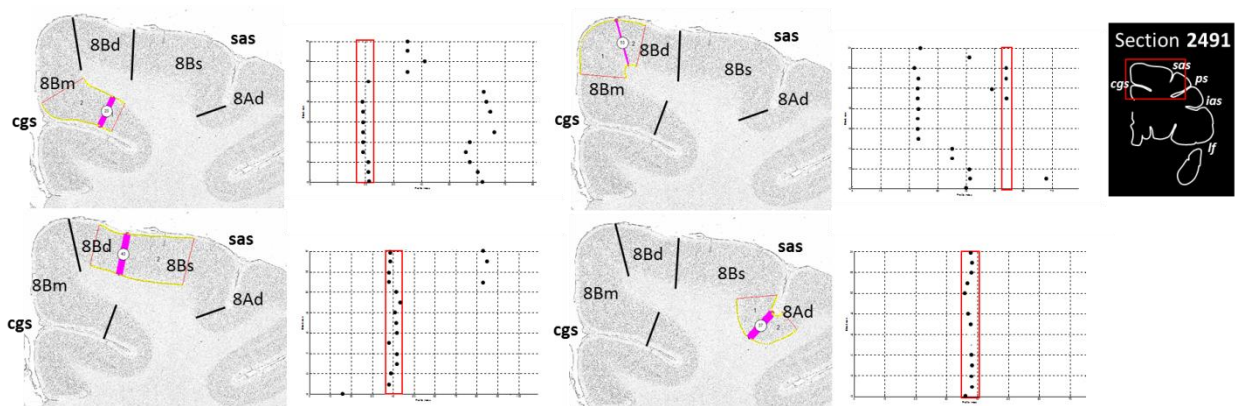


Figure 16 Positions of significant maxima in the Mahalanobis distance functions (abscissa) plotted against blocksize b (ordinate). The location of the significant maxima does not depend on the blocksize, but remains stable over large block size intervals and confirms the cytoarchitectonic subdivisions of Walker's (1940) area 8B, 8Bm (medial), 8Bd (dorsal), 8Bs (sulcal) identified by visual inspection. *cgs* – cingulate sulcus, *sas* – superior arcuate sulcus, *ps* – principal sulcus.

Ventrolateral (caudal) region (subdivision of Walker's area 45 and 44, *Fig. 17*).

Dysgranular area 44 can be recognized along the deeper portion of the ventral wall, and encroaching onto the dorsal wall, of the inferior branch of the arcuate sulcus. Area 44 is distinguished from the neighboring area 45B, located close to the fundus on the dorsal wall of the inferior branch of the arcuate sulcus, by dysgranular cortex and darkly stained pyramids in layer V, but without the characteristic clusters of pyramidal cells in the deeper part of layer III, as in granular area 45B. On the other hand, rostral to 45B on the prearcuate convexity, continuous, prominent pyramidal cells can be visualized in layers III and V that are located closer to the wider layer IV within area 45A than in 45B (*Fig. 17*).

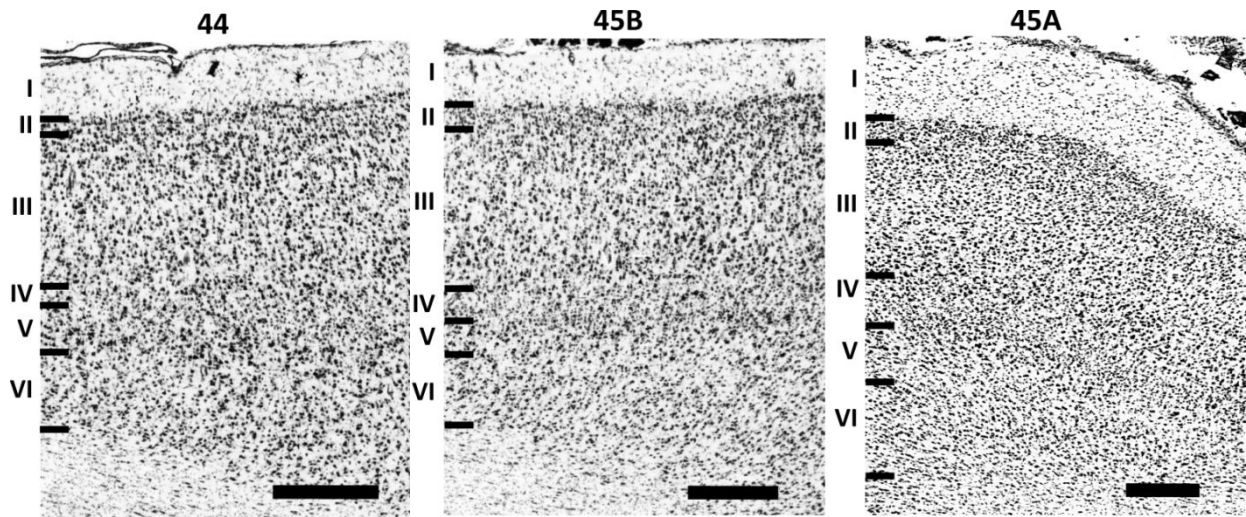


Figure 17 Visualization of the cortical layers in subdivisions of Walker's area 45, 45A (rostral), 45B (caudal); and area 44. Roman numerals indicate cortical layers. Scale bar 1 mm.

3.2.2 Motor regions

Medial and dorsal (rostral) premotor region (subdivision of areas F6 and F7, Fig. 18 and Fig. 19). Previous studies identified two areas, i.e., F6 and F7, in the rostral portion of the premotor cortex (Matelli *et al.*, 1985, 1991). Agranular premotor area F7 is characterized by the subdivision of layer VI into the pale, cell-sparse VI_a and the cell-dense, darkly stained VI_b sublaminae. This area was divided into three subareas according to differences in layer VI. Area F7d is located on the dorsal aspect of the hemisphere and abuts area F6, found on its medial aspect, and rostrally neighboring area 8B. Lateral to F7d is intermediate area F7i, occupying the rest of the dorsal surface above *sas*, and ventral area F7s that encompasses the middle part of the dorsal bank within the *sas*. Areas F7d and F7i have an evidently sublaminated layer VI, which is not clearly visible in F7s. Sublamina VI_a is much wider in F7d than in F7i. Subarea F7s can also be distinguished from the other two areas by its more prominent layer II. Area F6 does not have a sublaminated layer VI, which has an overall low cell body density in contrast to superficial layers, including the larger pyramids in layer V. Caudally neighboring area F3 can be distinguished from area F6 by the prominent pyramids in layer V due to lower cell-packing density in layer III unlike F6 (Fig. 18). New subdivisions of area F7 were also confirmed by observer-independent analysis, as presented in Fig. 19.

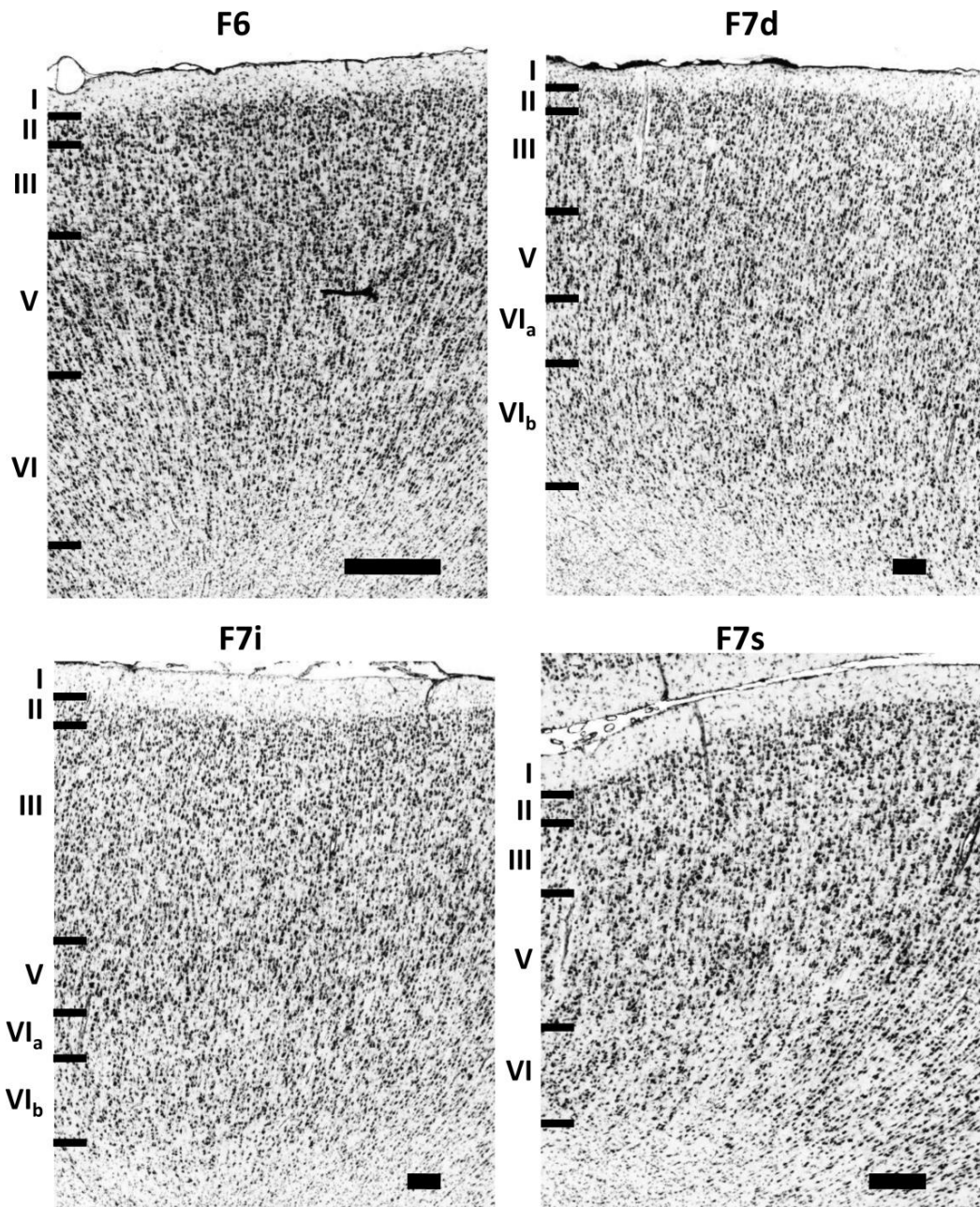


Figure 18 Visualization of the cortical layers in subdivisions of area F6 and F7 (Matelli *et al.*, 1985, 1991), F7d (dorsal), F7i (intermediate), F7s (sulcal). Roman numerals indicate cortical layers. Scale bar 1 mm.

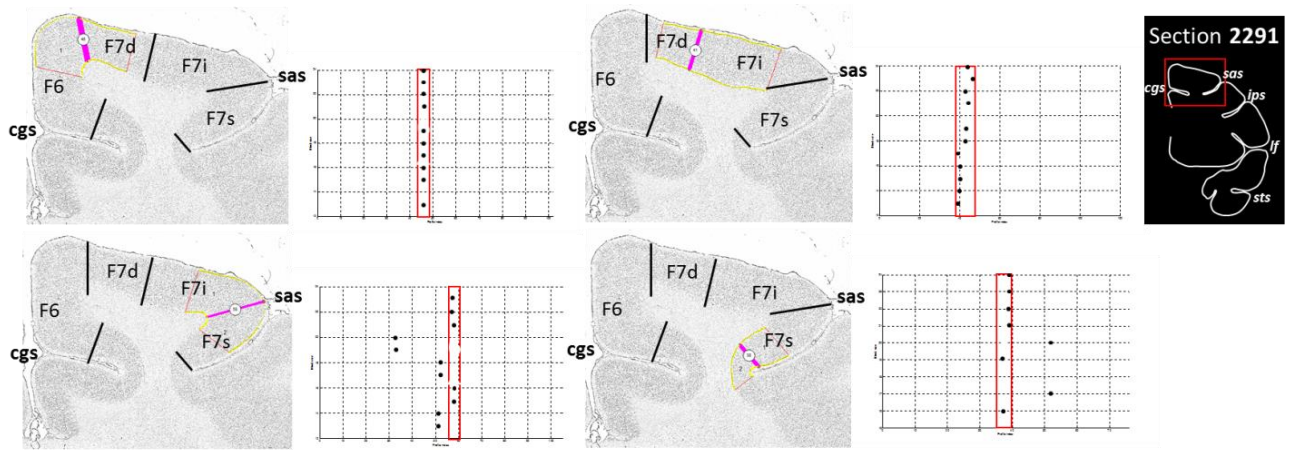


Figure 19 Positions of significant maxima in the Mahalanobis distance functions (abscissa) plotted against blocksize b (ordinate). The location of the significant maxima does not depend on the blocksize, but remains stable over large block size intervals and confirms the cytoarchitectonic subdivisions of area F7 (Matelli *et al.*, 1985, 1991), F7d (dorsal), F7i (intermediate), F7s (sulcal). *cgs* – cingulate sulcus; *spcd* – superior precentral dimple, *sas* – superior arcuate branch.

Medial and dorsal (caudal) premotor region (subdivision of areas F3 and F2, Fig. 20). Area F3 is located on the medial side of the hemisphere, caudal to area F6, and subdivisions of area F2 are found on the dorsal surface, caudal to F7 (Matelli *et al.*, 1985, 1991). Latest parcellation maps show distinct subareas recognized in area F2 (Matelli *et al.*, 1998; Rizzolatti and Luppino, 2001). This was also confirmed in the present analysis. The superior precentral dimple (*spcd*) constitutes the border between F2d and F2v, which extends ventrally to the fundus of the arcuate sulcus. Area F3 is characterized by the medium- to small-sized pyramids in layer III and the small-sized pyramidal cells in layer VI, which makes layer V more prominent with various scattered larger cells than in neighboring areas rostrally and caudally, F6 and 4m respectively. Pyramidal cells in layer III of area F2d are comparable in size to those of F3. However, in F2d layer V is thinner and with some bigger aggregate cells than in F3. Layer V of F2d is more prominent than that of F2v. In F2v pyramids are scattered in layer V, which has similar cell body-packing density to that of the other layers, making this subarea to appear less laminar than F2d. The difference between these two subdivisions within F2 can be recognized by the wider layer II in F2v than in F2d (Fig. 20).

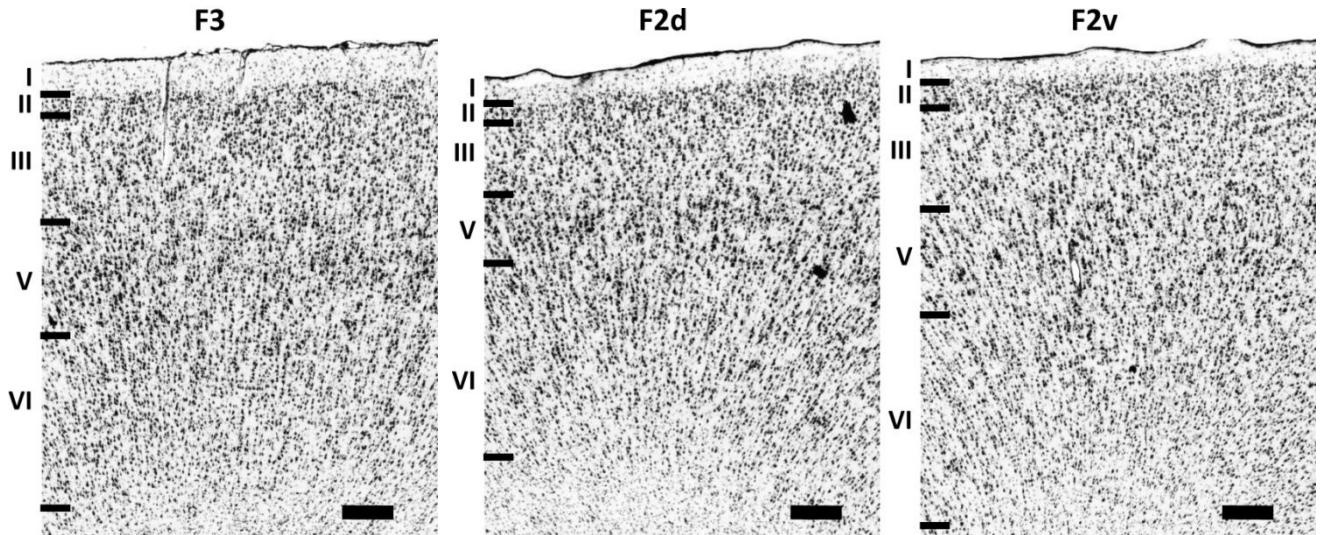


Figure 20 Visualization of the cortical layers in subdivisions of area F3 and F2 (Matelli *et al.*, 1985, 1991), F2d (dorsal), F2v (ventral). Roman numerals indicate cortical layers. Scale bar 1 mm.

Ventral (rostral) premotor region (subdivisions of area F5; *Fig. 21* and *Fig. 22*).

Although former study identified three areas within the ventral rostral premotor area (Belmalih *et al.*, 2008) as well, we were able to confirm only two previous subdivisions, i.e. areas F5a and F5c (Belmalih *et al.*, 2008), which correspond to the location of areas F5s and F5d, respectively, identified in the present study. Additionally, a ventral subdivision was identified on the postarcuate convexity, area F5v. Area F5s is located along the ventral wall of the *ias*, and is abutted ventro-rostrally by F5d, which is located on the dorso-caudal portion of the lateral convexity below the *ias*. Area F5s has a prominent layer V_a with a high cell packing density and scattered medium-sized pyramids in layer V_b which is much thinner than in the lateral subdivisions F5d and F5v. There is no distinct border between layers V and VI, but layers II and III can be clearly distinguished from each other. The main difference with neighboring area 44 on the ventral wall of the inferior branch of the arcuate sulcus is the lack of inner granular layer IV in F5s. Laterally neighboring area F5d is characterized by darkly stained small-sized pyramids with horizontal organization pattern in the lower part of layer III, and prominent medium-sized pyramids in layer V. As mentioned, both subareas F5d and F5v have subdivisions of layer V, but in F5v border between V_b and VI is clearer than in F5d. Moreover, F5v lacks horizontal organization in the lower part of the layer III (*Fig. 21*). This new subdivision of area F5 is also confirmed by observer-independent analysis, as presented in the *Fig. 22*.

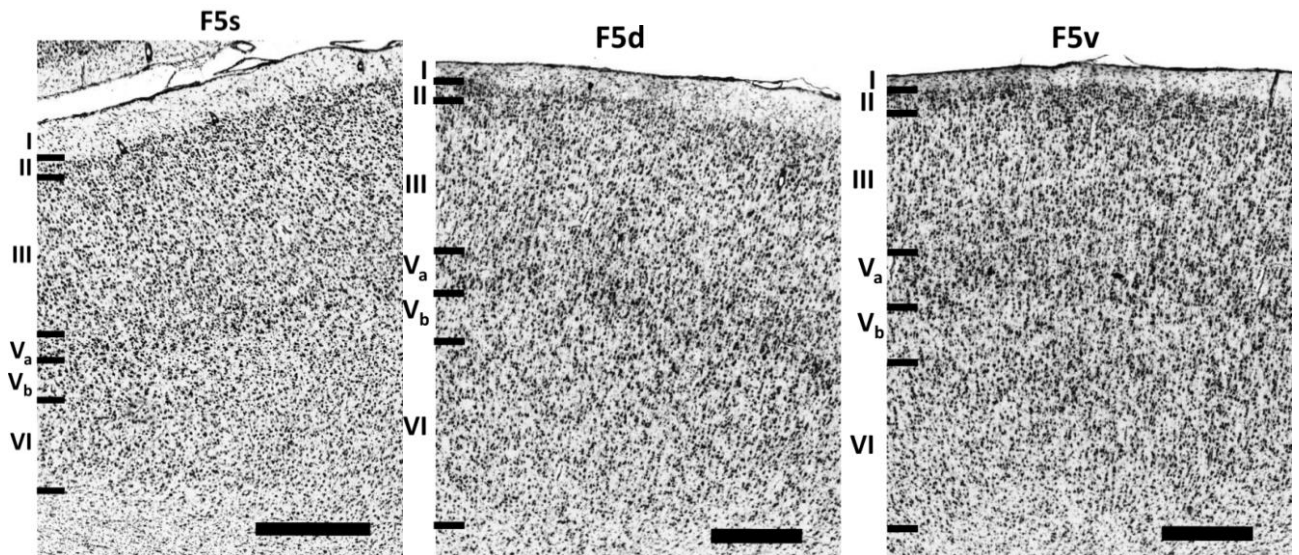


Figure 21 Visualization of the cortical layers in subdivisions of area F5 (Matelli *et al.*, 1985, 1991), F5s (sulcal), F5d (dorsal), F5v (ventral). Roman numerals indicate cortical layers. Scale bar 1 mm.

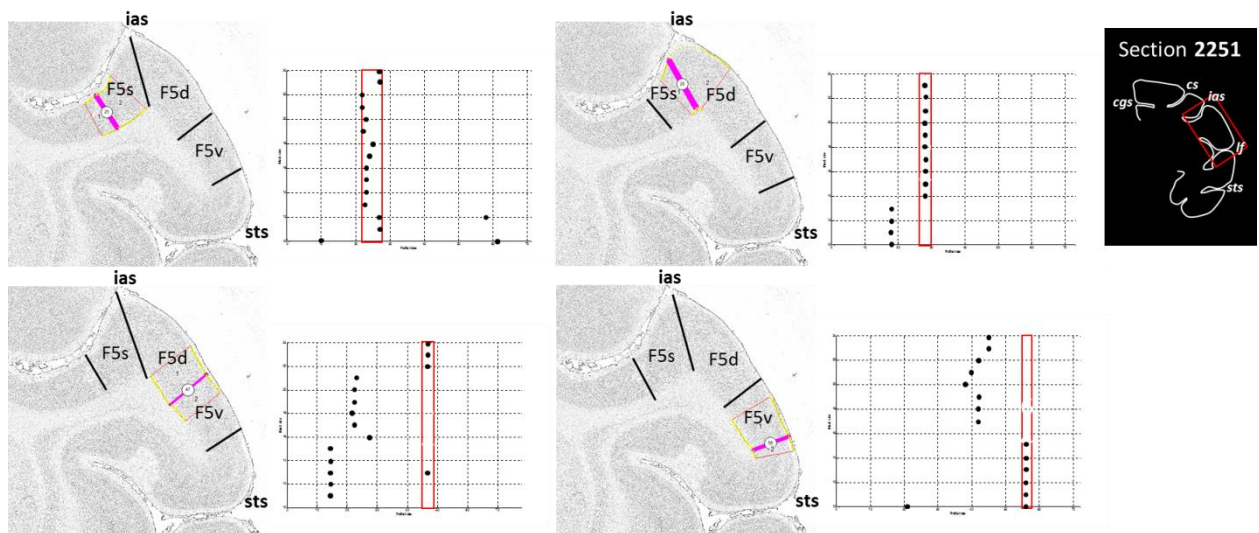


Figure 22 Positions of significant maxima in the Mahalanobis distance functions (abscissa) plotted against blocksize b (ordinate). The location of the significant maxima does not depend on the blocksize, but remains stable over large block size intervals and confirms the cytoarchitectonic subdivisions of area F5 (Matelli *et al.*, 1985, 1991), F5s (sulcal), F5d (dorsal), F5v (ventral). *cgs* – cingulate sulcus, *sas* – superior arcuate branch, *ias* – inferior arcuate branch, *lf* – lateral fissure, *sts* – superior temporal sulcus.

Ventral (caudal) premotor region (subdivision of area F4; Fig. 23). In previous maps (Matelli *et al.*, 1998; Rizzolatti and Luppino, 2001), caudal ventral premotor area F4 has been presented as a homogeneous region. However, in the present study three distinct subareas could be defined: F4s (sulcal), F4d (dorsal) and F4v (ventral) (Fig. 23). Unlike F5, this area does not have sublaminated layer V nor huge Betz cells. Area F4s occupies the

ventral wall of the arcuate sulcus caudal to areas 44 and F5s, and is characterized by a higher cell body-packing density in the upper part of the layer III, at the border with layer II, compared to the lower part, closer to the layer V. Furthermore, a horizontal organization of cells in layer VI is visible. Laterally neighboring on the dorsal portion of the lateral convexity is area F4d. This subarea has smaller cells over all layers than in F4s, with various large pyramids scattered in layer V. Unlike F4s and F4v, F4d has a more vertical cell organization in layer VI. F4v, unlike F4d, does not have large pyramids in layer V and, therefore, borders between layers are less clear, with exception for well recognizable layer II that is not so prominent in F4d.

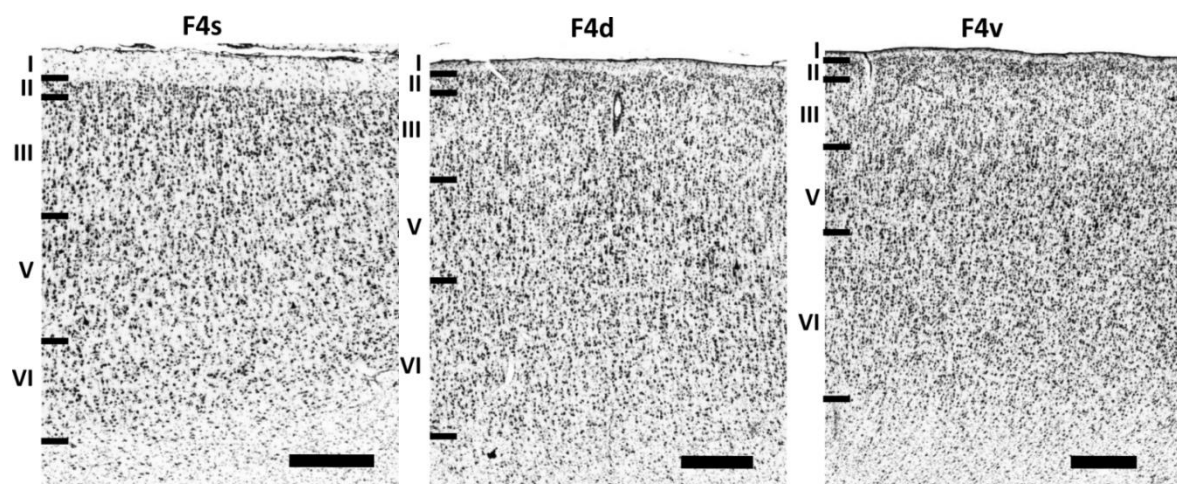


Figure 23 Visualization of the cortical layers in subdivisions of area F4 (Matelli *et al.*, 1985, 1991), F4s (sulcal), F4d (dorsal), F4v (ventral). Roman numerals indicate cortical layers. Scale bar 1 mm.

Medial and dorsal primary motor region (subdivisions of Brodmann's area 4; Fig. 24 and Fig. 25). Three areas were defined within the primary motor cortex: 4m (medial), 4d (dorsal) and 4s (sulcal). The main difference between motor cortical area 4 and rostrally adjacent premotor areas is the presence of the unusually large pyramidal cells (known as Betz cells; Betz, 1874) in sublayer V_b of all subdivisions of area 4. Area 4m is found on the medial aspect of the hemisphere, whereas 4d and 4s are found on its lateral aspect. Area 4s is located mainly within the *cs*, though it encroaches onto the surface of the hemisphere, where it is followed rostrally by area 4d. Area 4m is recognizable by the vertical cell organization in layer V_b. In comparison to the adjoining area 4d, pyramids in V_a are smaller in 4m, thus the border between layers III and V is not clear as in 4d. Moreover, 4m has wider layers I and V than 4d. Area 4d has the clearest lamination of all subareas 4, especially in comparison to the 4s. Area 4s occupies the rostro-dorsal wall of the *cs*, and the

border with caudally neighboring area 3a is located in the sulcus fundus. Within this part, only darkly stained layer II and the Betz cells in layer V_b can be clearly recognized (*Fig. 24*). Subdivisions of area 4 were confirmed by observer-independent analysis, as presented in the *Fig. 25*.

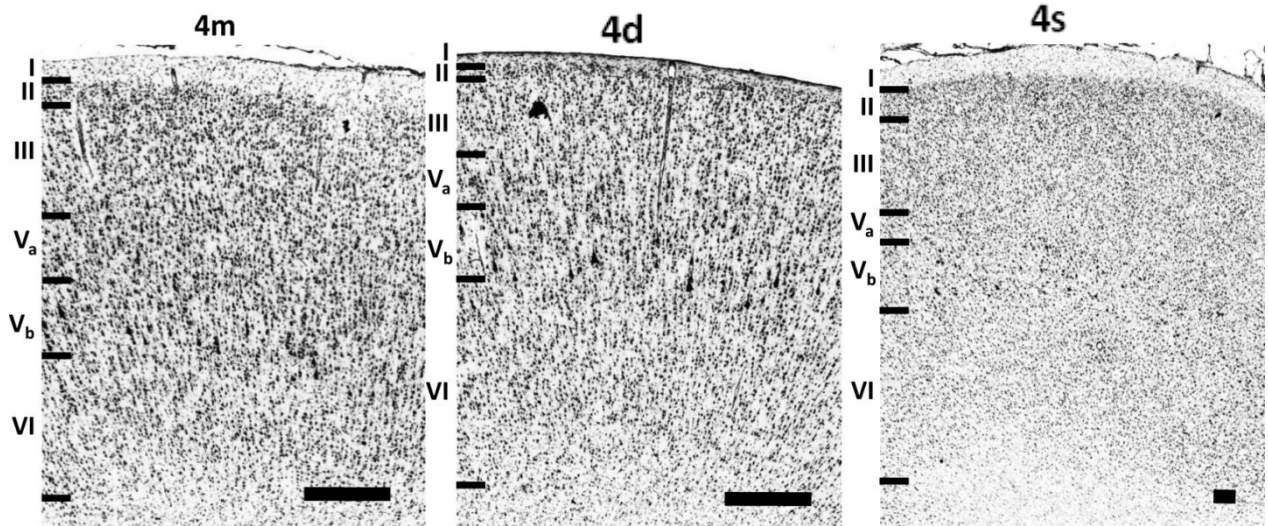


Figure 24 Visualization of the cortical layers in subdivisions of area 4 (Brodman, 1909), 4m (medial), 4d (dorsal), 4s (sulcal). Roman numerals indicate cortical layers. Scale bar 1 mm.

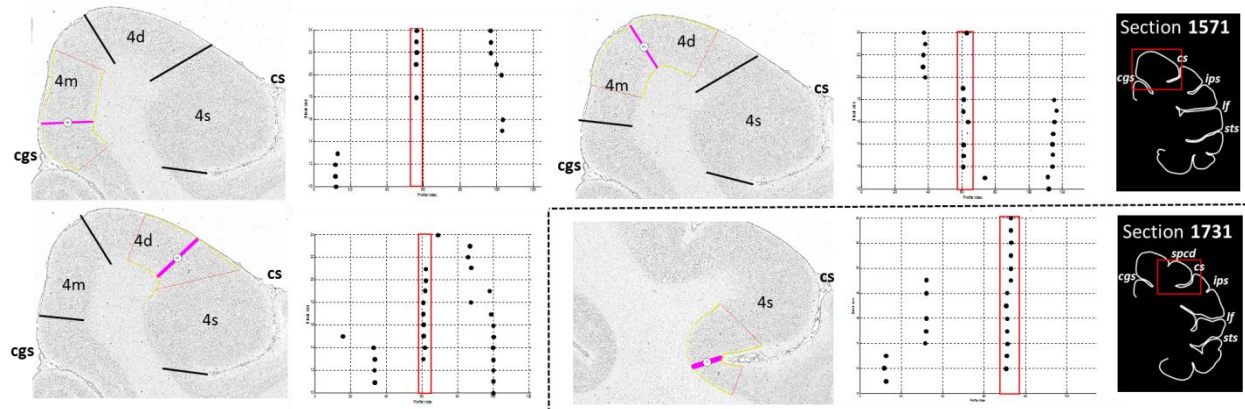


Figure 25 Positions of significant maxima in the Mahalanobis distance functions (abscissa) plotted against blocksize b (ordinate). The location of the significant maxima does not depend on the blocksize, but remains stable over large block size intervals and confirms the cytoarchitectonic subdivisions of area 4 (Brodman, 1909), 4m (medial), 4d (dorsal), 4s (sulcal). *cgs* – cingulate sulcus, *spcd* – superior precentral dimple, *cs* – central sulcus, *ips* – inferior parietal sulcus, *lf* – lateral fissure, *sts* – superior temporal sulcus.

3.3 Receptorarchitectonic analysis

The regional and laminar distribution patterns of 13 different receptor types were characterized, and their densities quantified in each cytoarchitectonically identified area (with

the exception of 13a and 14c, due to technical limitations) by means of receptor profiles extracted perpendicularly to the cortical surface. Although not all receptors show each areal border, and not all borders are equally clearly defined by all receptor types, if a border was detected by, at least, five (or sometimes by all) receptor types, this happened at the same position for all of these receptors at a given rostro-caudal level. Furthermore, the position of this border is reproducible in neighboring rostro-caudal levels. Regional and laminar differences in receptor densities confirmed cytoarchitectonically identified areas.

In general terms, most receptors are present at higher densities in the superficial than in the deeper areas, with maxima in layers I-II for 5HT_{1A} or II-IV for AMPA, NMDA, GABA_A, GABA_B, GABA_{A/BZ}, M₁, M₃, α_1 and α_2 . The opposite holds true for kainate receptors. Highest 5HT₂ receptor densities are reached in layer III. The distribution of the α_1 and the 5HT_{1A} receptors is of particular note because of their bimodal distribution: α_1 receptors present a local minimum in layers I-III and second lower maxima in layer V, whereas 5HT_{1A} receptors show extremely high densities in layers I-II and a second (lower) maximum in layers V-VI. Thus, each receptor, with the notable exception of the M₂ receptor, presented a distinct laminar distribution pattern, which remained constant throughout all examined areas. The M₂ receptor presents highest densities in layers III and V, separated by a local minimum in layer IV in all subdivisions of areas 10, 9, 46, F5, and of orbitofrontal areas, as well as in 8Ad, 8Av, 45A, 44, F4v. In areas 8m, 8Bd, 8Bs, F6, F3, F4d, as well as in subdivisions of F7 and F2, the M₂ receptors reach an absolute maximum in layer III, followed by a second, though lower one in layer V. Finally, subdivisions of the primary motor cortex are characterized by highest M₂ receptor densities in layer III.

3.3.1 Prefrontal regions

Fronto-polar region (subdivision of Walker's area 10, *Fig. 26* and *Fig. 27, Tab. 3*). The laminar distribution pattern of the examined receptors within the fronto-polar region, including the receptor fingerprint of four different subareas identified in the area 10, is shown in *Fig. 26*. Changes in laminar pattern of GABA_B, GABA_{A/BZ}, 5HT_{1A} and M₂ highlight the most clear cytoarchitectonic borders within area 10. Additional differences in the laminar distribution pattern are visible in M₁, kainate and α_1 between dorsal, 10md, and ventral, 10mv, subdivisions of the most rostro-medial part of the prefrontal cortex. Absolute receptor concentration (*Tab. 3*) measures show a higher level of AMPA, NMDA, GABA_A, GABA_B,

5HT_{1A} and M₃ receptors in ventral areas 10mv and 10o than in the dorsal areas 10md and 10d, which have a slightly higher concentration of α_1 receptors regarding ventral parts. In the dorsal areas, concentrations of the AMPA, NMDA, GABA_A, GABA_B, GABA_{A/BZ}, M₂, 5HT_{1A} and 5-HT₂ receptors are higher in

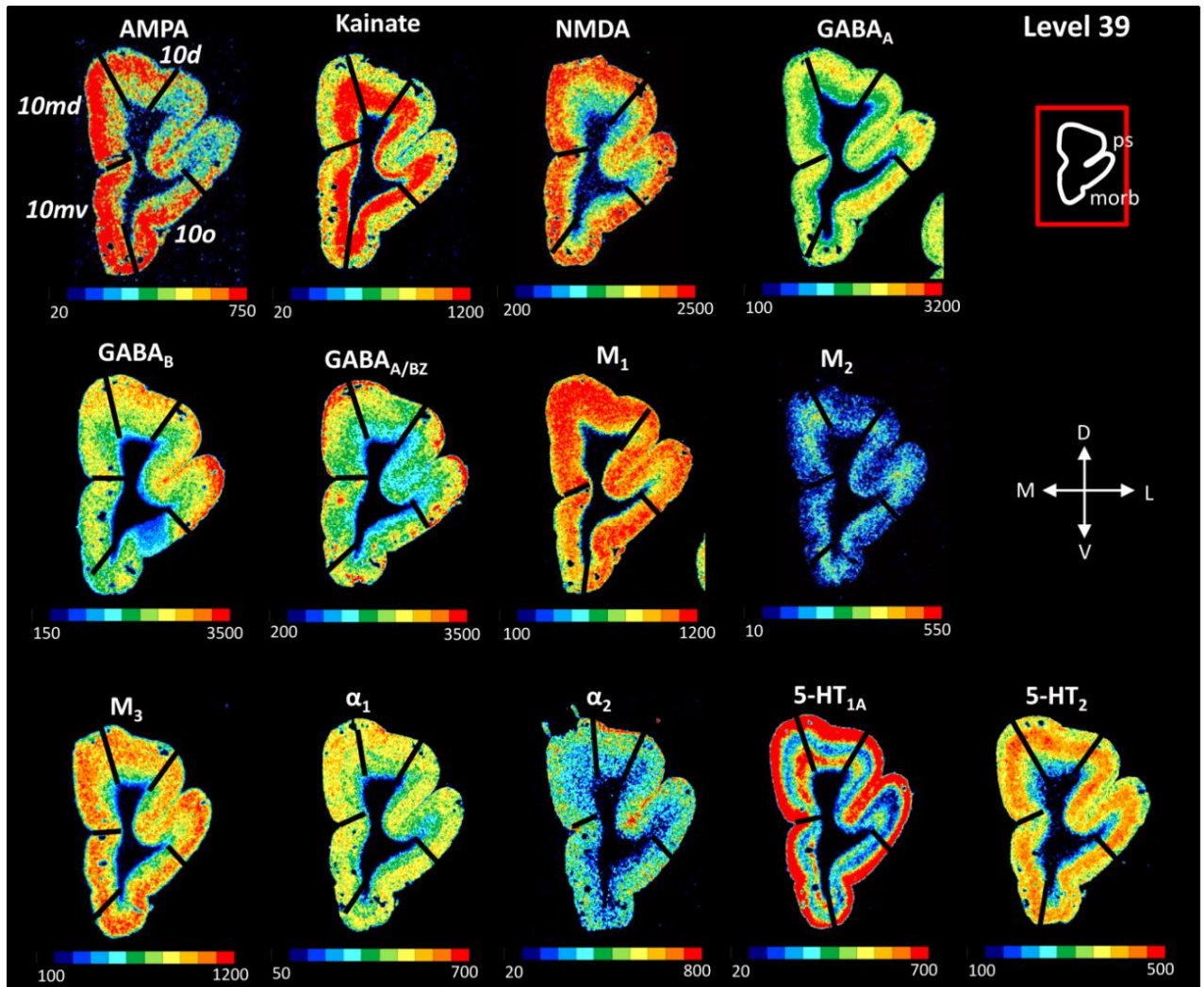


Figure 26 Regional and laminar receptor distribution patterns of the subdivisions of Walker's area 10. Scale bars code for receptor densities in fmol/mg protein.

10md than in 10d. Only the kainate, M₁ and M₃ receptors show a trend toward higher concentrations in 10d than in 10md. In the ventral areas, absolute concentrations of AMPA, NMDA, GABA_B, GABA_{A/BZ} and 5HT_{1A} are higher for area 10mv than 10o. Whereas all other receptor concentrations were higher in 10o than in 10mv, with the biggest difference in M₁ receptor concentration. The fingerprints of dorsal (10d and 10md) and ventral (10mv and 10o) subdivisions are visualized separately. Although differences between compared areas do not show significant difference in size, there are slight distinctions in shape of fingerprints,

especially for dorsal areas that have the most difference in NMDA and GABA_B receptors (*Fig. 27*). Kainate, M₂ and α_2 receptors do not reveal significant cytoarchitectonic borders within frontopolar area 10.

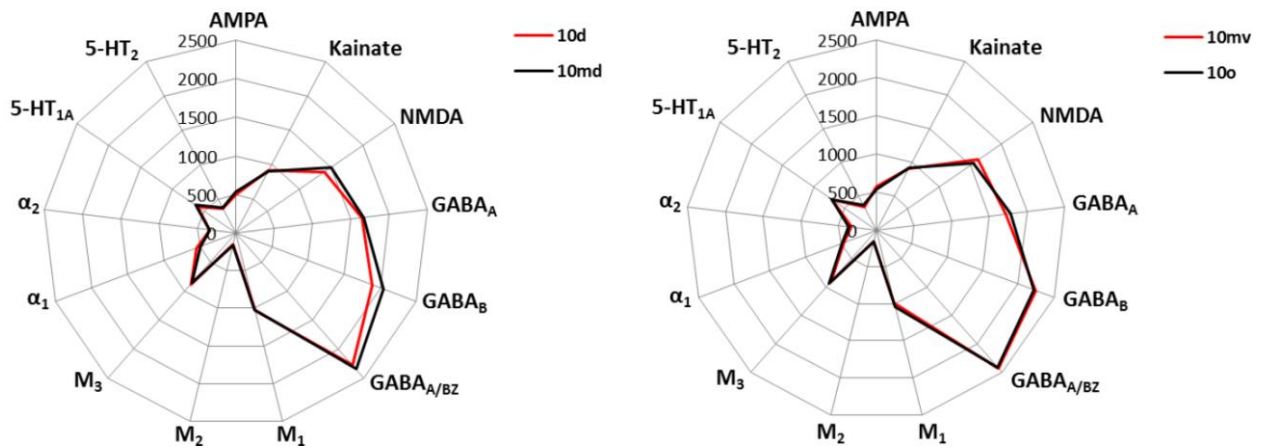


Figure 27 Receptor fingerprints of the subdivisions of Walker's area 10. Axis in polar coordinate plots code for receptor densities in fmol/mg protein.

Table 3 Absolute receptor concentrations (fmol/mg protein) measured in subareas of area 10; s.d. (standard deviation).

Area	AMPA	Kainate	NMDA	GABA _A	GABA _B	GABA _{A/BZ}	M ₁	M ₂	M ₃	α_1	α_2	5-HT _{1A}	5-HT ₂
10d	501	918	1396	1648	1888	2279	1038	146	887	547	339	600	363
s.d.	12	43	368	185	395	1169	378	51	117	91	55	144	83
10md	529	905	1495	1666	2039	2347	1026	159	862	492	341	635	372
s.d.	57	51	129	80	447	953	338	47	104	55	41	137	55
10mv	567	913	1626	1720	2243	2427	991	151	902	459	336	714	337
s.d.	126	48	166	165	598	979	403	41	80	125	46	247	72
10o	536	918	1545	1782	2222	2408	1040	158	943	483	366	707	367
s.d.	98	35	48	58	635	934	404	47	85	90	42	216	56

Orbitofrontal region (subdivision of Walker's areas 14, 11 and 13, *Fig. 28*, *Fig. 29* and *Fig. 30*, *Tab. 4*). The best delineation of rostral orbital areas 11m, 11l, 13b, and 14r is presented by the difference in laminar distribution patterns of GABA_A, GABA_B, 5HT_{1A}, kainate, M₁ and M₃ receptors (*Fig. 28*). Whereas for the caudal orbital areas 13m and 13l, laminar distribution of kainate, GABA_A, α_1 , M₂, M₃ and 5HT_{1A} receptors most clearly reveals cytoarchitectonic borders (*Fig. 29*). 11l showed higher concentration levels for AMPA, NMDA and especially for GABA receptors (GABA_A, GABA_B and GABA_{A/BZ}) in regard to the adjacent area 11m. These differences can be noted as well by the comparison of their receptor fingerprints (*Fig. 30*). It is interesting to remark that similar concentration levels in 11m and 11l were recorded for M₂ and serotonin receptors, 5HT_{1A} and 5HT₂. On the other

hand, the best difference between neighboring 11m and 13b was revealed by higher concentration levels of AMPA, NMDA, GABA_A, GABA_B, GABA_{A/BZ}, M₁ and M₃ recorded in 11m opposite to 13b. However, level of M₂ receptor in 13b is similar to values recorded for subareas 11. Although most receptors showed lower concentration levels in 14r, i.e. AMPA, NMDA, GABA_A, GABA_{A/BZ}, M₂, M₃ and α_1 , than in all other orbital areas, only for GABA_B receptors levels were higher in 14r than surrounding areas. Dysgranular areas 13 have the highest levels of AMPA, M₂ and α_2 in regard to all other orbital areas. The most significant difference between 13m and 13l was recorded for NMDA, GABA_B, GABA_A and GABA_{A/BZ}, whose concentration levels were higher in 13l. On the other hand, kainate and M₃ receptors were higher in 13m than in 13l (*Tab. 4*). Same distinction in the concentration levels between 13m and 13l is revealed by comparison of their fingerprints as they differ in size more than the shape. Furthermore, fingerprints of neighboring areas 13b and 14r were compared. They differ in both traits, i.e. shape and size, confirming previous defined distinction between these areas (*Fig. 30*).

Ventrolateral (rostral) region (subdivision of Walker's area 12; *Fig. 28, Fig. 29 and Fig. 31, Tab. 5*). Rostral ventro-lateral areas 12m and 12r are best delineated by the difference in laminar distribution patterns of GABA_A, GABA_B, 5HT_{1A}, kainate, M₁ and M₃ receptors (*Fig. 28*), whereas laminar distribution pattern of kainate, GABA_A, α_1 , M₂, M₃ and 5HT_{1A} receptors best identify cytoarchitectonic borders of the caudal subareas 12o and 12l of the ventro-lateral cortex (*Fig. 29*). Parcellation is visible in other receptor distributions too, but not so clear. However, changes in the absolute concentration levels, represented in *Tab. 5*, reveal more detailed differences in this region. Rostral areas 12r and 12m have higher concentration levels

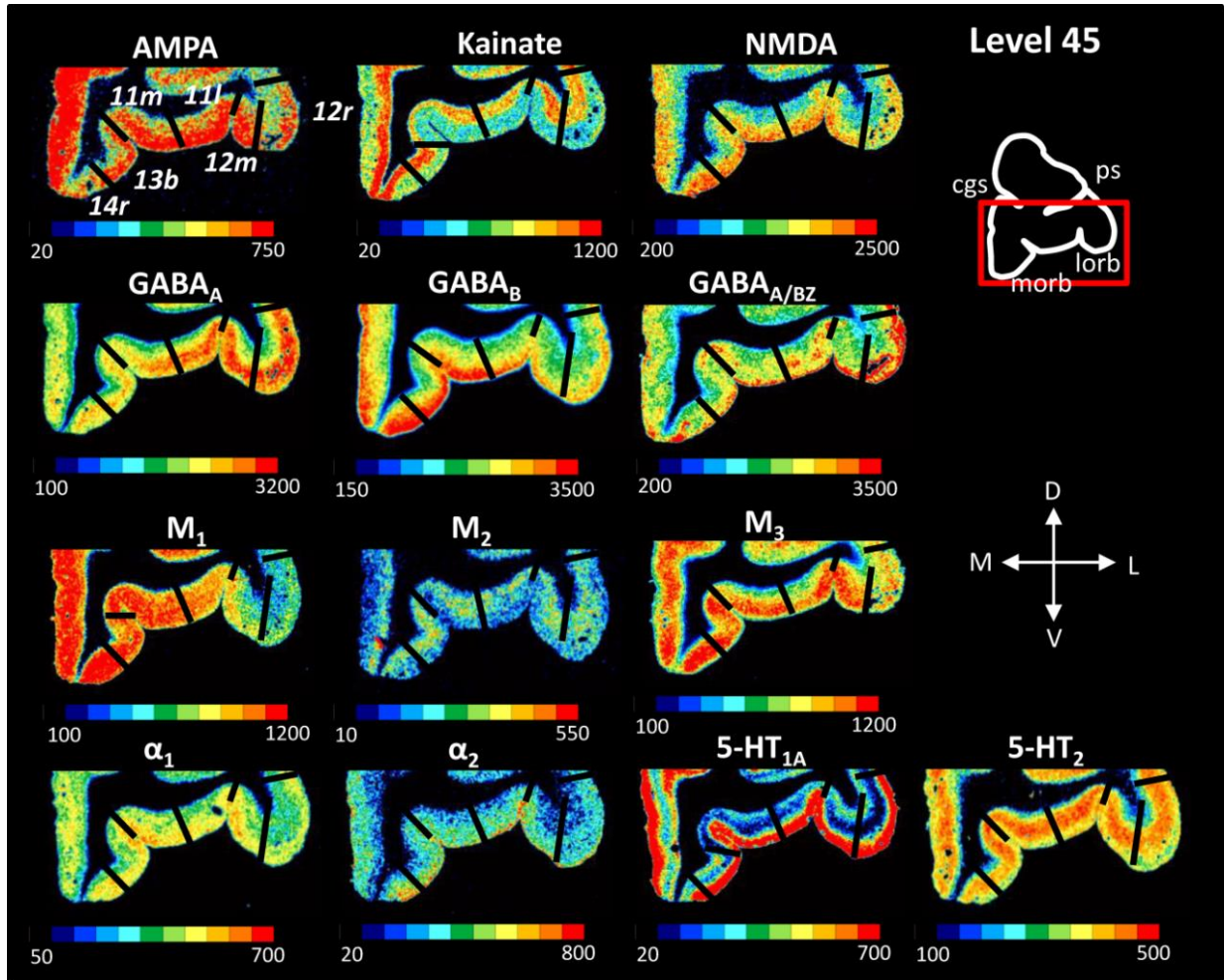


Figure 28 Regional and laminar receptor distribution patterns of the subdivisions of Walker's area 11, 11m (medial), 11l (lateral); Walker's area 14, 14r (rostral); Walker's area 13, 13b (rostral); Walker's area 12, 12r (rostral), 12m (medial). Scale bars code for receptor densities in fmol/mg protein.

measured for GABA_A, M₁ and M₃ than in 12o and 12l. However caudal areas have higher levels for AMPA and 5HT_{1A} receptors compared to rostral subdivisions. Thus, rostral areas have distinct shape of the receptor fingerprint from caudal ones (*Fig. 31*). For most receptor types concentration levels were higher in 12m than in 12r, especially significant were values for NMDA receptor levels. In 12r concentration levels were higher for kainate, GABA_A, GABA_B, GABA_{A/BZ} and 5HT_{1A} than in 12l, and these differences are reflected in the sizes of the receptor fingerprints. The absolute receptor concentration values were compared between 12l and 12o as well. The values were higher for almost all receptor types in 12o than in 12l, with exception in slightly higher concentration levels for kainate and α_1 in 12l. Receptor fingerprints showed difference in size when compared between these areas (*Fig. 31*).

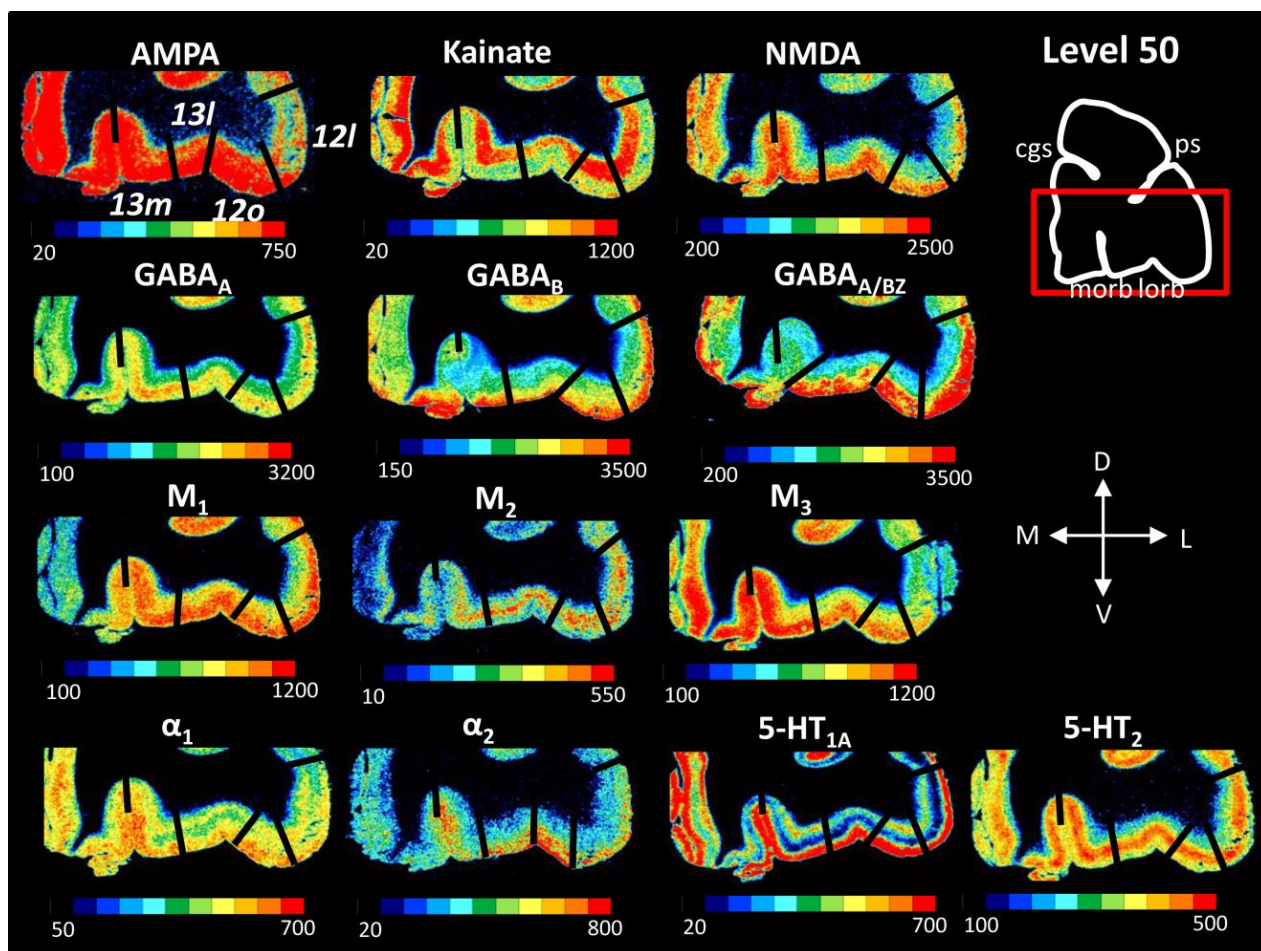


Figure 29 Regional and laminar receptor distribution patterns of the subdivisions of Walker's area 13, 13m (medial), 13l (lateral); Walker's area 12, 12o (orbital), 12l (lateral). Scale bars code for receptor densities in fmol/mg protein.

Table 4 Absolute receptor concentrations (fmol/mg protein) measured in subareas of area 11, 14 and 13; s.d. (standard deviation).

Area	AMPA	Kainate	NMDA	GABA _A	GABA _B	GABA _{A/BZ}	M ₁	M ₂	M ₃	α_1	α_2	5-HT _{1A}	5-HT ₂
11m	604	771	1630	1804	2515	2002	1074	174	997	488	349	533	374
s.d.	70	59	137	78	397	193	256	74	147	37	36	213	66
11l	625	823	1605	1945	2740	2102	1021	173	972	474	369	533	372
s.d.	79	149	85	147	518	187	288	60	65	43	32	137	56
14r	513	820	1348	1465	2523	1655	936	151	808	476	279	542	331
s.d.	192	104	380	179	224	364	460	53	102	132	121	160	24
13b	549	822	1577	1642	2379	1892	1016	178	933	483	361	565	368
s.d.	102	125	243	116	340	422	324	59	50	84	83	253	56
13m	796	952	1567	1716	1797	1713	964	287	1030	485	430	409	397
13l	764	798	1646	1831	2155	2215	929	290	910	457	424	372	385

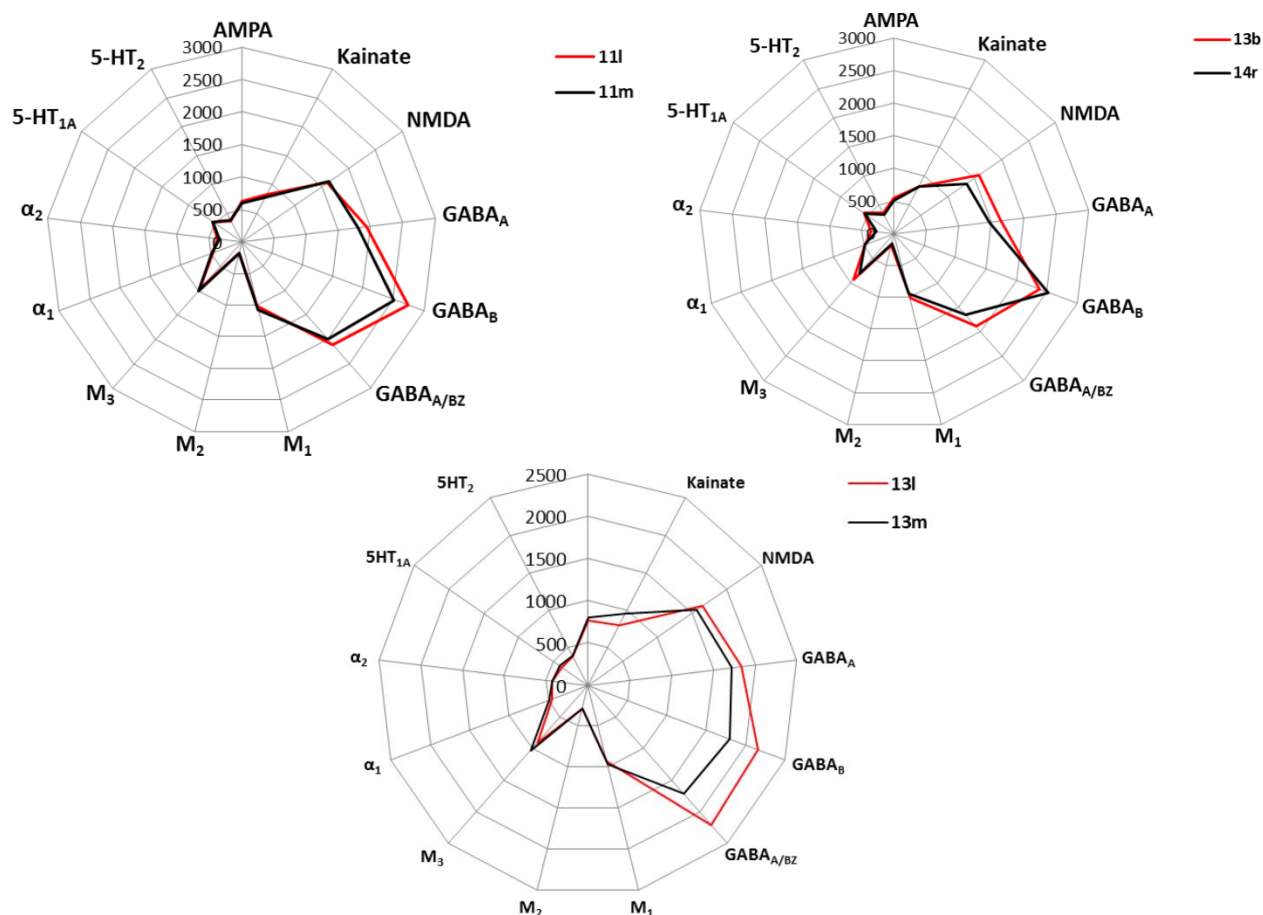


Figure 30 Receptor fingerprints of the subdivisions of Walker's areas 11, 14 and 13. Axis in polar coordinate plots code for receptor densities in fmol/mg protein.

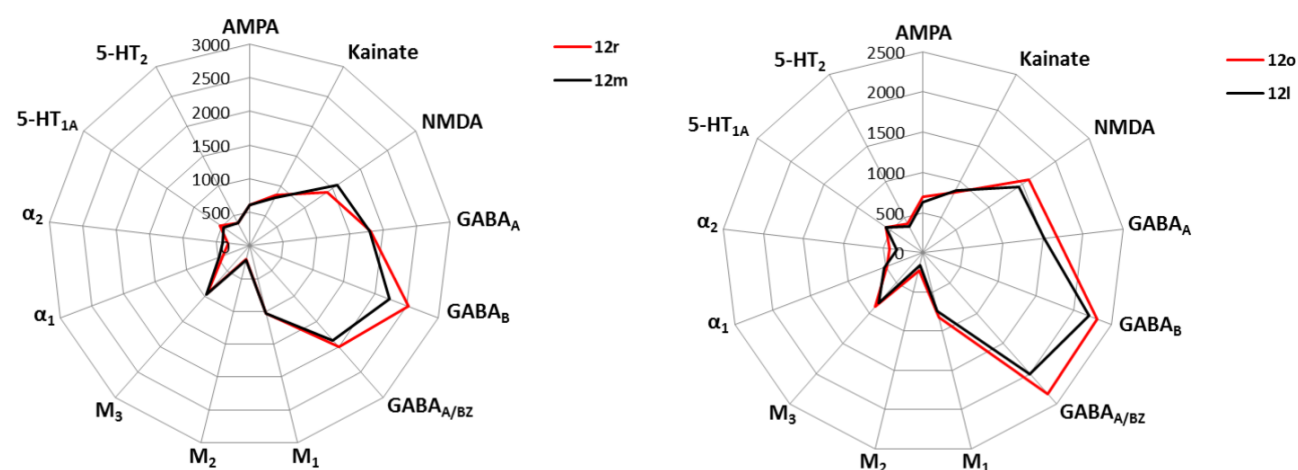


Figure 31 Receptor fingerprints of the subdivisions of Walker's area 12. Axis in polar coordinate plots code for receptor densities in fmol/mg protein.

Table 5 Absolute receptor concentrations (fmol/mg protein) measured in subareas of area 12; s.d. (standard deviation).

Area	AMPA	Kainate	NMDA	GABA _A	GABA _B	GABA _{A/BZ}	M ₁	M ₂	M ₃	α ₁	α ₂	5-HT _{1A}	5-HT ₂
12r	606	852	1409	1818	2531	2004	1028	195	948	433	319	535	380
s.d.	134	147	44	297	256	158	355	89	74	35	38	112	40
12m	614	803	1582	1794	2227	1871	1035	221	955	486	395	472	382
s.d.	72	21	148	251	182	417	305	67	37	46	46	60	44
12o	696	851	1595	1674	2311	2329	823	223	894	488	421	563	408
s.d.	194	33	76	378	88	105	88	82	36	37	32	110	41
12l	629	876	1446	1512	2199	2000	745	161	827	514	330	558	372
s.d.	118	68	19	251	142	404	432	87	54	85	40	172	47

Medial and dorsal (rostral) region (subdivision of Walker's area 9, Fig. 32 and Fig. 33, Tab. 6). Area 9 of Walker has clear subdivisions, not just cytoarchitectonically, but also by the difference in receptor laminar patterns between subareas 9d and 9m. Almost all receptors show a clear border (Fig. 32). Area 9d showed considerably higher concentrations for the NMDA, GABA_A, GABA_B, GABA_{A/BZ} M₁ and M₃, although slightly higher concentration can be

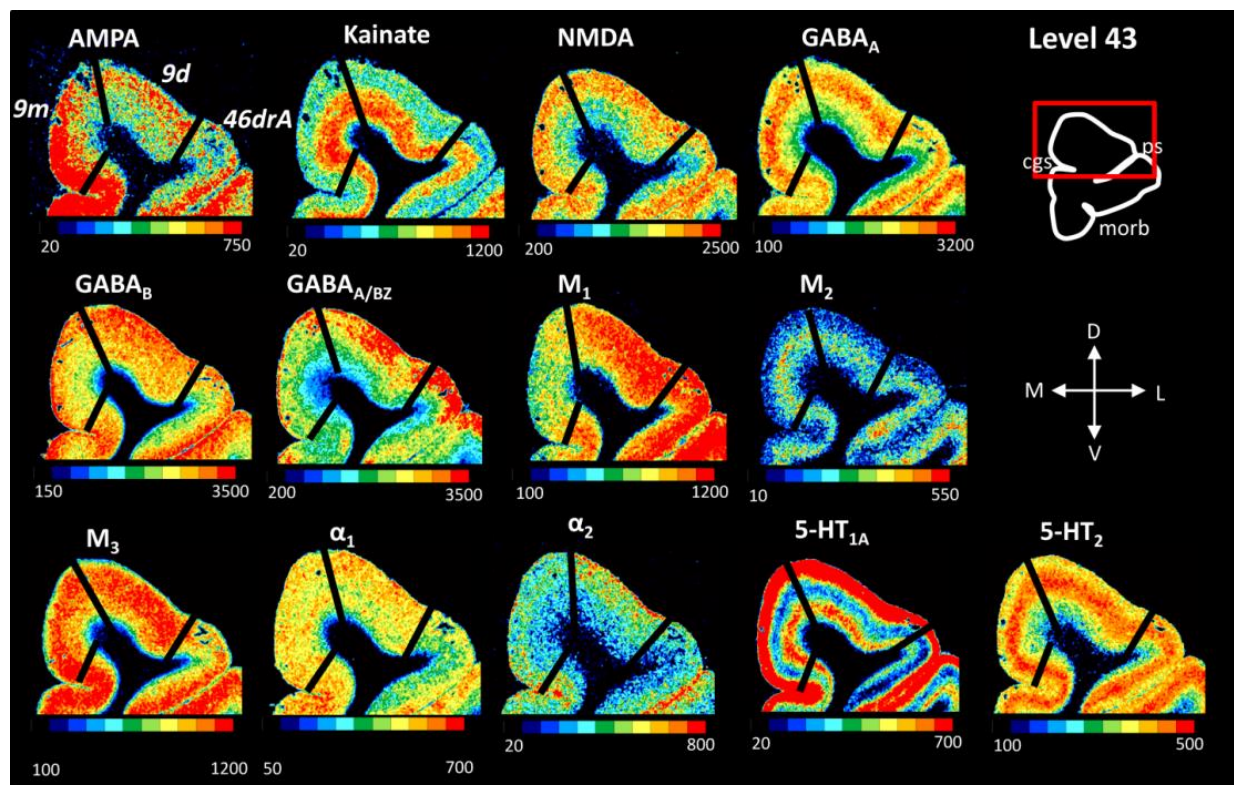


Figure 32 Regional and laminar receptor distribution patterns of the subdivisions of Walker's area 9. Scale bars code for receptor densities in fmol/mg protein.

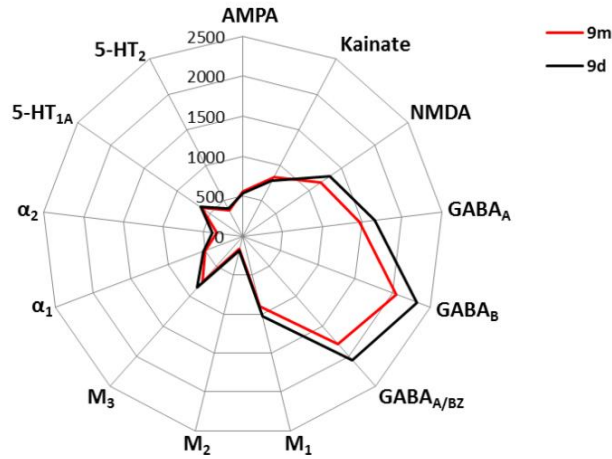


Figure 33 Receptor fingerprints of the subdivisions of Walker's area 9. Axis in polar coordinate plots code for receptor densities in fmol/mg protein.

Table 6 Absolute receptor concentrations (fmol/mg protein) measured in subareas of area 9; s.d. (standard deviation).

Area	AMPA	Kainate	NMDA	GABA _A	GABA _B	GABA _{A/BZ}	M ₁	M ₂	M ₃	α_1	α_2	5-HT _{1A}	5-HT ₂
9m	557	839	1182	1466	2051	1792	895	166	765	507	323	631	372
s.d.	60	63	274	444	221	459	287	38	29	40	30	160	52
9d	540	780	1326	1658	2323	2060	1022	180	858	529	379	644	390
s.d.	108	52	255	403	242	540	237	40	38	37	46	78	72

noticed for M₂, α_1 , α_2 , 5HT_{1A} and 5HT₂ too. On the other hand, higher concentrations are found only for AMPA and kainate receptors in area 9m (*Tab. 6*). The same trend can be recognized when comparing the shapes of the receptor fingerprints, where a difference is noted in the size but not in the shape (*Fig. 33*).

Region within the principal sulcus (subdivision of Walker's area 46; *Fig. 34, Fig. 35 and Fig. 36, Tab. 7*). Along the principal sulcus, anterior and posterior portions of Walker's area 46 were defined. The dorsal wall is occupied by areas a46dr, a46d (*Fig. 34*), p46dr and p46d (*Fig. 35*), the ventral one by areas a46vr, a46v (*Fig. 34*), p46vr and p46v (*Fig. 35*). Changes in the laminar distribution patterns of AMPA, GABA_A, GABA_B, GABA_{A/BZ}, kainate and M₃ receptors most clearly reveal delineation of subdivisions within Walker's area 46 for both, anterior and posterior subareas. Higher concentration levels were recorded for AMPA, NMDA, GABA_A and GABA_B receptors in areas closer to the fundus of *ps*, a46v/p46v and a46d/p46d, especially for the ventral part. Only kainite levels were higher

for areas extending on the free lateral surface around *ps*, a46vr/p46vr and a46dr/p46dr. When comparing anterior and posterior concentration levels, higher concentration levels were recorded for NMDA, GABA_A, M₁, M₂, M₃ and α_1 in anterior portion. All posterior subareas had higher levels only for GABA_{A/BZ} with highest concentrations measured in p46v (*Tab. 7*). Receptor fingerprints of anterior and corresponding posterior areas (*Fig. 36*) were compared to demonstrate that the most prominent differences in the shape of the receptor fingerprints are similar between areas within *ps* in regard to areas on the surface of the *ps*. However bigger differences are recognized in ventral areas, i.e. for GABA_{A/BZ}, NMDA and M₁ receptors in a46v and p46v, and kainite, NMDA, GABA_A and M₁ in a46vr and p46vr.

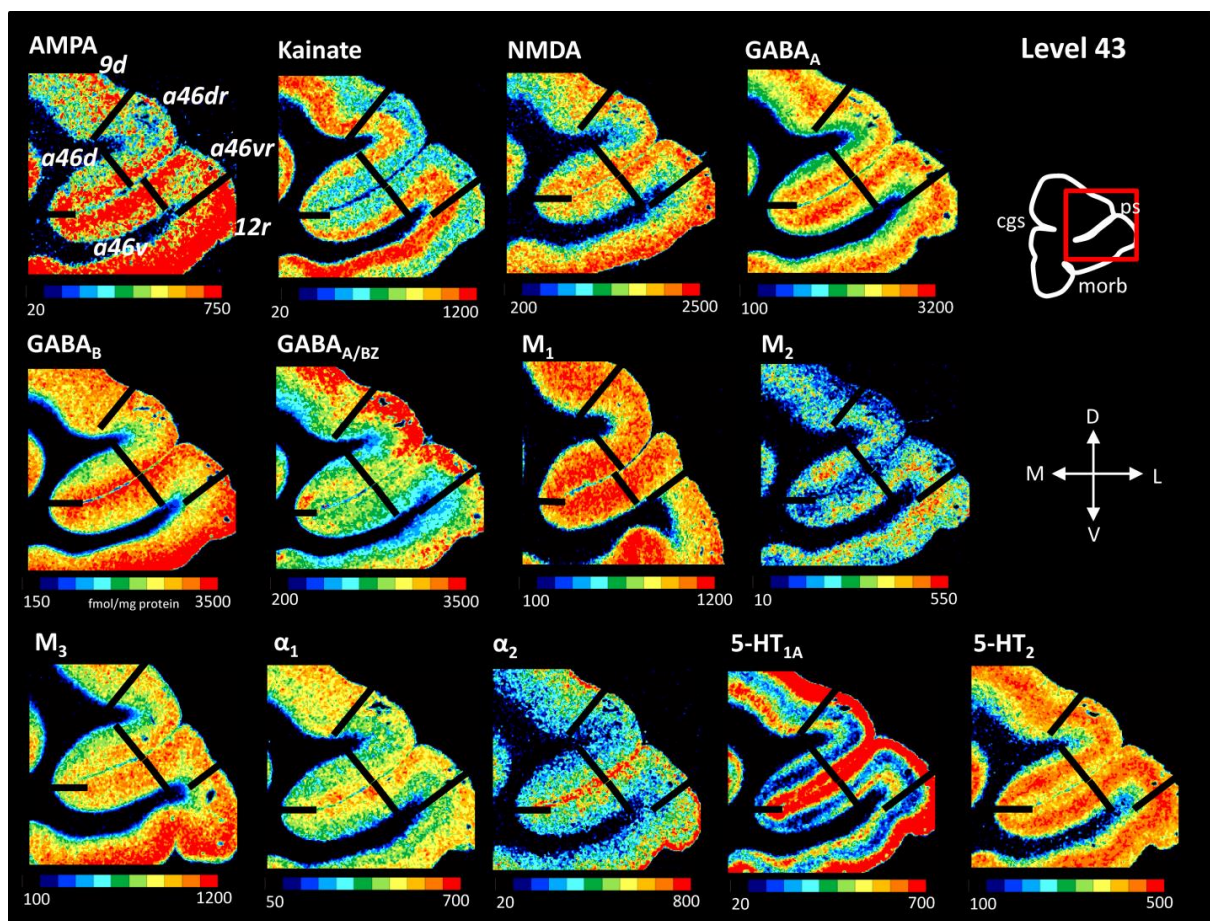


Figure 34 Regional and laminar receptor distribution patterns of the subdivisions of Walker's area 46, anterior areas. Scale bars code for receptor densities in fmol/mg protein.

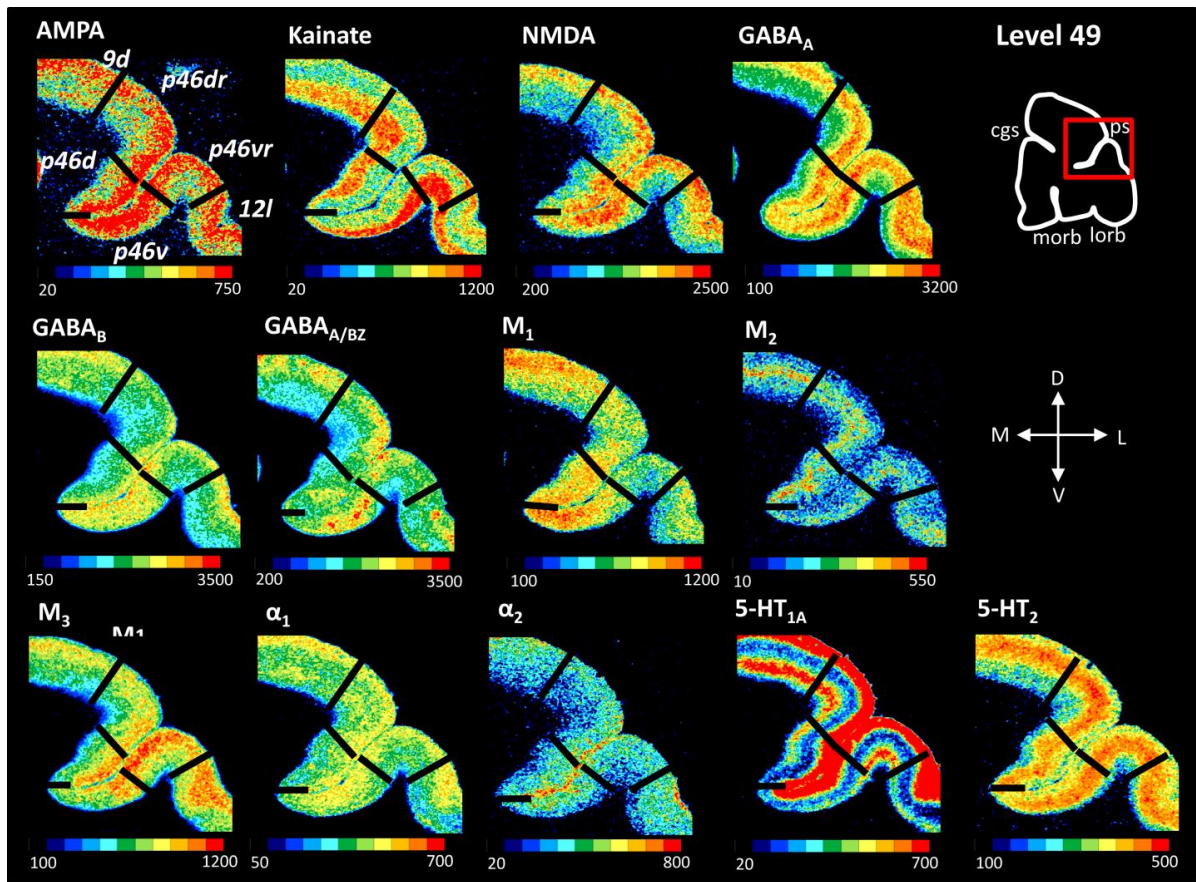


Figure 35 Regional and laminar receptor distribution patterns of the subdivisions of Walker's area 46, posterior areas. Scale bars code for receptor densities in fmol/mg protein.

Table 7 Absolute receptor concentrations (fmol/mg protein) measured in subareas of area 46; s.d. (standard deviation).

Area	AMPA	Kainate	NMDA	GABA _A	GABA _B	GABA _{A/BZ}	M ₁	M ₂	M ₃	α ₁	α ₂	5-HT _{1A}	5-HT ₂
a46dr	518	827	1228	1617	2008	1799	993	199	850	463	335	512	379
s.d.	80	88	203	265	99	401	309	33	87	82	61	105	46
p46dr	531	804	1093	1373	1947	1829	867	190	806	429	296	472	375
s.d.	56	14	336	277	94	259	303	56	80	69	15	33	28
a46d	555	673	1372	1676	2109	1774	1076	190	857	491	394	453	386
s.d.	65	38	32	260	89	444	194	46	37	37	58	117	64
p46d	568	705	1261	1651	2085	2034	1019	184	846	450	395	484	390
s.d.	79	22	288	317	113	189	368	51	16	70	36	90	30
a46v	615	685	1467	1777	2418	1826	1118	195	915	490	409	472	404
s.d.	19	87	21	339	7	407	195	47	28	37	20	98	57
p46v	583	684	1327	1745	2455	2308	970	169	884	468	404	517	395
s.d.	100	54	210	372	62	166	299	46	46	71	80	118	37
a46vr	535	813	1309	1623	2079	1859	987	192	883	430	328	482	374
s.d.	55	63	143	305	198	408	275	62	34	56	16	88	29
p46vr	514	768	1124	1375	2000	1894	625	169	815	398	322	439	367
s.d.	32	37	82	309	129	215	40	38	62	83	51	63	41

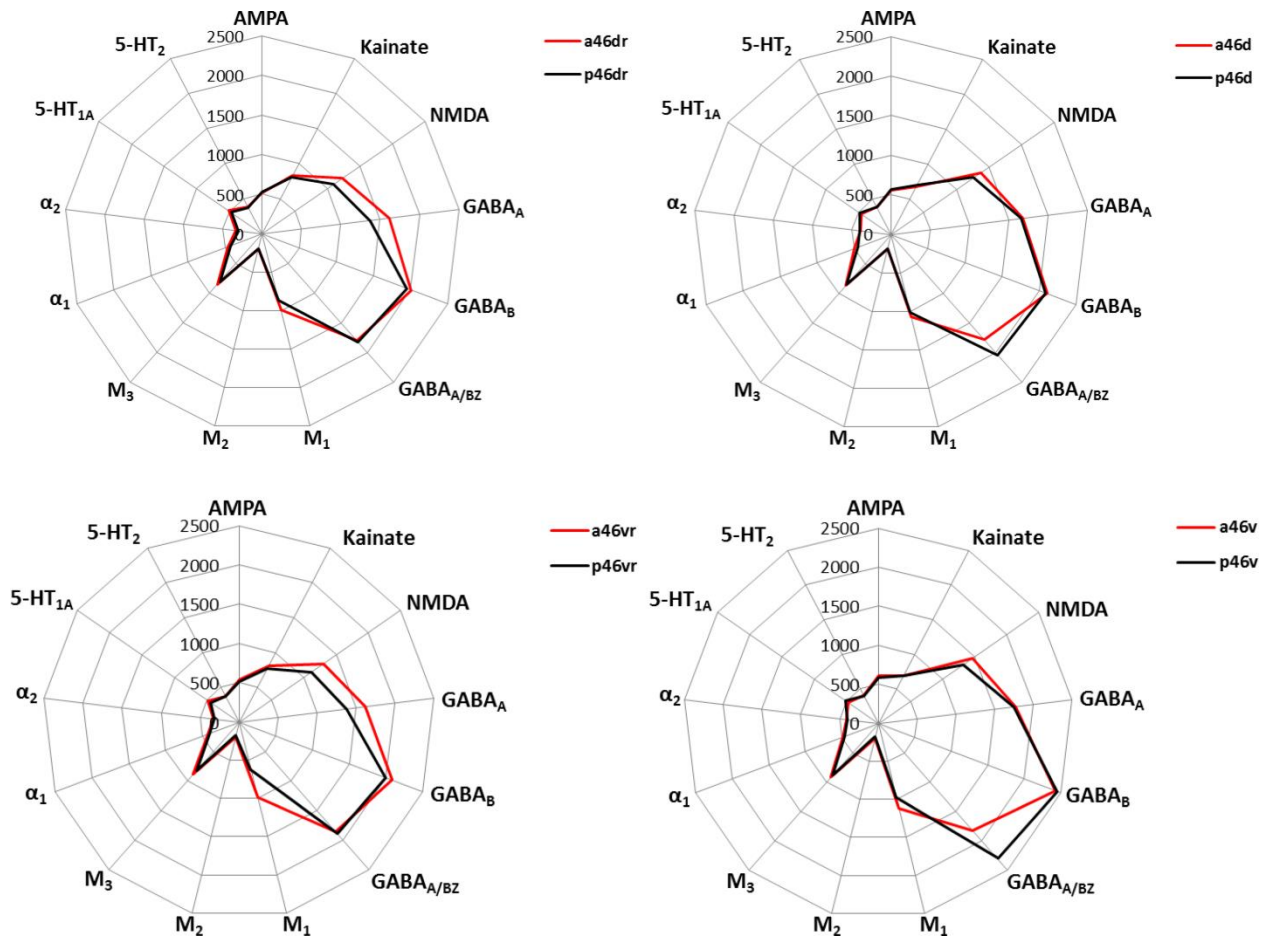


Figure 36 Receptor fingerprints of the subdivisions of Walker's area 46. Axis in polar coordinate plots code for receptor densities in fmol/mg protein.

Medial and dorsolateral (caudal) region (subdivision of Walker's areas 8B and 8A, Fig. 37 and Fig. 38, Tab. 8). Area 8B was subdivided into areas 8Bm, 8Bd and 8Bs, which were visible not only from cytoarchitectonic analysis, but also by differences in the laminar receptor distribution patterns of AMPA, kainate, M₁, M₃ and 5-HT_{1A} (Fig. 37), as well as in absolute concentration receptor levels (Tab. 8). Area 8Bd presented higher kainate, GABA_{A/BZ}, M₁, M₂ and α_1 receptor densities than did 8Bs. Both areas presented comparable 5-HT₂ receptor densities. 8Bm showed the highest concentration of AMPA and kainate receptors of all three subdivisions of area 8B and the lowest densities of GABA_A, GABA_B, GABA_{A/BZ}, M₁, M₃ and α_2 receptors. Most prominent differences in the laminar receptor pattern between subdivisions of area 8B and area 8Ad were visible for α_1 , 5-HT_{1A}, 5-HT₂, kainate and M₁ receptors. On the other hand, the laminar receptor distribution pattern of NMDA, α_1 , α_2 , GABA_B, AMPA, M₃, and 5-HT_{1A} receptors revealed clear differences between 8Av and neighboring areas, i.e., 46 dorsally and 45A ventrally. Area 8Av presented clearly lower AMPA, NMDA, GABA_B, M₁, M₂, M₃, α_1 , α_2 , 5-HT_{1A} and 5-HT₂ receptor

densities than subareas 8B or 8Ad. In 8Ad the highest concentrations were measured for NMDA and GABA_B receptors, whereas GABA_{A/BZ} densities were the lowest in this area. Subdivisions of areas 8B and 8A show slight differences in shape and size of their fingerprints (Fig. 38).

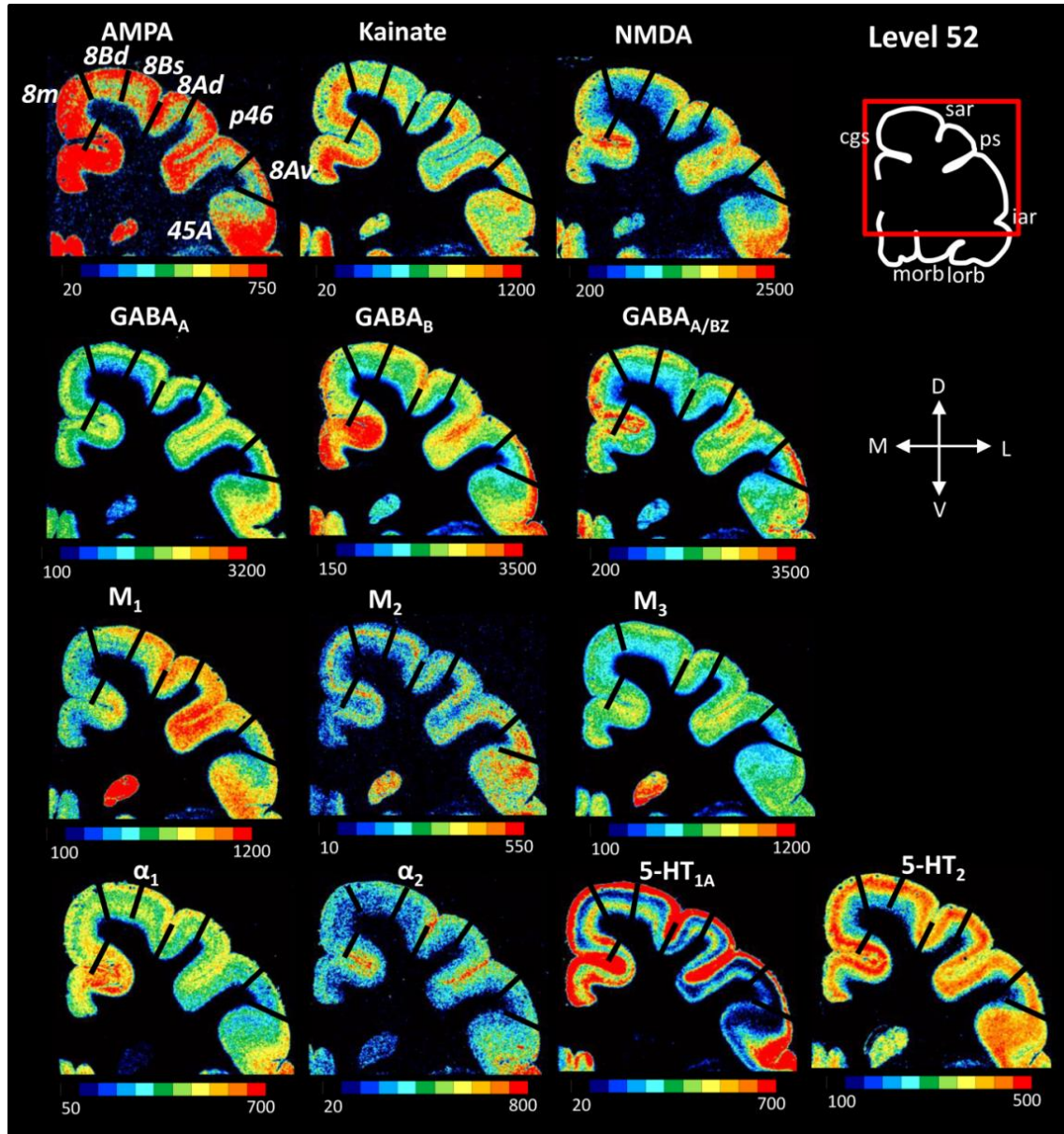


Figure 37 Regional and laminar receptor distribution patterns of the subdivisions of Walker's area 8B and 8A. Scale bars code for receptor densities in fmol/mg protein.

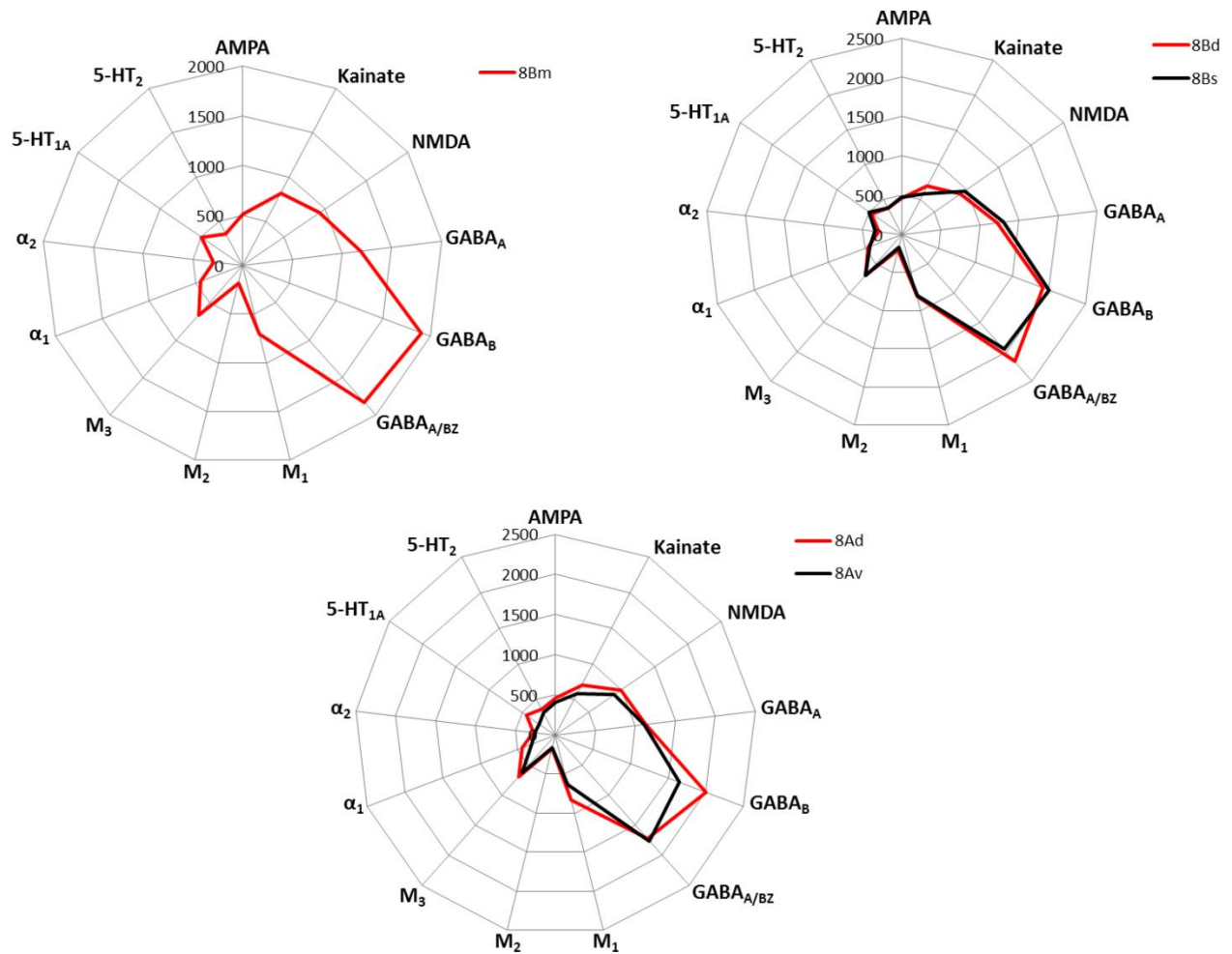


Figure 38 Receptor fingerprints of the subdivisions of Walker's area 8B and 8A. Axis in polar coordinate plots code for receptor densities in fmol/mg protein.

Table 8 Absolute receptor concentrations (fmol/mg protein) measured in subareas of area 8B and 8A; s.d. (standard deviation).

Area	AMPA	Kainate	NMDA	GABA _A	GABA _B	GABA _{A/BZ}	M ₁	M ₂	M ₃	α ₁	α ₂	5-HT _{1A}	5-HT ₂
8Bm	515	818	932	1188	1903	1824	707	179	660	451	292	496	356
s.d.	137	29	410	309	323	233	185	44	108	93	32	82	30
8Bd	455	696	904	1220	1920	2164	814	201	695	457	301	460	375
s.d.	82	42	356	154	109	285	164	52	103	86	42	73	39
8Bs	474	586	967	1297	1998	1960	806	169	704	437	336	501	374
s.d.	56	31	366	230	466	114	81	41	98	77	18	133	48
8Ad	468	710	988	1133	2004	1725	832	170	686	446	280	431	367
s.d.	56	58	295	81	91	325	270	36	181	68	17	48	41
8Av	405	588	892	1114	1644	1766	628	159	628	319	259	243	321
s.d.	66	125	66	174	251	469	258	27	240	121	67	124	82

Caudal ventrolateral region (subdivision of areas 44 and 45; *Fig. 39, Fig. 40 and Fig. 41, Tab. 9*). The cytoarchitectonic border between areas 44 and 45B can be clearly recognized by changes in the laminar distribution pattern of kainate, GABA_B, GABA_{A/BZ},

M₁, M₂, M₃, α_1 , 5-HT_{1A} and 5-HT₂ receptors (*Fig. 39*). In contrast, AMPA, NMDA, GABA_A, M₃ and α_2 receptors do not clearly reveal this border. Whereby the borders between area 45A and neighboring areas 12l and p46vr were best recognized by α_1 , AMPA, GABA_B, 5HT_{1A}, M₁ and M₃ laminar distribution patterns (*Fig. 40*). Area 44 had higher concentration levels recorded for NMDA, GABA_B, α_1 , α_2 , 5HT₂ and 5-HT_{1A} receptors in regard to areas 45A and 45B. The most prominent differences between 45A and 45B were recorded for NMDA, M₁, α_1 and 5HT_{1A} where concentration levels were higher in 45B than in 45A. Area 45A had highest levels of kainite and GABA receptors in regard to areas 44 and 45B (*Tab. 9*). *Fig. 41* demonstrates differences in the shape of the receptor fingerprints between subareas 45, where fingerprints are similar in size and partly in shape, with most prominent differences in kainate, NMDA and GABA receptors, and area 44 that has the shape of the fingerprint more similar to the 45B than 45A.

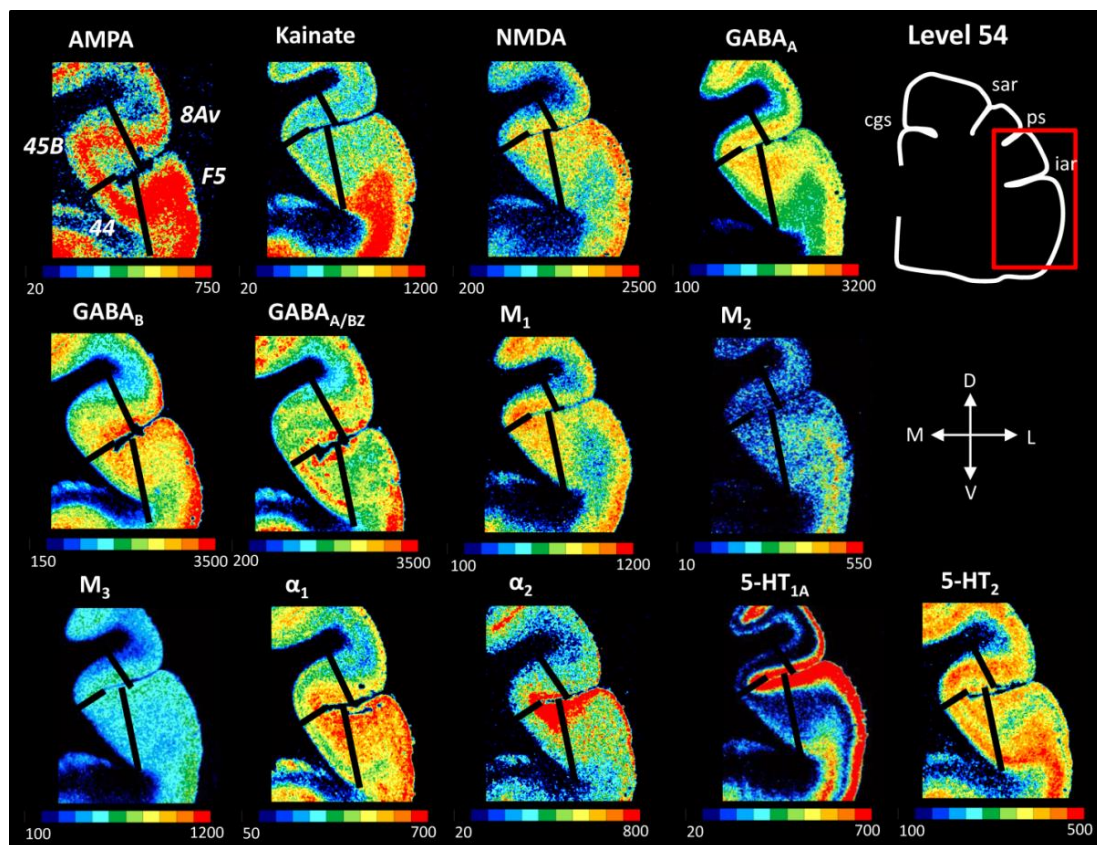


Figure 39 Regional and laminar receptor distribution patterns of the subdivisions of Walker's area 45, 45B (caudal); and area 44. Scale bars code for receptor densities in fmol/mg protein.

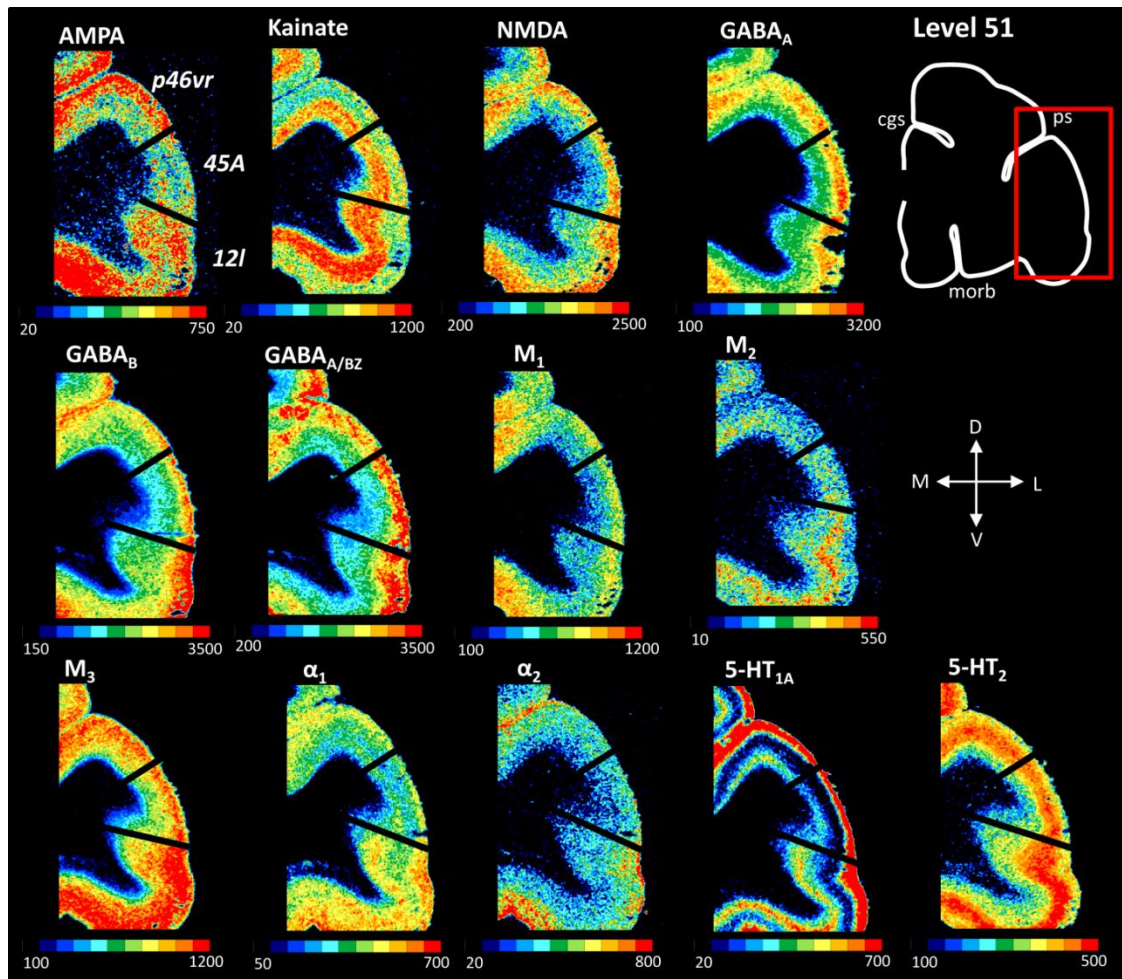


Figure 40 Regional and laminar receptor distribution patterns of the subdivisions of Walker's area 45, 45A (rostral). Scale bars code for receptor densities in fmol/mg protein.

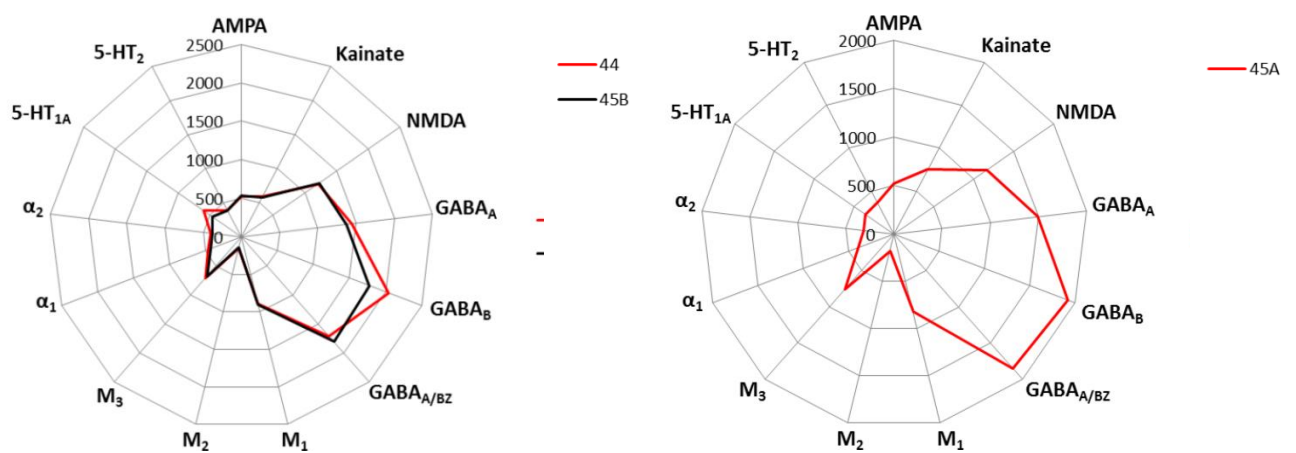


Figure 41 Receptor fingerprints of the subdivisions of Walker's area 45 and 44. Axis in polar coordinate plots code for receptor densities in fmol/mg protein.

Table 9 Absolute receptor concentrations (fmol/mg protein) measured in subareas of area 45 and 44; s.d. (standard deviation).

Area	AMPA	Kainate	NMDA	GABA _A	GABA _B	GABA _{A/BZ}	M ₁	M ₂	M ₃	α ₁	α ₂	5HT _{1A}	5HT ₂
44	530	593	1210	1443	2040	1711	890	155	707	463	401	605	394
<i>s.d.</i>	121	69	197	132	192	212	371	20	191	93	74	221	67
45A	519	752	1163	1494	1921	1851	825	176	759	397	319	356	369
<i>s.d.</i>	41	35	48	302	209	489	230	64	16	71	30	108	48
45B	543	577	1225	1369	1778	1810	902	144	682	430	376	456	388
<i>s.d.</i>	130	42	237	158	311	206	351	14	144	72	92	133	59

3.3.2 Motor regions

Medial and dorsal (rostral) premotor region (subdivision of areas F6 and F7, Fig. 42 and Fig. 43, Tab. 10). Changes in the laminar distribution patterns of kainate, α₁, GABA_A, 5HT_{1A}, AMPA, M₁ and M₃ mirror the cytoarchitectonic parcellation of dorso-rostral and medial premotor areas F7 and F6 (Fig. 42). The border between areas F7i and F7s was difficult to recognize in α₂, GABA_{A/BZ}, GABA_B, 5HT₂ and M₂ receptor autoradiographs. However, absolute receptor concentrations for AMPA, NMDA, GABA_A, GABA_B, M₁, M₃ and α₂ showed lower receptor levels in F7i than in F7s. Only for kainate were higher concentration levels measured in area F7i with regard to levels in F7s. Medial area F6 differed from both subdivisions of area F7 with regard to the AMPA, kainate, NMDA, GABA_A, GABA_B, M₁, α₁, α₂ and 5HT_{1A} receptors, whereby mentioned receptors showed higher concentration levels in F6. Area F7d had significantly higher concentration of GABA_{A/BZ} binding sites, as well as higher concentrations of M₂, M₃ and 5HT₂ receptors, in contrast to neighboring areas. Lowest concentrations were recorded in AMPA, NMDA and α₁ receptor levels for this area (Tab. 10). Comparison of receptor fingerprints shows the most significant differences for GABA_B receptor levels among areas (Fig. 43). However, the shape of the receptor fingerprint for F6 vary the most in 5HT_{1A}, kainate and NMDA levels in regard to subdivisions of area F7. F7d shows difference in GABA_{A/BZ} levels in compare to surrounding areas, whereas the most prominent difference between F7i and F7s receptor fingerprints can be recognized in NMDA, M₁ and AMPA receptor levels.

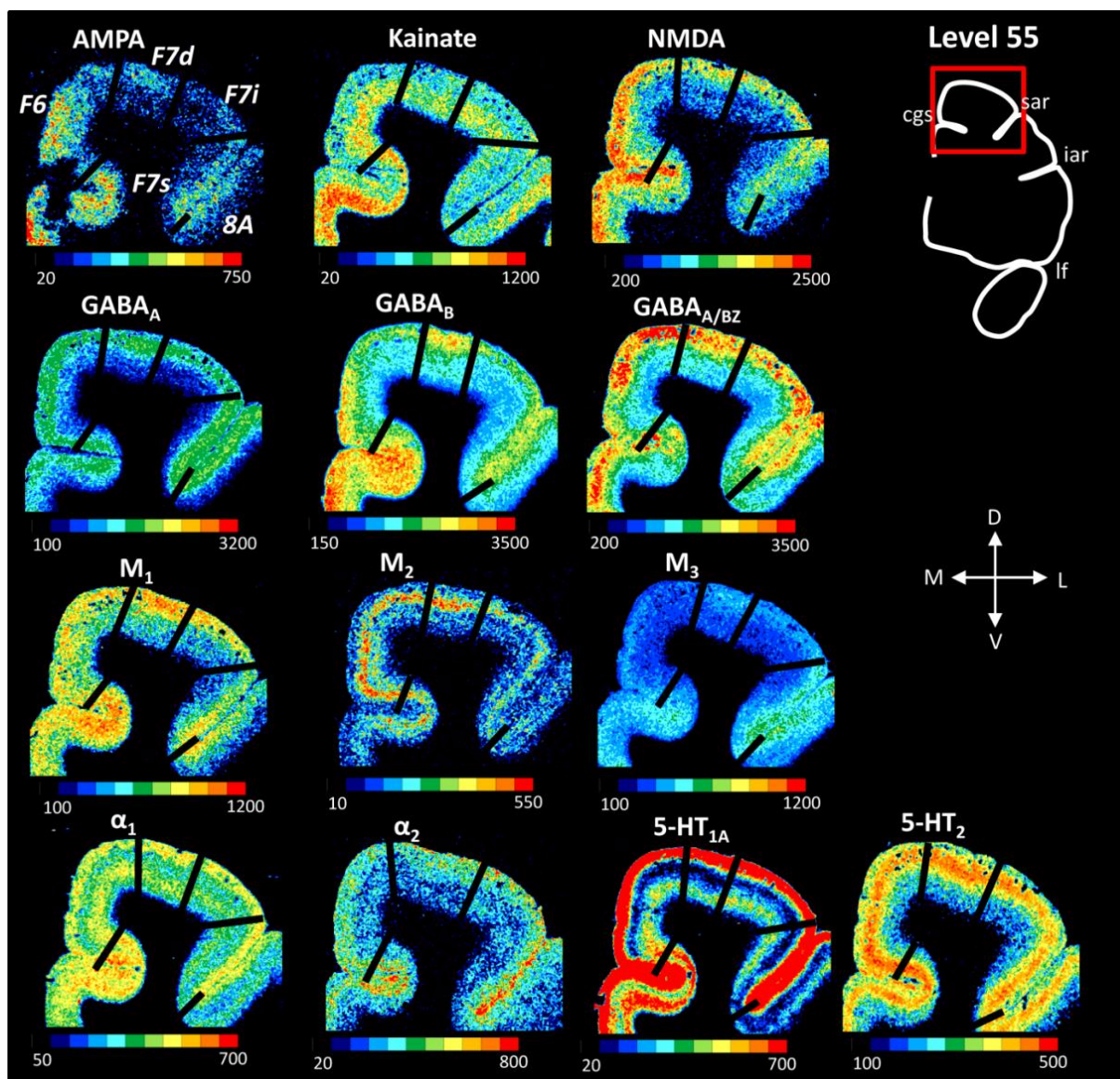


Figure 42 Regional and laminar receptor distribution patterns of the subdivisions of area F6 and F7 (Matelli *et al.*, 1985, 1991). Scale bars code for receptor densities in fmol/mg protein.

Table 10 Absolute receptor concentrations (fmol/mg protein) measured in subareas of area F6 and F7 (Matelli *et al.*, 1985, 1991); s.d. (standard deviation).

Area	AMPA	Kainate	NMDA	GABAA	GABAB	GABAA/BZ	M1	M2	M3	α_1	α_2	5-HT _{1A}	5-HT ₂
F6	440	723	966	1070	1839	1492	861	180	563	479	319	565	368
s.d.	103	79	302	128	67	173	304	44	212	86	41	134	83
F7d	338	597	723	1015	1776	1892	831	206	583	440	287	430	378
s.d.	81	94	299	141	135	241	215	44	172	76	42	60	76
F7i	341	587	743	880	1512	1475	718	160	545	421	292	410	354
s.d.	101	66	240	71	159	255	244	36	194	78	34	90	88
F7s	409	568	856	1023	1580	1470	807	165	579	422	307	425	366
s.d.	63	76	289	64	226	148	284	32	179	86	55	90	75

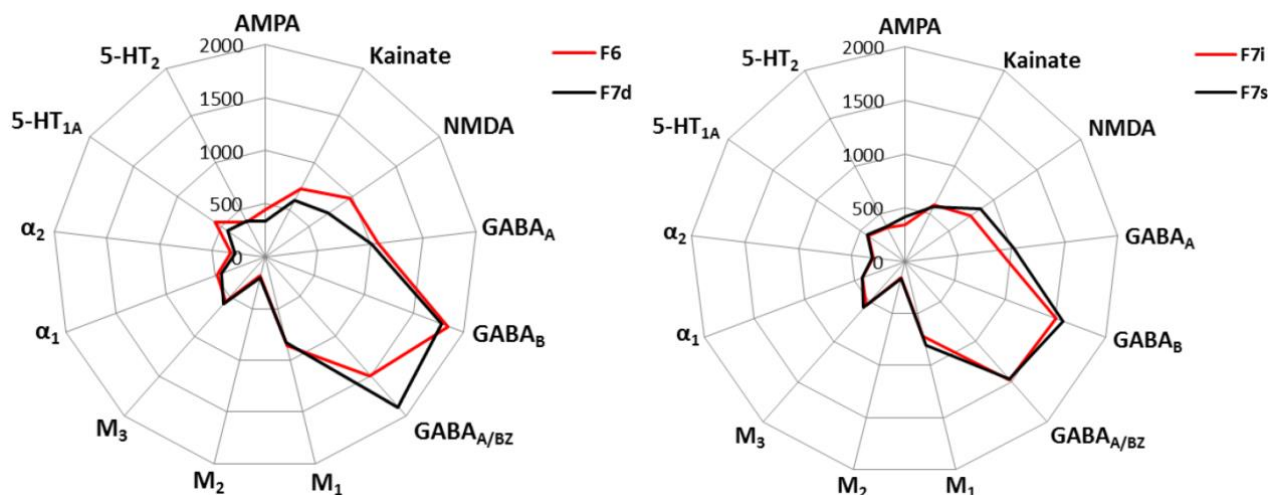


Figure 43 Receptor fingerprints of the subdivisions of area F6 and F7 (Matelli *et al.*, 1985, 1991). Axis in polar coordinate plots code for receptor densities in fmol/mg protein.

Medial and dorso-caudal) premotor region (subdivision of areas F3 and F2; Fig. 44 and Fig. 45, Tab. 11). Almost all receptor types show clear changes in their densities throughout all layers of F2d and F2v, thus clearly highlighting the border between these two areas (presented in Fig. 44). Absolute concentration levels measured (Tab. 11) in F2v were considerably lower than those of F2d for 11 different receptor types, i.e. AMPA, kainate, NMDA, GABA_B, GABA_{A/BZ}, M₁, M₂, M₃, α_1 , α_2 and 5-HT_{1A}. Conversely, differences between F2d and F3 are mainly restricted to the GABA_A, GABA_B, GABA_{A/BZ}, and M₁, receptors, which were higher in F2d, as well as the NMDA receptors with higher densities in F3. Receptor fingerprints showed (Fig. 45) similarity in shape for F3 and F2d, but slight difference in the size. However, F2v had highly distinct fingerprint in shape and size in regard to F2d and F3.

Table 11 Absolute receptor concentrations (fmol/mg protein) measured in subareas of area F3 and F2 (Matelli *et al.*, 1985, 1991); s.d. (standard deviation).

Area	AMPA	Kainate	NMDA	GABA _A	GABA _B	GABA _{A/BZ}	M ₁	M ₂	M ₃	α_1	α_2	5-HT _{1A}	5-HT ₂
F3	377	709	896	885	1749	1554	815	188	564	489	333	566	342
s.d.	140	42	307	340	100	256	265	35	152	68	43	71	63
F2d	368	671	825	934	1910	1804	877	177	583	512	362	606	362
s.d.	51	81	195	252	78	67	217	44	144	58	43	88	75
F2v	345	575	673	920	1442	1429	808	171	534	448	284	393	352
s.d.	44	51	154	203	44	130	221	30	122	70	50	60	87

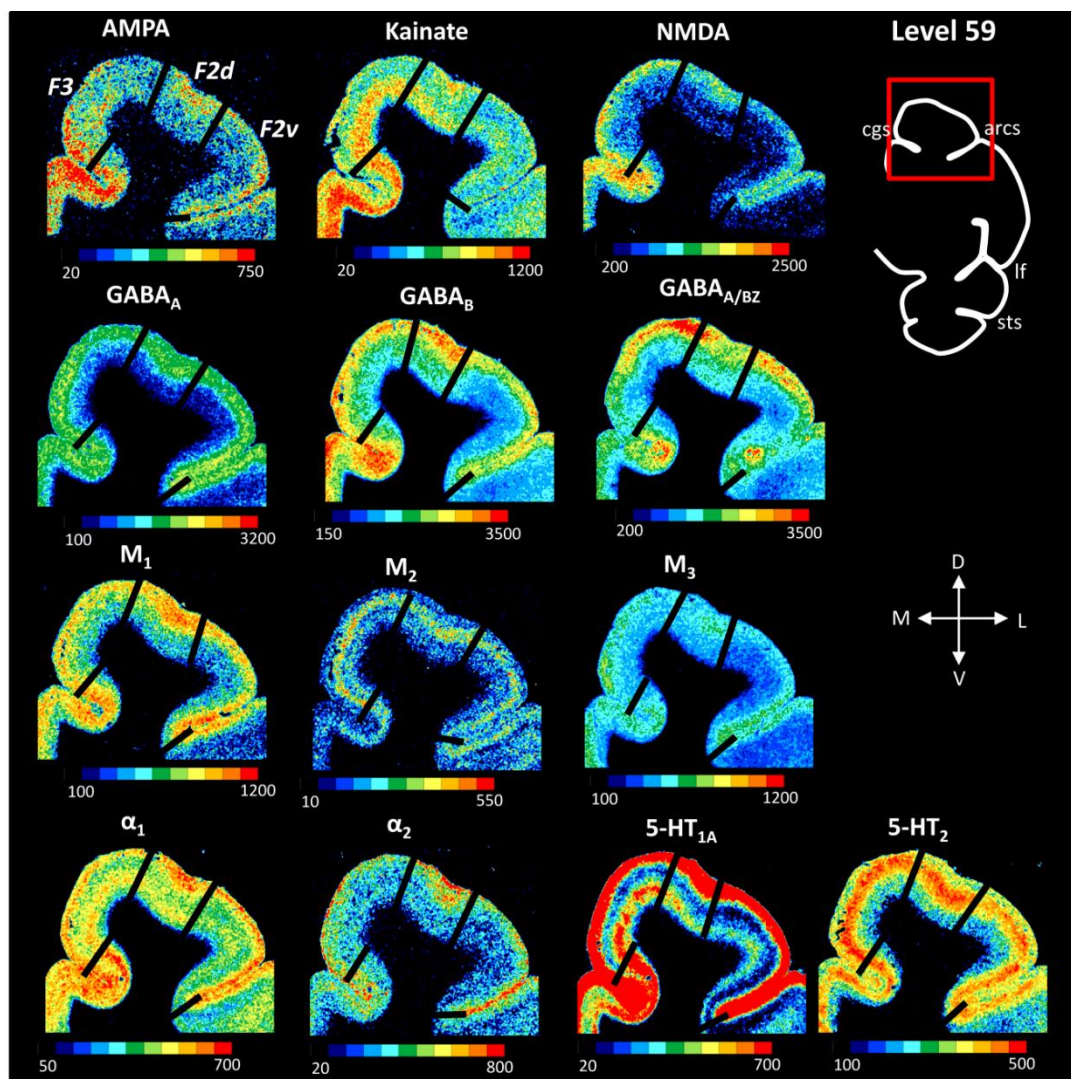


Figure 44 Regional and laminar receptor distribution patterns of the subdivisions of area F3 and F2 (Matelli *et al.*, 1985, 1991). Scale bars code for receptor densities in fmol/mg protein.

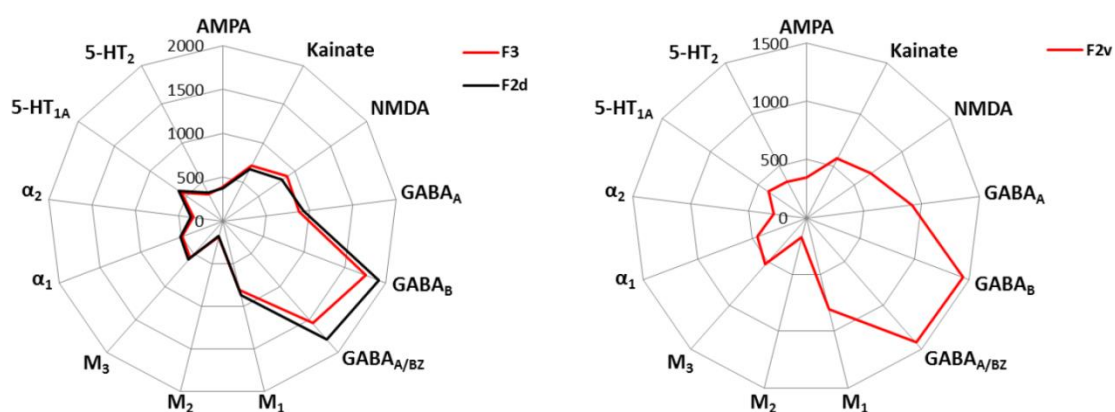


Figure 45 Receptor fingerprints of the subdivisions of area F3 and F2 (Matelli *et al.*, 1985, 1991). Axis in polar coordinate plots code for receptor densities in fmol/mg protein.

Ventral (rostral) premotor region (subdivision of area F5; Fig. 46 and Fig. 47, Tab. 12). Differences in the density of GABA_{A/BZ}, GABA_B, M₃, α_1 , 5HT_{1A} and NMDA

receptors across all layers reveal the cytoarchitectonic borders defined for the three different subareas of F5, in particular that between F5d and F5v (*Fig. 46*). The concentration of almost all receptors (*Tab. 12*) was highest in F5v, except for 5HT₂ receptors, that did not show any significant difference regarding dorsally neighboring area F5d, and AMPA receptors, that showed slightly

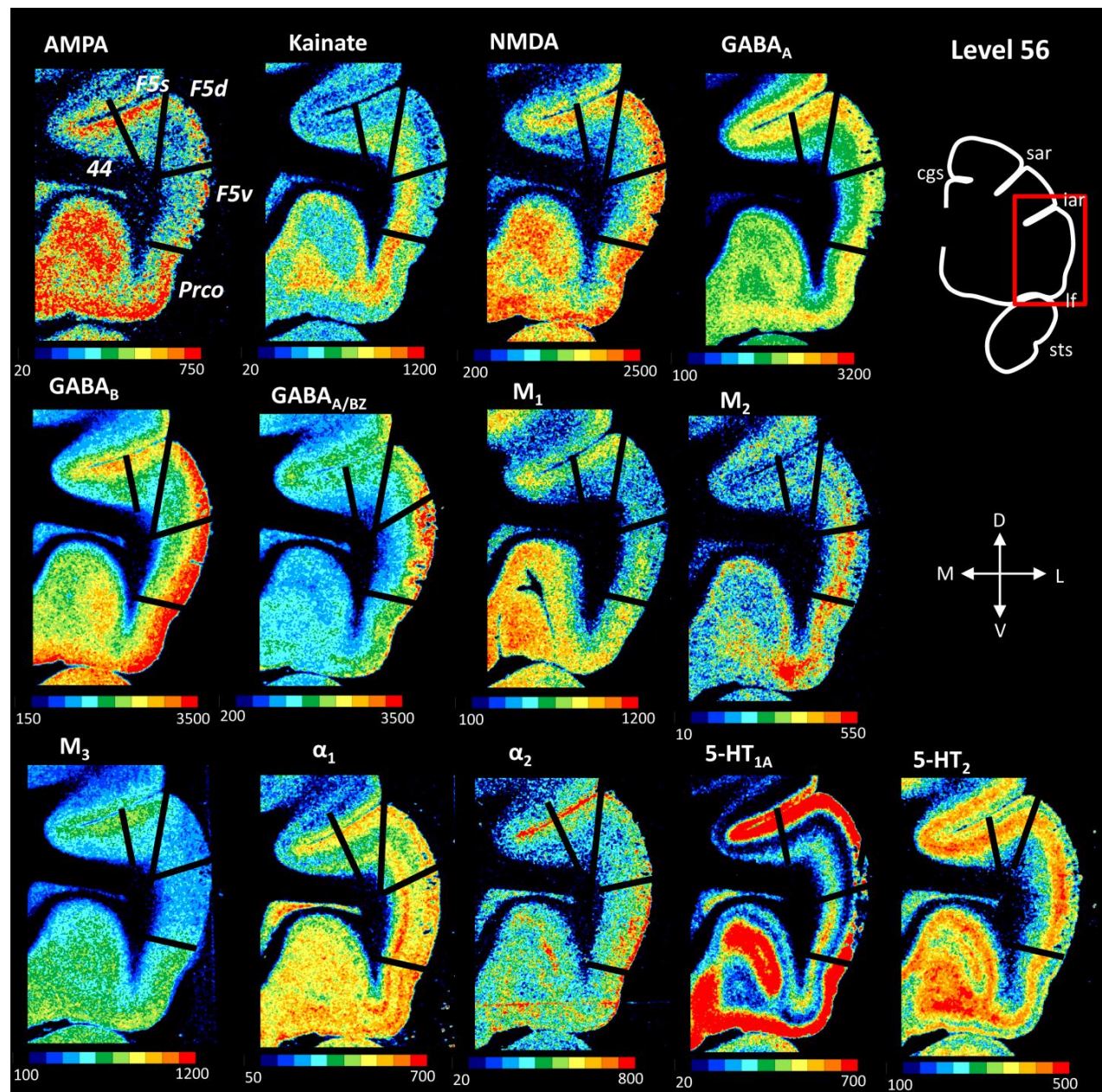


Figure 46 Regional and laminar receptor distribution patterns of the subdivisions of area F5 (Matelli *et al.*, 1985, 1991). Scale bars code for receptor densities in fmol/mg protein.

higher values in F5d than in F5v. The border between F5d and F5s was revealed only by differences in mean AMPA, kainate and GABA_{A/BZ} densities, which were higher in F5d than

F5s. Subdivisions of the area F5 showed differences in the size of the receptor fingerprints (Fig. 47). This was especially recognizable between F5d and F5v.

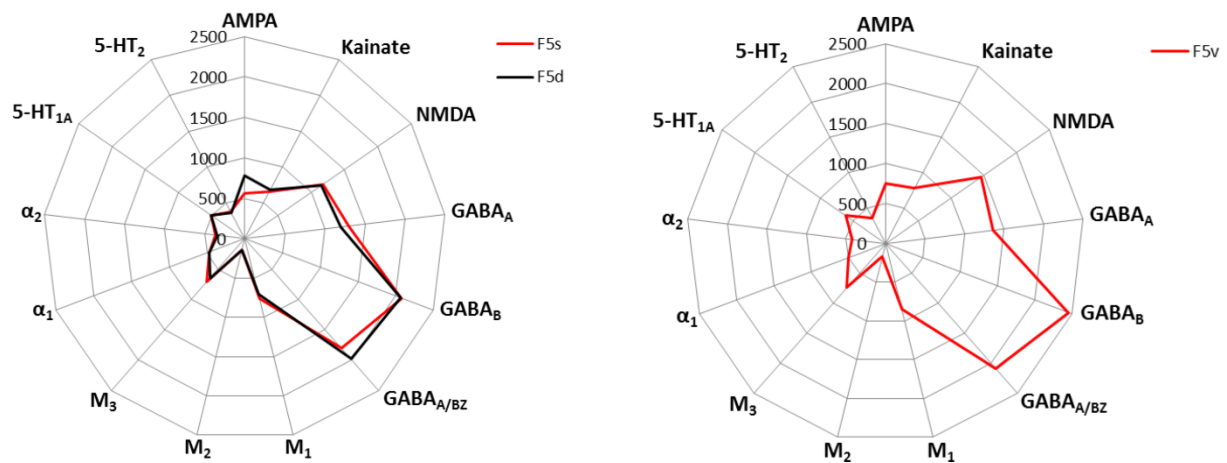


Figure 47 Receptor fingerprints of the subdivisions of area F5 (Matelli *et al.*, 1985, 1991). Axis in polar coordinate plots code for receptor densities in fmol/mg protein.

Table 12 Absolute receptor concentrations (fmol/mg protein) measured in subareas of area F5 (Matelli *et al.*, 1985, 1991); s.d. (standard deviation).

Area	AMPA	Kainate	NMDA	GABAA	GABAB	GABAA/BZ	M1	M2	M3	α_1	α_2	5-HT _{1A}	5-HT ₂
F5s	563	664	1176	1292	2078	1802	766	146	707	469	363	513	379
s.d.	239	22	257	70	412	300	440	33	215	78	53	140	67
F5d	777	683	1153	1198	2065	1983	705	146	646	467	348	510	360
s.d.		43	166	137	298	269	389	58	218	42	28	146	35
F5v	748	776	1455	1359	2450	2087	849	168	736	504	420	611	361
s.d.	73	50	121	200	328	200	381	96	197	34	17	144	48

Ventral (caudal) premotor region (subdivision of areas F4; Fig. 48 and Fig. 49, Tab. 13). Almost all receptor types show the border (Fig. 48) between areas F4d and F4v, because of the prominently higher concentrations for all 13 receptors in F4v (Tab. 13). Conversely, the border between areas F4s and F4d is revealed by more subtle changes in receptor densities, restricted to only some layers and found mainly for α_1 , AMPA, GABA_{A/BZ}, GABA_A, GABA_B, M₁ and M₃ receptors. Thus, the absolute receptor concentration levels between F4s and F4d do not show significant differences at the mean (averaged over all layers) receptor concentration level. Whereas high differences in size of the receptor fingerprints between F4d and F4v is demonstrated in the Fig. 49.

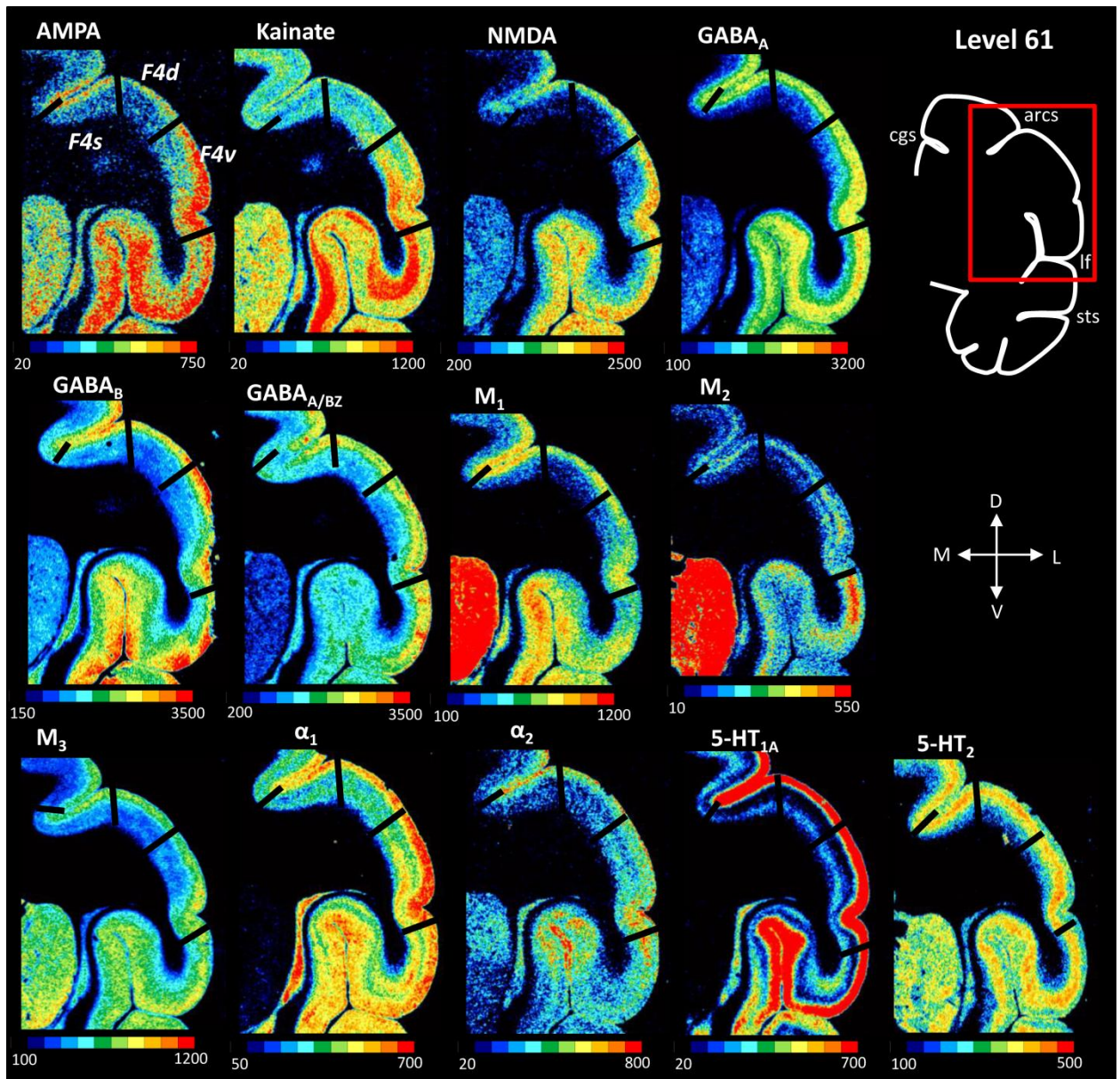


Figure 48 Regional and laminar receptor distribution patterns of the subdivisions of area F4 (Matelli *et al.*, 1985, 1991). Scale bars code for receptor densities in fmol/mg protein.

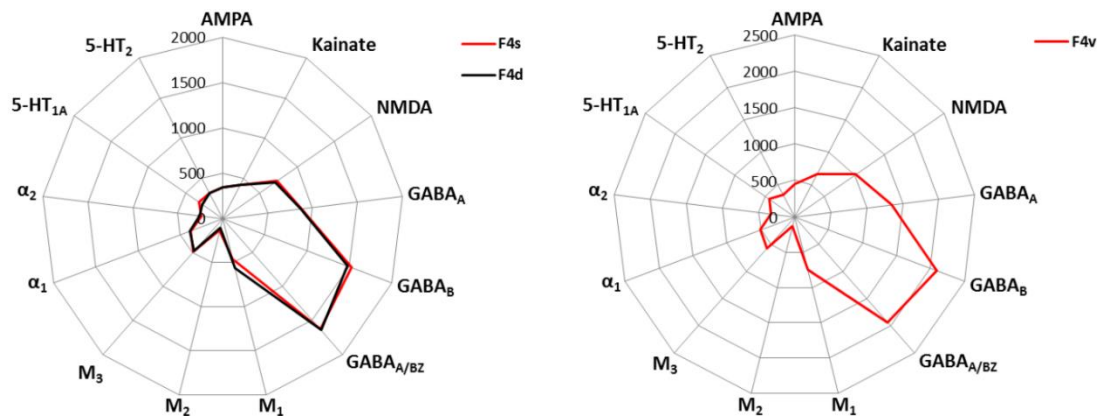


Figure 49 Receptor fingerprints of the subdivisions of area F4 (Matelli *et al.*, 1985, 1991). Axis in polar coordinate plots code for receptor densities in fmol/mg protein.

Table 13 Absolute receptor concentrations (fmol/mg protein) measured in subareas of area F4 (Matelli *et al.*, 1985, 1991); s.d. (standard deviation).

AREA	AMPA	Kainate	NMDA	GABAA	GABAB	GABAA/BZ	M1	M2	M3	α_1	α_2	5-HT _{1A}	5-HT ₂
F4s	342	424	728	881	1522	1632	456	133	492	377	235	320	314
<i>s.d.</i>	82	17	154	103	136	308	33	38	86	91	8	73	64
F4a	344	424	709	868	1476	1639	562	100	472	386	258	273	317
<i>s.d.</i>	38	41	62	133	264	430	198	24	69	17	37	7	89
F4b	449	662	1021	1349	2095	1931	747	135	578	502	326	422	345
<i>s.d.</i>	118	221	337	367	97	243	428	49	32	2	96	12	56

Medial and dorsal precentral motor region (subdivision of Brodmann's area 4; Fig. 50 and Fig. 51, Tab. 14). Receptor architectonic differences between the cytoarchitectonically identified subdivisions of area 4 are mostly subtle and restricted to only a few cortical layers (Fig. 50). Areas 4d and 4s can be delineated by the lower NMDA and GABA_{A/BZ} but higher GABA_B densities (mainly in the infragranular layers) in 4s than in 4d. Measured receptor concentration levels (Tab. 14) show that area 4m can be distinguished from area 4d by its higher AMPA, GABA_B, and GABA_{A/BZ}, but lower M₁ and M₃ densities in the supragranular layers as well as by its higher kainate, α_1 , α_2 , and 5HT_{1A}, but lower 5HT₂ concentrations in the infragranular layers. 4m and 4d show similarity in the shape and size of the receptor fingerprint with slight differences (Fig. 51). On the other hand, dorsal subdivisions 4d and 4s differ in size and shape, especially in regard to GABA_{A/BZ}, GABA_B and NMDA receptors.

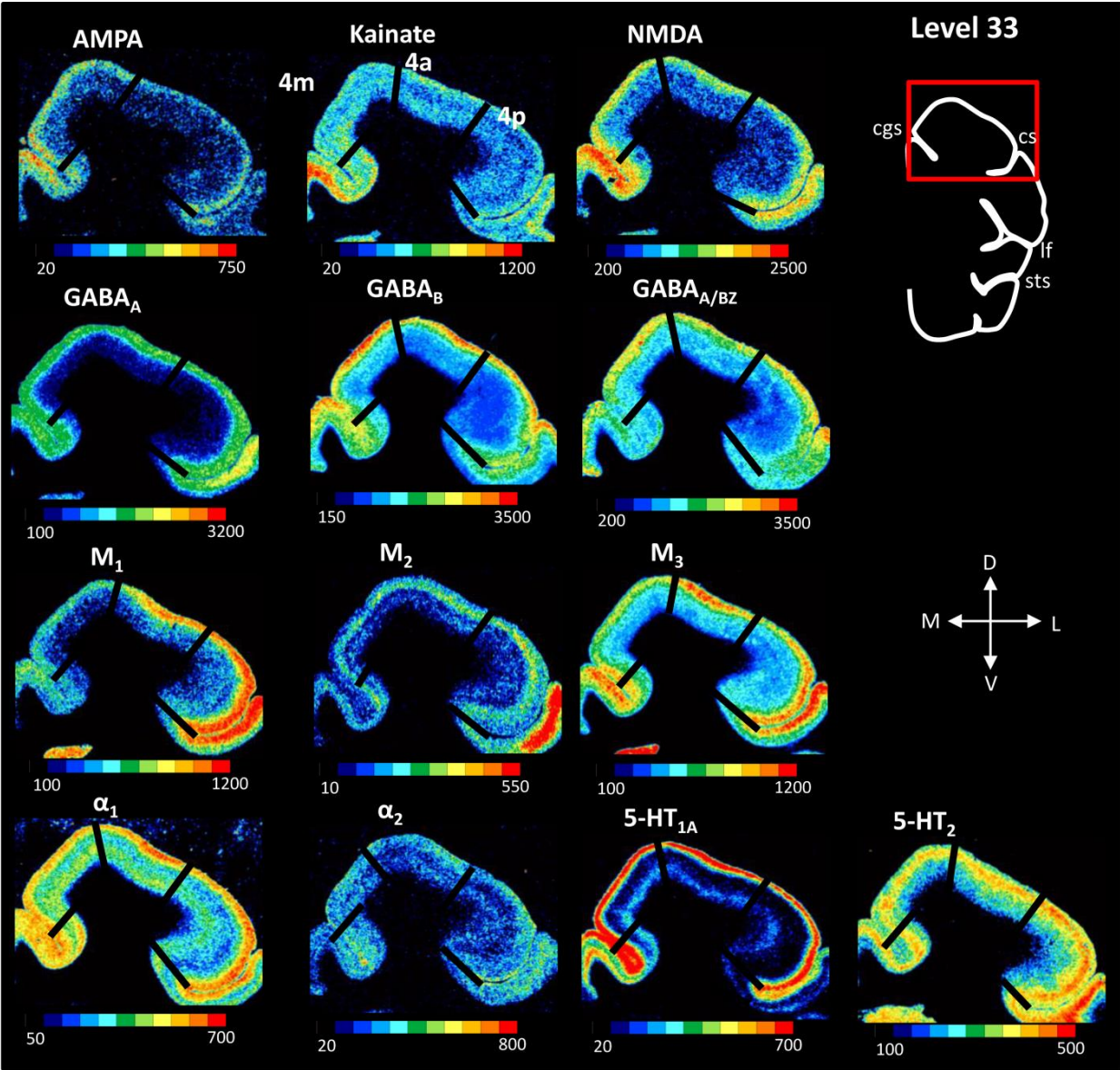


Figure 50 Regional and laminar receptor distribution patterns of the subdivisions of Brodmann's area 4. Scale bars code for receptor densities in fmol/mg protein.

Table 14 Absolute receptor concentrations (fmol/mg protein) measured in subareas of Brodmann's area 4; s.d. (standard deviation).

Area	AMPA	Kainate	NMDA	GABAA	GABAB	GABAA/BZ	M1	M2	M3	α_1	α_2	5-HT _{1A}	5-HT ₂
4m	334	324	924	795	1084	1597	417	88	534	359	141	215	250
s.d.	60	86	241	148	133	581	134	83	40	16	54	25	48
4d	301	292	936	781	1116	1606	488	85	563	352	141	194	275
s.d.	70	75	257	178	18	621	88	72	52	17	53	51	57
4s	289	255	832	724	1255	1489	461	83	540	334	166	204	282
s.d.	81	76	228	237	37	432	174	60	15	18	52	25	53

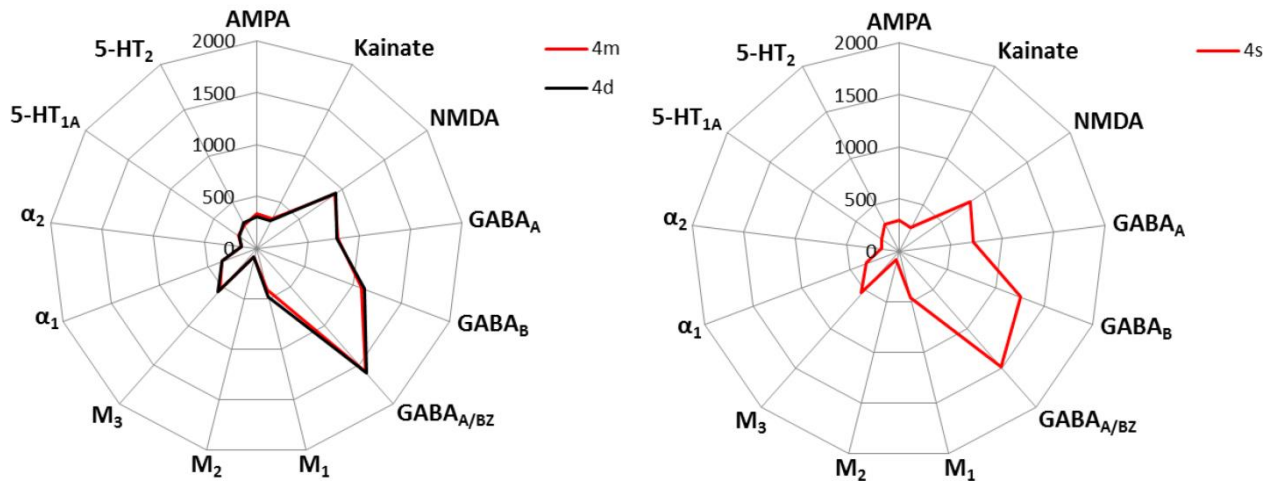


Figure 51 Receptor fingerprints of the subdivisions of Brodmann's area 4. Axis in polar coordinate plots code for receptor densities in fmol/mg protein.

3.4 Hierarchical cluster analysis

In order to reveal similarities between receptor fingerprints of the different areas in the frontal lobe, a hierarchical cluster analysis was conducted (*Fig. 52*).

A fundamental separation is found between the most caudal areas, and all other cortical areas studied here, as well as a dorso-ventral trend of grouping within main cluster groups with occasional similarities between areas that do not share borders and occupy different regions of the frontal lobe. Three main groups of clusters with similar receptor distributions were identified within frontal areas defined here:

- (i) "Rostroventral" cluster (group A, *Fig. 53*): comprises all subdivisions of fronto polar area 10 (cluster 2; *Fig. 52 and Fig. 53*), as well as orbital areas, ventrolateral prefrontal area 12, and all subdivisions of area 46 which are located in the depths of the principal sulcus (i.e. a46d, p46d, a46v and p46v). Areas 13m and 13l (cluster 1; *Fig. 52 and Fig. 53*) are clearly segregated from all the other orbitofrontal areas 13b, 11m and 11l, which most closely resemble all subdivisions of ventrolateral prefrontal area 12 and the subdivisions of area 46 located in the depths of the principal sulcus (cluster 3; *Fig. 52 and Fig. 53*).

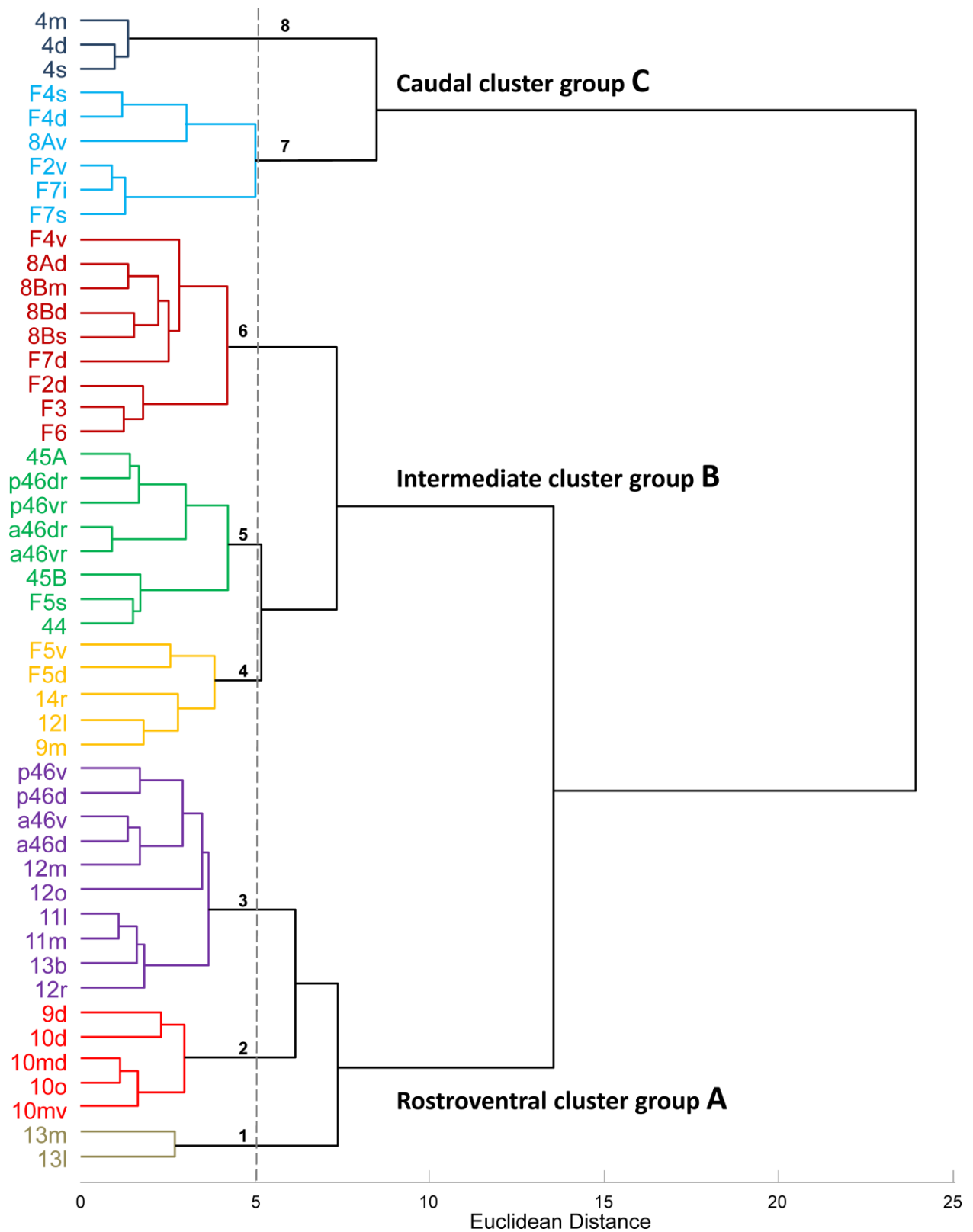


Figure 52 Hierarchical cluster analysis of the macaque monkey lobe (k-mean clustering represented 8 as the most acceptable number of clusters).

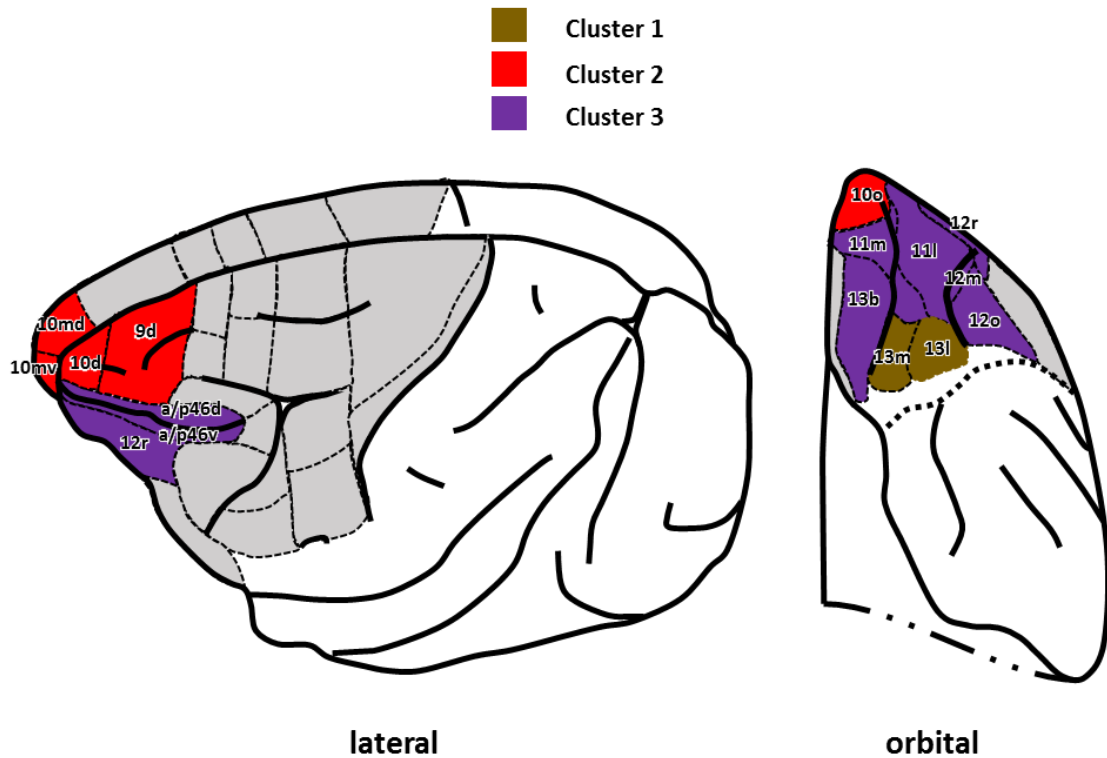


Figure 53 Schematic drawing of a macaque brain showing the extent and location of areas contained within cluster A in the dendrogram depicted in *Fig. 52*.

- (ii) “Intermediate” cluster (group B, *Fig. 54*): encompasses mainly premotor and ventrolateral prefrontal areas. Group B also contained all subdivisions of prefrontal area 8, which were closely associated with premotor areas F7d, F4v and F2d, as well as with supplementary motor area F3 and pre-supplementary motor area F6 (cluster 6; *Figs. 52* and *54*). Rostroventral premotor areas F5d and F5v showed greater similarity to ventrolateral prefrontal area 12l, dorsomedial prefrontal area 9m, and orbital area 14r (cluster 4; *Figs. 52* and *54*) than to neighboring premotor areas. Finally, the subdivisions of area 46 located within the outer portion of the iar, i.e. areas a46dr, p46dr, a46vr, and p46vr, clustered with areas of Broca’s region, and with premotor areas (cluster 5; *Figs. 52* and *54*).
- (iii) “Caudal” cluster (group C, *Fig. 55*): the three subdivisions of the primary motor cortex (i.e. areas 4d, 4s and 4m) are clearly separated from lateral premotor areas (cluster 8; *Figs. 52* and *55*). Premotor areas (cluster 7; *Figs. 52* and *55*) present a dorso-ventral segregation around the arcuate sulcus, with a dorsal group comprises areas F2v, F7i and F7s, while premotor areas F4s and F4d, together with prearcuate area 8Av, build the ventral group.

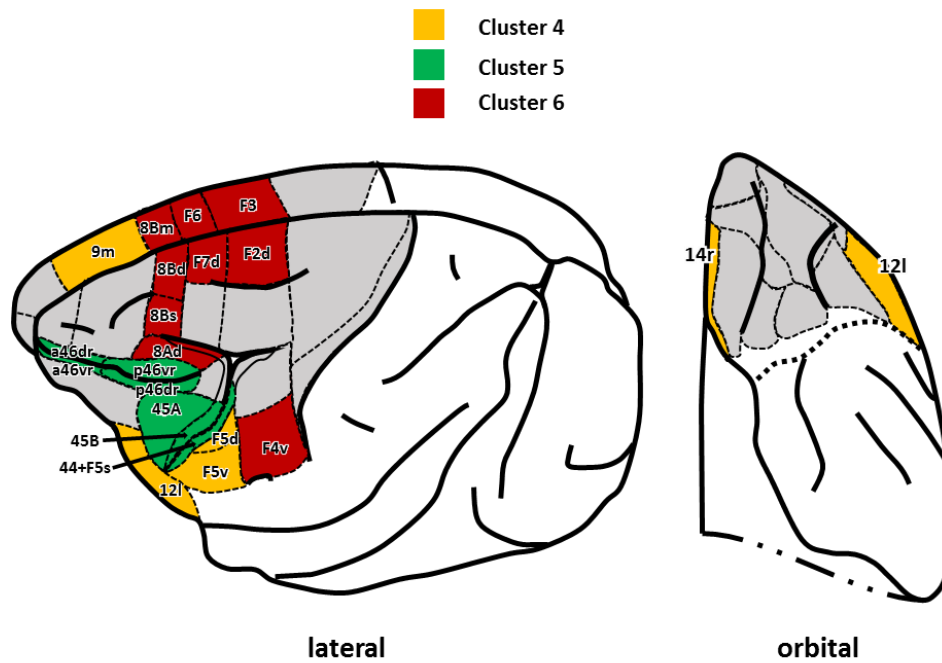


Figure 54 Schematic drawing of a macaque brain showing the extent and location of areas contained within cluster B in the dendrogram depicted in *Fig. 52*.

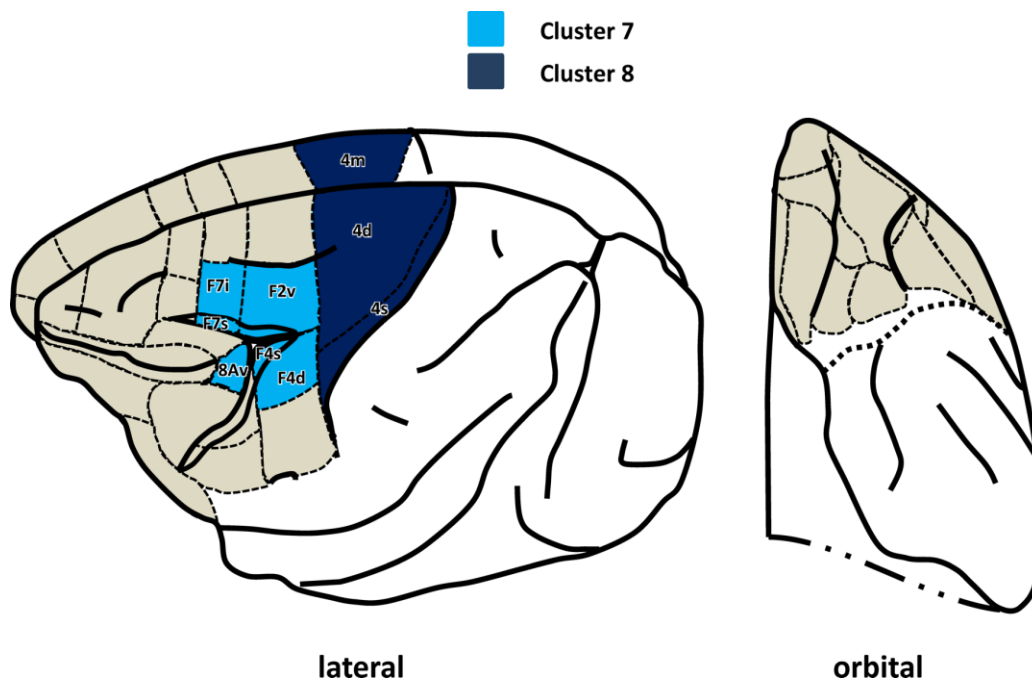


Figure 55 Schematic drawing of a macaque brain showing the extent and location of areas contained within cluster C in the dendrogram depicted in *Fig. 52*.

3.5 Principal component analysis

A principal component analysis was carried out to reduce the 13-dimensional space resulting from the analysis of 13 different receptors area to a 2-dimensional plot depicting the Euclidean distances between the fingerprints of each area, which explained 79.664% of the variance in the sample of areas examined. As presented in *Fig. 56*, differences in the 1st principal component confirmed the existence of three main cluster groups as revealed by the hierarchical cluster analysis (dashed red lines in *Fig. 56*). Within group B, the 2nd principal component segregated supplementary motor area F3, pre-supplementary motor area F6 and premotor area F2d from remaining premotor and lateral prefrontal areas (dashed black line within cluster B in *Fig. 53*). Finally, differences in the 2nd principal component segregated orbital areas 13m and 13l as well as the subdivisions of frontopolar area 10 from the remaining areas of group A.

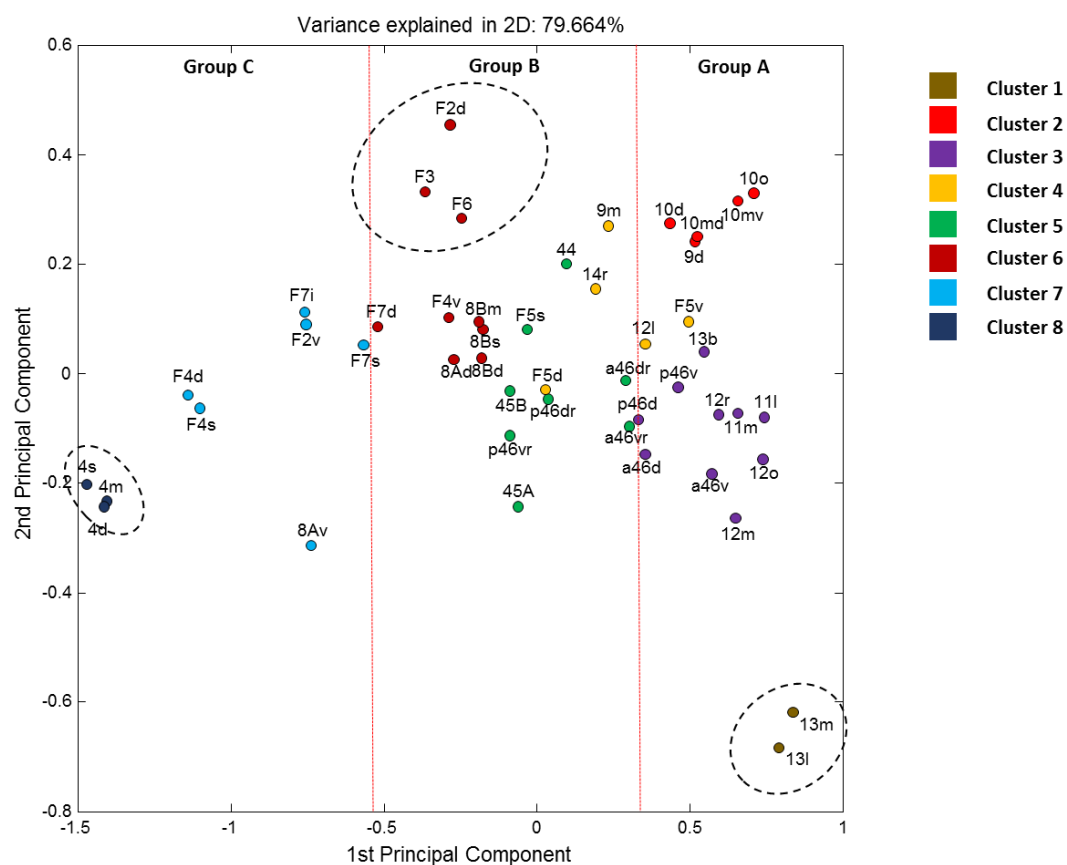


Figure 56 Principal component analysis

4 Discussion

In the present study, 50 different areas were identified in the macaque frontal lobe, of which 16 belong to the motor cortex, 18 to the prefrontal cortex, and 16 to the orbitofrontal cortex. For the first time, a microstructural analysis of the macaque frontal lobe is provided based on quantifiable tools such as a statistically testable cytoarchitectonic approach and multi-receptor autoradiography (specifically, the areal distribution of 13 different receptor types was examined), to create detailed parcellation map of the macaque frontal lobe. Each cortical area was thus characterized by distinct cyto- and receptorarchitectonic properties. Cytoarchitectonic borders between areas were determined first by visual inspection, and their position was subsequently confirmed by a quantitative and statistically testable approach (Schleicher *et al.*, 1986; Zilles and Schleicher, 1991). The position of these borders was further confirmed by changes in the laminar distribution pattern of at least 5 different receptors compared to the neighboring areas, as well as by differences in absolute receptor concentration levels. Based on this approach, some previously published parcellation schemes could be confirmed. It also revealed the existence of several frontal areas that had not been described in previous maps, such as a subdivision of areas 10, 8B, F7, F5 and 4. The ensuing novel parcellation scheme was presented in a 2D flat map (*Fig. 4* and *Fig. 5*), in order to compare delimitation results from the multivariate analysis to the ones in previous microparcellations (Walker, 1940; Preuss and Goldman-Rakic, 1991; Morecraft *et al.*, 1992; Carmichael and Price, 1994; Barbas and Pandya, 1989; Petrides and Pandya, 1994, 2002; Caminiti *et al.*, 2017). Finally the density of each of the 13 receptor types was quantified in 48 of the 50 areas. Multivariate analyses of the ensuing receptor fingerprints revealed structurally and functionally relevant clusters of areas which share similar neurochemical and properties.

4.1 Comparison among different parcellation maps

Orbitofrontal and ventrolateral region in the prefrontal cortex.

The first parcellation scheme of the macaque orbito-medial prefrontal cortex was proposed by Walker (1940), who identified 5 relatively large cytoarchitectonic areas: area 10 on the frontal pole, area 11 on the rostral orbital surface, areas 13 and 12 on the medial and

lateral orbital surface, and area 14 located on the ventromedial convexity (*Fig. 1*). These findings were largely replicated by Barbas and Pandya (1989) and Morecraft *et al.* (1992), whereas Preuss and Goldmann-Rakic (1991) carried out a further parcellation of the orbito-medial region, recognizing subdivisions in area 13, i.e. 13L and 13M, and in area 14, i.e. 14M, 14A, 14VL and 14L, but no subdivisions were identified in areas 10 and 11. Moreover, these parcellation maps did not counterpart with the connectional diversity of this region (Charmichael and Price, 1994). Thus, Charmichael and Price (1994) published a more detailed map of this region based on the analysis of nine different histochemical and immunohistochemical stains, recognizing over 20 distinct subareas.

The present parcellation scheme largely confirms that of Charmichael and Price (1994), except for the frontal pole region (area 10). They subdivided rostral granular area 10 into areas 10m, extending on the medial and dorsal surface of the hemisphere, and 10o, on the orbital surface of the medioventral gyrus, which is caudally replaced with area 14r (Carmichael and Price, 1994). The present analysis confirmed the location and extent of subarea 10o on the orbital portion of the frontal pole, but detected three subdivisions within 10m, i.e. on the medial surface, dorsal portion 10md and a ventral 10mv, and a distinct subarea on the dorsal surface of the frontal pole, 10d. All subdivisions of area 10 are granular, with very-well developed layers II and IV, but with slight differences in its thickness between defined subareas. Area 10d has a wider layer IV and blurry border between layer VI and white matter in comparison to the medial subareas 10md and 10mv. Medial areas are characterized by horizontal pattern in layer IV, however only in 10md can the same pattern be recognized in layers III and V as well. Area 10o can be distinguished from 10mv by more prominent granular layers II and IV. This cytoarchitectonic parcellation was further confirmed by the receptor architectonic analysis, which clearly revealed the existence of newly defined subareas 10. Differences in absolute concentrations were noted for GABA_A, GABA_B, GABA_{A/BZ}, M₁ and NMDA receptors, as higher levels were recorded in 10mv than in 10md, whereas hierarchical dendrogram showed clear distinction between 10d and all other subareas 10.

Area 10 was delimited caudally on the ventromedial convexity by area 14, which was subdivided into rostral dysgranular and caudal agranular parts, 14r and 14c respectively (Carmichael and Price, 1994). The location and extent of both areas could be confirmed with the present cytoarchitectonic analysis (*Fig. 5*), but it was not possible to quantify receptor densities in 14c due to tangential sectioning at that rostro-caudal level.

Walker's (1940) areas 11 and 13 occupy the rostral and caudal portion of the orbital gyrus, respectively. Both areas have been subdivided into medial and lateral parts, i.e. 11m, 11l, 13m and 13l (Carmichael and Price, 1994). Overall, areas 11m and 11l are granular, whereas areas 13m and 13l are part of the dysgranular cortex rostral to the agranular insular region. The main difference between the medial and lateral subdivisions of areas 11 and 13 is found in their layer V. Areas 11m and 11l differ in sublaminae V_a and V_b , which are continuous in area 11l and broken into aggregates of cells in area 11m, whereas area 13l has blurry sublamination of layer V that cannot be seen in 13m. Receptorarchitectonic analysis revealed differences in the concentration levels of GABAergic ($GABA_A$ and $GABA_B$ receptors as well as $GABA_{A/BZ}$ binding sites) receptors, which were higher in the lateral than in the medial subdivision of 11. On the other hand, 13m had higher level of kainate receptors than 13l. On the medial bank of the medial orbital sulcus, at a site included in area 14 by Walker (1940), two more areas were classified based on their connectivity patterns as being further subdivisions of area 13, i.e. rostral dysgranular area 13b and caudal agranular 13a (Amaral and Price, 1984). The location and extent of both areas could be confirmed with the present cytoarchitectonic analysis (*Fig. 5*), but it was not possible to characterize the receptor architecture of 13a due to tangential sectioning at that rostro-caudal level. Interestingly, the hierarchical cluster analysis revealed that area 13b differed considerably from adjacent area 14r and orbital subdivisions of area 13, but was more similar to areas 11m and 11l.

Finally, the lateral orbital cortex is occupied by area 12, which can be subdivided into four areas. Areas 12r and 12o occupy the rostral, whereas 12l and 12m are on the caudal portion of the lateral orbital surface and on the ventrolateral convexity. Unlike neighboring areas, 12r has dysgranular cortex, whereas area 12m can be distinguished by its well-developed layer IV and bipartite layer V. Area 12o has a thin and weakly stained layer IV, and no obvious sublamination in layer V. Finally, most posterolateral area 12l is granular cortex with clear subdivision in layers III and V, whose pyramids are smaller than in dorsally neighboring area 45A. All borders could be confirmed by the observer-independent cytoarchitectonic approach, as well as by differences in receptor architecture. $GABA_{A/BZ}$, $GABA_B$, $GABA_A$ concentrations were higher in 12r than in 12m, whereas kainate levels were higher in 12m. Areas 12o and 12l differed mainly in their $GABA_{A/BZ}$, NMDA and AMPA densities, which were higher in 12o than in 12l.

Dorsal and ventrolateral region of the prefrontal cortex.

This region encompasses dorsal prefrontal areas 8 and 9, lateral area 46, as well as ventrolateral areas 45 and 44. Walker (1940) identified and labeled area 9 on the rostral portion of the medial and dorsal surface of the prefrontal cortex neighboring rostral with area 10 and caudal with area 8B. Whereas some authors confirmed this parcellation scheme (e.g., Barbas and Pandya, 1989; Carmichael and Price, 1994), others (e.g., Preuss and Goldman-Rakic, 1991; Petrides and Pandya, 1994, 2002; Caminiti *et al.*, 2017) described dorsal (9d) part, located on the convexity superior to the principal sulcus, and a medial (9m) subdivision on the medial surface of the hemisphere, dorsal to the cingulate sulcus. In the present quantitative cytoarchitectonic analysis the existence of dorsal and medial subdivisions of area 9 could be confirmed, both of which are granular in nature, although layer IV was more prominent in 9d than in 9m. The receptor analysis further confirmed this subdivision. Receptor fingerprints did not show much difference in shape but rather in size, thus indicating comparable specific balances between the different receptors in both areas (Zilles *et al.*, 2002).

Walker (1940) defined area 46 within and around principal sulcus on the lateral surface of the prefrontal cortex caudal to area 10, while on the most posterior end of principal sulcus, area 46 was replaced by area 8A. Area 46 could be identified along entire principal sulcus. This location of area 46 in the macaque monkey has been confirmed in various anatomical studies (Preuss and Goldman-Rakic, 1991; Petrides and Pandya, 1994, 2002; Caminiti *et al.*, 2017), however it was widely acknowledged that this large region is not homogenous and distinct subdivisions with many discrepancies among parcellation schemes were made by different authors. Preuss and Goldman-Rakic (1991) identified four subareas along the principal sulcus. Two areas within the sulcus on the dorsal and ventral wall close to the fundus (inner subareas), areas 46d and 46v respectively, and two areas on the dorsal and ventral shoulders of the sulcus and extending onto the free surface of the hemisphere (outer areas), areas 46dr and 46vr, respectively. Other authors (Petrides and Pandya, 2006; Morecraft *et al.*, 2012, Caminiti *et al.*, 2017) identified rostro-caudal differences within Walker's area 46, but only described a dorso-ventral segregation in the caudal portion, thus resulting in a parcellation with a rostral area 46 and caudal areas 9/46d and 9/46v located on the dorsal and ventral banks of the principal sulcus, respectively, and extending onto the free surface of the hemisphere. The existence of dorso-ventral subdivisions along the entire length of the principal sulcus (i.e., the parcellation proposed by Preuss and Goldman-Rakic (1991))

could be corroborated by the present quantitative cytoarchitectonic analysis. However, based on the receptor architectonic analysis, we could also confirm the existence of differences between the anterior and posterior portions of the principal region, which were especially prominent along the ventral bank of the sulcus. Higher concentrations of GABA_{A/BZ} binding sites, but lower M₁ receptor densities were measured in posterior subareas as compared with anterior subareas. Therefore, a new parcellation scheme for Walker's area 46 is proposed which results in its subdivision into 8 areas: a46d, a46dr, p46d and p46dr, located from rostral to caudal and from the fundus to the surface along the dorsal wall of the principal sulcus, as well as a46v, a46vr, p46v and p46vr, located from rostral to caudal and from the fundus to the surface along the ventral wall of the principal sulcus.

Further on the caudal portion of the medio-dorsal prefrontal surface, Walker (1940) and Petrides and Pandya (1994) delineated dysgranular area 8B as a transitional region between granular prefrontal and agranular premotor areas, as well as the granular area 8A on the prearcuate convexity. Preuss and Goldman-Rakic (1991) and Morecraft *et al.* (2012) recognized within area 8B two distinct areas 8Bm and 8Bd, which is supported by the results of the quantitative cyto- and receptorarchitectonic analysis as well. However, area 8Bd was further subdivided into two areas, 8Bd and 8Bs. Moreover, unlike previous maps, in the present parcellation scheme the location of 8B has been defined more caudally, occupying the medial and dorsal surface above *sas*, that was previously identified as the most rostral part of premotor areas F6 and F7, respectively. Area 8Bd and 8Bs are found on the dorsal surface of the hemisphere rostrally and above the *sas*, and 8Bs extends onto the dorsal wall of the *sas*. Cytoarchitectonically 8Bm differs from dorsal subdivision 8Bd by its weak lamination and smaller pyramids in layers III and V. 8Bm and 8Bs share similar cytoarchitectonic traits, however, the main difference between them is that in 8Bs has more prominent pyramids scattered in layer V. Receptor analysis further confirmed the border between 8Bd and 8Bs, with higher kainate, NMDA and GABA_{A/BZ} densities in 8Bd than in 8Bs. Area 8Bm differed from 8Bd by its higher AMPA and kainate, but lower M₁ receptor densities. On the other hand, granular area 8A, located within prearcuate region, is separated from the premotor representation of the forelimb and mouth by the arcuate sulcus (Bruce *et al.*, 1985; Stanton *et al.*, 1989), while rostrally neighboring with area 46 and area 45A ventrally.

Area 8A has been associated with the frontal eye field (FEF), originally investigated by Bruce *et al.* (1985) and Stanton *et al.* (1989), in monkeys. FEF corresponds to an architectonically defined area (Stanton *et al.*, 1989) where intracortical microstimulation with

low current intensities evokes saccades (Bruce *et al.*, 1985). Dorsally larger-amplitude saccades were evoked, whereas smaller-amplitude was represented more ventrally (Bruce *et al.*, 1985), indicating dorso-ventral differences within the region. Walker's area 8A has been subject of numerous architectonic analyses, resulting with the maps that differ in the number and extent of areas depicted. Preuss and Goldman-Rakic (1991) marked the rostral part of Walker's 8A as a single area 8Ar occupying the dorsal and ventral surface of the prearcuate convexity, which is delimited caudally by 8Am within the ventral wall of the *sas*, and area 8Ac within the posterior part of the dorsal wall of the *ias*. Furthermore, their area 8Ar extends ventrally on the cortical surface rostral to the *ias*, where it was delimited rostrally by area 12vl. This parcellation scheme, however, differs from those proposed by Petrides and Pandya (1999), who identified dorsal (8Ad) and ventral (8Av) subdivisions, or Gerbella *et al.* (2007), who described a rostro-caudal segregation (area 8r located rostral to area 8/FEF). The results of the present quantitative multimodal analysis are in accordance with the map of Petrides and Pandya (1999). An area 8Ad was defined on the ventral bank of the *sas* and extending ventrally onto the free surface of the prearcuate convexity, and an area 8Av on the anterior wall of the *ias* and extending dorsally onto the convexity. Furthermore, in the present parcellation scheme, and contrary to the map of Preuss and Goldman-Rakic (1991), areas 8Av and 12l share no common border, since area 8Av could no longer be identified on the cortical surface adjoining the most rostral portion of the *ias*, since it had been replaced at this position by area 45A. Cytoarchitectonic differences were further confirmed by the receptor architectonic analysis, that revealed lower levels of AMPA, NMDA, GABA_B, M₁, M₂, M₃, α_1 , α_2 , 5HT_{1A} and 5HT₂ receptor densities in 8Av than in 8Ad.

Finally, the ventrolateral region encompasses areas 44 and 45, which are thought to be the homologs of Broca's region in humans (Petrides and Pandya, 2002). Walker (1940) identified his area 45 within the lower limb of the arcuate sulcus. Petrides and Pandya (2002), however, found area 45 to extend rostrally onto the adjacent lateral surface of the hemisphere for a considerable distance, reaching as far as the *ipd*. This is also in contrast with the parcellations proposed by (Walker, 1940) and (Preuss and Goldman-Rakic, 1991), who described area 45 mainly within the *ias*, and only encroaching onto the free surface, where it was replaced dorsally by area 46 and ventrally by area 12 (in the map of Walker, 1940), or rostrally by area 8Ar (in the map of Preuss and Goldman-Rakic, 1991). Furthermore, Petrides and Pandya (1994, 1999, 2002) subdivided monkey area 45 into areas 45A and 45B, which was confirmed in the present analysis as well. Area 45A occupies the ventral portion of the

prearcuate convexity ventral to area 8Av, and extends rostrally into the *ipd* where is substituted by 12r dorsal to *ipd*, and by 12l ventral to the dimple. Caudally 45A is delimited by 45B, which occupies the rostro-dorsal wall of the *ias*. The subdivision of area 45 is based primarily on the differences in development of layer IV. This layer is wider and more prominent in area 45A than in area 45B. The results of the present quantitative multimodal approach not only support the presence of an area 45, and not of area 12, on the prearcuate convexity, but also confirm the existence of areas 45A and 45B. Area 45A presented higher kainate, GABA_A and GABA_{A/BZ}, but lower 5HT_{1A} and NMDA densities than 45B. In the same time, area 44 has also been subject of controversy. Area 44 has now been described as the dysgranular area between the caudally adjacent agranular premotor cortex and granular area 45 (Petrides and Pandya, 1994; Petrides *et al.*, 2005), and this view could be confirmed by the present analysis. Walker (1940) and Preuss and Goldman-Rakic, (1991a) did not identify an area 44 in their maps, because they considered that area 45 not only occupied the rostral, but also the caudal wall of the *ias*. Matelli *et al.* (1985, 1991) did not identify area 44 either, since they thought that their area F5 continues rostrally into the *ias*, where it was followed by area 45. Thus, cortex on the posterior wall of the *ias* was considered to constitute a specialized region of the premotor cortex for orofacial movements (Deacon, 1992; Preuss, 1995).

Motor region.

The motor region in the frontal lobe was originally subdivided into two cytoarchitectonic distinct areas. Precentral motor area 4, characterized by giant pyramidal cells (Betz cells) in layer V, and premotor area 6, lacking these pyramids (Brodmann, 1909). Functionally, area 4 represents the primary motor cortex (Brodmann, 1909), whereas area 6 consists of the supplementary (SMA) and pre-supplementary (pre-SMA) motor areas (Penfield and Welch, 1951; Woolsey *et al.*, 1952) on the mesial surface, and the premotor cortex (Fulton and Sheehan, 1935) on the lateral cortical convexity. The development of new and more powerful anatomical and functional techniques revealed that this cortical region, particularly the premotor areas, is a complex mosaic of structurally and functionally distinct areas responsible for processing different aspects of motor behavior (Rizzolatti *et al.*, 1987; Wise, 1985; Barbas and Pandya, 1987; Preuss and Goldman-Rakic, 1991; Matelli *et al.*, 1985, 1991, 1998; Dum and Strick, 2002; Geyer *et al.*, 2000). The present results will be discussed in the framework of the map of Matelli *et al.* (1985, 1991, 1998), since it is the currently most widely accepted subdivision of the motor region in the macaque brain. They

defined a primary motor area F1, and subdivided Brodmann's area 6 into a supplementary motor area F3, a pre-supplementary motor area F6 (both located on the mesial cortical surface), dorsal premotor areas F2 and F7 on the dorsolateral premotor convexity, as well as ventral premotor areas F4 and F5 on the ventrolateral premotor convexity.

Previously published maps of this region differ considerably in the number and extent of areas depicted, as well as in nomenclatures used. On the mesial surface caudal to area 8B, Preuss and Goldman-Rakic (1991) identified a large area 6M, which has been subdivided into a rostral part (area F6 of Matelli *et al.*, 1985, 1991 and Caminiti *et al.*, 2017, pre-SMA of Morecraft *et al.*, 2012) and a caudal (area F3 or SMA of Matelli *et al.*, 1985, 1991 and Caminiti *et al.*, 2017, area 6m of Morecraft *et al.*, 2012). The existence of these two areas was confirmed by histochemical, cytoarchitectonic and functional data (Matelli *et al.*, 1985, 1991; Luppino *et al.*, 1993; Rizzolatti *et al.*, 1996; Geyer *et al.*, 1998), and is further corroborated by the results of the present study. A characteristic cytoarchitecture could be identified, with densely packed medium size pyramids in the superficial layers in area F6 unlike deeper layers V and VI. On the other hand, area F3 has more prominent layer V in compare to adjacent layers III and VI, which gives visual appearance as if F3 is more laminated than F6. Areas F3 and F6 showed high similarity in the shape and size of the receptor fingerprint. However, differences in the absolute concentration levels were recorded for NMDA and M₁ receptors, which were higher in F6 than in F3. Furthermore, lower concentration levels for GABA_{A/BZ} were noted in F6 in regard to F3 levels.

Laterally to area F6, rostral premotor area F7 (Matelli *et al.*, 1985, 1991), or 6DR (Petrides and Pandya, 2006; Morecraft *et al.*, 2012), was subdivided into three subareas, i.e. dorsal area F7d, intermediate area F7i and ventral area F7s, based on distinct receptor fingerprints and on cytoarchitectonic differences, mainly, in layer VI. Area F7d is found at a position comparable to that of the rostro-dorsal oculomotor area SEF (supplementary eye field, Schlag and Schlag-Rey, 1987). Preuss and Goldman-Rakic (1991) referred to the entire dorsolateral premotor cortex as area 6D, they described distinct specializations within the dorsal wall of the *sas*, which could partly correspond to the present area F7s. Layer VI is sublaminate in F7d and F7i, but not in F7s, whereby the sublamina VI_a is much wider in F7d than in F7i. Area F7d had higher GABA_{A/BZ}, M₂, M₃ and 5HT₂ receptors, in contrast to neighboring areas F7i and F6. For the densities of AMPA, NMDA, GABA_A, GABA_B, M₁, M₃ and α_2 receptors were lower in F7i than in F7s. Only for kainate receptor densities were higher in F7i than in F7s.

Further caudally to F7, within area F2 (Matelli *et al.*, 1985, 1991), also referred to as 6DC (Petrides and Pandya, 2006; Morecraft *et al.*, 2012), distinct cytoarchitectonic and receptor distribution patterns could be identified enabling its subdivision into dorsal F2d and ventral F2v parts with regard to the superior precentral dimple (*prcd*). A comparable subdivision of area F2 was made based on SMI-32 immunohistochemical (Geyer *et al.*, 1998, 2000), cytoarchitectonic and functional (Matelli *et al.*, 1998) analyses. Both subdivisions of F2 were poorly laminated and presented some big pyramids in layer V, which have rostrocaudal gradient in size, in particular, closer to the border with area 4, where pyramids are bigger, but still not as prominent as in area 4. Layers II and V were thinner and more prominent in F2d than in F2v. As for receptor architecture, absolute concentration levels measured in F2v were lower for 11 different receptor types, e.g. AMPA, kainate, NMDA, GABA_B, GABA_{A/BZ}, M₁, M₂, M₃, α_1 , α_2 and 5HT_{1A} compared to F2d, further confirming obvious subdivision within caudal premotor cortex.

The ventral surface of the rostral premotor region, that encompasses area F5, was recently subdivided into three distinct subareas based on cyto-, myelo- and chemoarchitecture (Belmalih *et al.*, 2008). Two of these areas occupy the ventral wall of the inferior arcuate branch, F5p posteriorly and F5a anteriorly, and area F5c is located on the ventral convexity below the inferior arcuate branch (Belmalih *et al.*, 2008). However, Maranesi *et al.* (2012) consider area F5p of Belmalih *et al.* (2008) to be a part of area F4, based on the results of a study with intracortical microstimulation and extracellular recordings. This would be in agreement with the present results, since no rostro-caudal subdivision was found in the portion of area F5 buried within the *ias*, which was marked as subarea F5s. However, the most caudal portion of the present area F5d partly corresponds to F5p of Belmalih *et al.* (2008) as the authors specified that this area also occupies a small part of the lateral surface in the most caudal part of the postarcuate convexity. Thus, most of area F5v, together with area F5d, both identified in the present study, are found within area F5c of Belmalih *et al.* (2008). Furthermore, the dorsal part of area F5c of Belmalih *et al.* (2008) (F5d of the present study), is reported to have different connections than its ventral part of the F5c (which could correspond to F5v of the present study) (Gerbella *et al.*, 2011). Areas F5d and F5v of the present study can be distinguished based on their distinct cyto- and receptor architecture. Area F5d is characterized by darkly stained small-sized pyramids in the lower part of layer III, and prominent medium-sized pyramids in layer V. Subdivisions of layer V and the poor staining of pyramids in layer III differentiate F5v from F5d. Furthermore, higher NMDA,

GABA_B, GABA_A and GABA_{A/BZ} densities were measured in F5v than in F5d. Additionally, AMPA, kainate and GABA_{A/BZ} densities were higher in F5d than in F5s. The receptor fingerprints of the F5d and F5v are comparable in shape, but distinct in size, indicating similar receptor balance of these F5 subdivisions. On the other hand, areas F5s and F5d have similar size of the receptor fingerprints, with most prominent difference in shape between subareas in AMPA and GABA_{A/BZ} receptors.

Further, on the ventral surface, three cytoarchitectonically distinct subareas were identified within caudal area F4, i.e. area F4s occupying the ventral wall of the *arcs* and two areas on the free surface of the hemisphere, F4d dorsally and F4v ventrally. A similar subdivision of the precentral convexity was reported by Maranesi *et al.* (2012) who identified functionally distinct areas F4d (comparable in position and extent to area F4d of the present study) and F4v (comparable in extent and location to area F4v of the present study). Area F4d is involved in forelimb (reaching and grasping) and mouth movements, and integrates different types of visual properties (Maranesi *et al.*, 2012). Area F4s, which is located in a cortical region which is visually responsive and represents eye movements, as well as eye position-related movements (Boussaoud *et al.*, 1993; Fujii *et al.*, 1998, 2000) is characterized by aggregates of pyramidal cells in layer V and deeper part of layer III, a horizontal striation is visible in layers II, VI and III. In area F4d the horizontal striation is only visible in layer VI. Area F4v has a denser layer V with smaller pyramids than does F4d. Furthermore, results from the receptorarchitectonical analysis confirmed clear subdivision on the lateral convexity as the densities of all 13 examined receptors were higher in F4v than in F4d. Receptor concentration differences were more subtle when compared between F4s and F4d. The most distinctive measure was noticed in higher kainate receptor density of F4s than of F4d.

In the macaque monkey, the primary motor cortex (F1, Brodmann's area 4) covers the rostral wall of the central sulcus, as well as the rostrally adjacent cortex on the precentral convexity (where it reaches the superior precentral dimple) and on the medial surface is characterized by an overall low cell packing density, a poor lamination, the lack of a visible layer IV, and the presence of prominent giant pyramids (Betz cells; Betz, 1874) in layer V. To date, maps of the monkey brain depict area F1 as being a cytoarchitectonically homogenous region (Caminiti *et al.*, 2017; Matelli *et al.*, 1985, 1991, 1998; Preuss and Goldman-Rakic, 1991; Petrides and Pandya, 2006; Morecraft *et al.*, 2012) although some authors have proposed that it may be composed of architectonically and functionally distinct areas (Gould *et al.*, 1986; Preuss *et al.*, 1997; Rathelot and Strick, 2009; Strick and Preston,

1982; Stepniewska *et al.*, 1993), as is the case for the human (Geyer *et al.*, 1996) and New World owl monkey (*Aotus trivirgatus*) (Stepniewska *et al.*, 1993) primary motor cortex. It has been proposed that two distinct subregions can be defined within the primary motor cortex based on the location of the cortico-motoneuronal (CM) cells as identified by retrograde tracking experiments (Rathelot and Strick, 2009). On the other hand, the present quantitative multimodal analysis revealed the existence of three distinct subdivisions within the macaque primary motor cortex: area 4m on the medial surface, area 4d occupying the precentral convexity, and area 4s, located mostly within the central sulcus where, in the fundus, it abuts somatosensory area 3a. When compared with the previous proposed subdivision by Rathelot and Strick (2009), most CM cells were found within the central sulcus, at a location comparable to that of 4s of the present study, whereas the surface of the precentral gyrus, where area 4d was identified, only presented a few scattered CM cells. Another reason for noticed differences in cyto- and receptor architecture detected in the present study of the precentral region could be due to somatotopical representations of different body parts. However, this is not considered to be reliable parcellation criteria because regions are overlapping and have multiple representation locations (Park *et al.*, 2001). Nevertheless, in monkeys, the somatotopical map of the primary motor cortex shows that the medial surface (where area 4m was identified) is mostly occupied by the representation of the trunk and tail region, whereas the leg and hand regions are overlap on the precentral convexity (where area 4d was identified), and the hand region extends along the dorsal wall of the central sulcus (where area 4s was identified) (Graziano and Gandhi, 2000). Area 4s had the poorest lamination, and only layer V could be clearly identified due to the presence of numerous Betz cells. Areas 4d and 4m were clearly laminated with strong vertical striations, particularly in area 4d, in layer VI. The position of cytoarchitectonic borders identified here was paralleled by changes in receptor architecture. Area 4s presented lower AMPA, kainate, NMDA, GABA_A, GABA_{A/BZ}, M₂ and α_1 , but higher, GABA_B densities than areas 4d or 4m. In comparison to other frontal areas, all three subdivisions of area 4 were characterized by their very low receptor densities. This is comparable to the situation in the human brain, where the primary motor cortex was found to have significantly lower receptor densities than any other neocortical area (Zilles and Palomero-Gallagher, 2017; Palomero-Gallagher and Zilles, 2017).

4.2 Hierarchical organization of the frontal lobe

Receptor fingerprints not only segregate allocortical and isocortical areas, but also vary between cortical types (e.g., primary or multimodal association areas) and functional systems (Palomero-Gallagher and Zilles, 2017; Zilles and Palomero-Gallagher, 2017). It is important to note that receptor densities do not necessarily correlate with cell packing densities (volume density of cell bodies in a specific region or cortical layer), because one cell can express many different receptors on its surface (Zilles *et al.*, 2002). Rather, differences in the size and shape of receptor fingerprints are related to the hierarchical structure of cortical functional organization (Zilles *et al.*, 2002; Zilles and Amunts, 2009). Indeed, the fact that cortical areas have stronger reciprocal connection with neighboring than with distantly located areas, and up to 94% of all cortical connections tend to be predominantly local (Averbeck and Seo, 2008), is reflected by the present hierarchical cluster analyses. Macroanatomically related areas often clustered together as they share similar neurochemical and cytoarchitectonic properties, and the most rostral and caudal areas within the frontal lobe are significantly different regarding their molecular organization.

The similarities or differences of the multivariate receptor fingerprints between 48 of the 50 frontal areas identified in the present study were analyzed using hierarchical cluster and principal component analyses. It was not possible to include the fingerprints of areas 14c and 13a in this analysis since, due to their macroanatomical location, there were not enough non-tangentially sectioned sites to enable quantification of receptor densities. The k-means clustering identified 8 as the highest acceptable number of clusters, which segregated the examined areas into three main cluster groups following both rostro-caudal and dorso-ventral streams (*Fig. 52* and *Fig. 56*). The distinct cytoarchitecture and molecular structure of each area is accompanied by their particular connections with other cortical areas, as well as with different subcortical structures. Microparcellation studies like the present one reveal the numerous distinct areas involved in the different aspects of cognition control and guided behavior, as well as their well-tuned reciprocal neural networks at the molecular, micro-, and macroscopic levels. Studies in both, human and monkeys, revealed a rostro-caudal distinction of functional organization within the lateral frontal cortex. Based on the fMRI studies in human, it was suggested that three distinct processes occur in the frontal lobe: (i) preparation and execution of movements by the motor areas as action is selected based on the sensory inputs; (ii) gathering of contextual information by the posterior prefrontal areas; and (iii)

selection by the most rostral prefrontal areas of reliable information from the posterior prefrontal areas, based on the inputs from the temporal region (Koechlin *et al.*, 2003; Koechlin and Summerfield, 2007). Furthermore, there are two gradual direction trends in the functional organization of the premotor cortex: (i) posterior - anterior direction, where posterior areas are active during more “simple” movements (when the task is routine) and anterior areas control more “complex” movements (tasks with additional or new motor/cognitive inputs); (ii) dorsomedial - ventrolateral direction, where dorsomedial areas are active in movement guidance based on internal inputs (the internal feedback loops and/or proprioception), whereas, activation of the ventrolateral areas is guided by the external inputs (visual or auditory stimuli; Passingham, 1993; Rizzolatti *et al.*, 1998; Geyer *et al.*, 2000). This counterparts with the present multivariate analyses, that show a rostro-caudal trend with a grouping of areas into three main groups, i.e., rostroventral (group A; see *Fig. 53*), intermediate (group B; see *Fig. 54*) and caudal (group C; see *Fig. 55*), which present further clusters segregating areas in a dorso-ventral direction (clusters 1-8; see *Fig. 52 and Fig. 56*).

Rostroventral cluster (group A, *Fig. 53*).

The rostroventral cluster group includes posterior orbitofrontal areas 13l and 13m in one cluster (*cluster 1*), all subdivisions of frontopolar area 10 (areas 10d, 10md, 10mv, 10o) and the dorsal portion of area 9 (9d) in a second cluster (*cluster 2*), and all remaining orbital areas except for 12l and 14r (i.e., areas 11l, 11m, 12r, 12m, 12o, 13b) together with the subdivisions of area 46 located close to the fundus of the principal sulcus (areas a46d, p46d, a46v, p46v) in cluster 3 (*Fig. 52 and Fig. 56*). Detailed studies on the connectivity revealed that distinct subareas of the orbito-frontal and medio-ventral region can be separated into two different functional networks, i.e. orbital and medial prefrontal network (Carmichael and Price, 1996), while in the same time, being part of two distinct connectional trends in the prefrontal cortex, i.e. basoventral and mediodorsal trend (Barbas and Pandya, 1989). Interestingly, clusters of the group A encompass areas that mainly belong to the basoventral trend, with exception of the dorsally located areas 9d and the dorsal subdivisions of area 46, that are part of the mediodorsal trend. At the same time, areas found within clusters 1 and 3 are part of the orbital prefrontal network, whereas areas in cluster 2 mostly belong to the medial prefrontal network. ‘Orbital’ areas receive inputs from distinct sensory regions and appear to be involved in sensory integration (Carmichael and Price, 1996). Furthermore, they are more sensitive to external, environmental-related information (visual stimuli). On the other hand, ‘medial’ areas, which are the main target for the descending projections from the

hypothalamus and brainstem, are more sensitive to internal, subject-related information (self-initiated behavior) (Bouret and Richmond, 2010).

All the here identified subdivisions of Walker's area 10 were located within a single cluster (*Fig. 52* and *Fig. 56*). Area 10 is thought to be at the top of the functional hierarchy, and highly evolved in humans, where it mediates the most complex and abstract cognitive tasks (Medalla and Barbas, 2014). Macaque area 10 corresponds only to the ventromedial part of the human frontal pole (Carmichael and Price, 1996; Sallet *et al.*, 2013), that plays major role in the monitoring of outcomes expected for the ongoing course of action (Koechlin, 2014). Furthermore, within the frontal region, area 10 presents the densest reciprocal connections with auditory association areas and together with dorsolateral areas 46 and 9, makes a central node in the working memory system (Medalla and Barbas, 2014). This could be related to the present results too, where subarea 10d showed the highest similarity with dorsally neighboring area 9d in regard to other subdivisions of area 10. On the other hand, functional distinction of the structural subdivisions in area 10 that were recognized in present study require further studies in order to understand detailed role of each of them in overall functional organization of the prefrontal cortex. Though, it is interesting to notice that subareas 10mv and 10o had very similar shape and size of the receptor fingerprint, but hierarchical analysis showed more difference among them than expected. 10o and 10md showed most similarity and together they grouped with 10mv.

Area 11m has dense reciprocal connection to the neighboring area 11l (Carmichael and Price, 1996), with which is also closely related from the neurochemical point of view (*Fig. 52* and *Fig. 56*). Moreover, area 11m receives strong afferents from the posterior cingulate gyrus (Öngür and Price, 2000), which is reciprocally connected to numerous cortical areas associated with vision and eye movements. These include prefrontal area 46 (Barbas and Mesulam, 1985), posterior parietal association cortex (Cavada and Goldman-Rakic, 1989; Andersen *et al.*, 1990), supplementary eye field (Huerta and Kaas, 1990) and frontal eye field (Barbas and Mesulam, 1981; Leichnetz and Goldberg, 1988), regions that are specialized for spatial information. On the other hand, areas 11m and 11l were found to show highest similarity to the mediolateral subdivision of the area 13, 13b, and with rostral ventrolateral area 12r. Area 12r receives strong projections from the rostral cingulate cortex (Öngür and Price, 2000), that plays a crucial role in the neural network underlying decision making in primates (Walton and Mars, 2007). Visual neurons of 12r are active during an object identification and it is suggested its role in working memory for object identity

(Wilson *et al.*, 1993). Moreover, neurons that are linked to the hand-related activity have also been recorded in this area (Simone *et al.*, 2017; Bruni *et al.*, 2015). Therefore, it seems that area 12r plays role in control of object-orientated hand action (Caminiti *et al.*, 2017).

Moreover, information from 11m is further projected to the medial network areas, while the adjacent area 11l innervates posterior orbital areas, such as area 13, which are part of the orbital network as well. Studies revealed that areas 13 and 11 seem to be the earliest sites at which visual information about objects congregates with olfactory, auditory, gustatory and visceral inputs (Barbas, 2007). Object-related information comes from the perirhinal cortex to the granular orbitofrontal areas (e.g., areas 11 and 12), whereas visceral inputs, that provide information about internal body status, are projected via the agranular orbitofrontal cortex (i.e., areas 11l and 11pm) (Kringelbach and Rolls, 2004; Rudebeck and Murray, 2014) to dysgranular areas 13 and, if necessary, based on this projection, orbitofrontal cortex modulates behavior and internal body reaction to alter undesirable action (Nauta, 1971). Area 13 is considered to be a functionally higher area in the hierarchical organization of motivational/reward system within the prefrontal cortex (Goulas *et al.*, 2014) due to dense projections from the amygdala that additionally contribute to emotional and motivational integration of different stimuli (Barbas 2007; Ghashghaei *et al.* 2007; Murray and Izquierdo, 2007). This is reflected in the dendrogram where cluster 1 (*Fig. 52* and *Fig. 56*), that includes subdivisions 13m and 13l, is segregated from the all other orbitofrontal areas. The distinction of these areas is even more clearly visible in the 2-dimensional plot of the principal component analysis (*Fig. 56*).

Intermediate cluster (group B, *Fig. 54*).

The intermediate cluster includes mostly posterior prefrontal areas and some premotor areas. Additionally, a dorso-ventral trend is visible within this main cluster, with smaller clusters, that grouped areas located mostly dorsally (*cluster 6*), around the principal sulcus (*cluster 5*) or ventrally (*cluster 4*) within the frontal lobe. Cluster 6 includes medial premotor areas F3 and F6 closely grouped with the dorsal subdivision of area F2 (i.e., F2d), and areas associated with the frontal oculomotor system, i.e. dorsal portion of area F7 (i.e., area F7d), all subdivisions of area 8B, area 8Ad (dorsal part of the FEF). Interestingly, the most ventral portion of caudal premotor area F4 (area F4v) is also found within cluster 6, although it doesn't share any common border with clustered areas. The subdivisions of area 46 located on the walls of the principal sulcus and extending onto the free surface of the hemisphere

were all found within cluster 5, together with both subdivisions of area 45, as well as with area 44 and the most rostral subdivision of area F5 (F5s). Finally, the lateral subdivisions F5d and F5v, which occupy the postarcuate convexity clustered with medio-ventral areas 12l and 14r, and with the medial portion of area 9, 9m (cluster 4) (*Fig. 52* and *Fig. 56*).

The lateral prefrontal cortex in primates is an anatomically and functionally heterogeneous region that plays a crucial role in executive functions, such as planning, organizing, selecting and modulating behavior based on context and social environment (Rozzi and Fogassi, 2017). Functional dorso-ventral segregation in the lateral prefrontal cortex has been suggested by Barbas and Pandya (1989) and Goldman-Rakic (1996) based on the anatomical, physiological, and behavioral evidence. Visual system sends an object's identity information (e.g. the color, shape and texture of the visual stimuli) to the prefrontal areas via the ventral stream, which includes mainly inferior temporal areas, while dorsal stream is responsible for object spatial location information, which is processed in posterior parietal and superior temporal areas. Therefore, dorsolateral prefrontal region is involved in working memory for spatial information, whereas non-spatial (e.g., object-related information) working memory is coded in the ventrolateral prefrontal region. Similar segregation of the frontal areas is constructed in the dendrogram (*Fig. 52*) by the separation of areas within intermediate cluster B into a dorsal, a periprincipal and a ventral cluster.

Functionally distinct areas on the medial premotor surface, F3 and F6, have strong reciprocal connections with each other (Matelli *et al.*, 1998), and also show a great similarity of their receptor fingerprints, as they are grouped together with the dorsal subdivision of F2, i.e. F2d. Whereas, rostral to F2d is the dorsal subdivision of F7, i.e. F7d, that has more similarity to the posterior prefrontal areas, i.e. all subdivisions of area 8B and subarea 8Ad, as well as to ventral part of the premotor area F4, i.e. F4v, than to the other subdivisions of F7, i.e. F7i and F7s. Electrical stimulation of SMA (area F3) in monkeys revealed a complete somatotopical map of the body motor representation, in addition to the one in the primary motor cortex (Woolsey *et al.*, 1952), whereas movements in pre-SMA (area F6) are mostly arm-related (Mitz and Wise, 1987; Luppino *et al.*, 1991), and involved in target localization (Hoshi and Tanji, 2000, 2004). F3 is the source of dense, topographically organized corticospinal projections and strong corticocortical connections to F1 and other premotor areas (F2, F4 and F5; Luppino and Rizzolatti, 2000). On the other hand, rostral premotor areas F6 and F7 cannot control movement directly, but serve as the major transmitting point for limbic and prefrontal information to all caudal and rostral premotor areas. While the area

F2d corresponds to the previously described dimple area F2dc (Matelli *et al.*, 1998) that receives projections from areas PEip and PEc, two higher-order areas involved in amplification of the somatosensory stimuli, in order to plan and coordinate, mostly, hindlimb movements (Matelli *et al.*, 1998). These three areas (F3, F6 and F2d) are closely grouped in the clustering analyses, reflecting a similar molecular organization, which may underlie the functional synchronization required to plan voluntary limb movements based on visual and/or somatosensory guidance, when the animal moves toward the object to accomplish the reaching distance.

As mentioned before, further grouped areas in cluster 6 include areas 8B and 8Ad of the posterior dorsolateral prefrontal cortex, as well as the dorsal portion of the rostral premotor area F7 (F7d), all of which are associated with oculomotor and visuospatial functions and receive main inputs from inferior parietal, e.g. area PG, which encodes eye orientation (Sakata *et al.*, 1980) and intraparietal, e.g. area LIP, which encodes eye movement (Cavada and Goldman-Rakic, 1989; Andersen *et al.*, 1990; Snyder *et al.*, 1997; Huerta and Kaas, 1990). These frontal areas are densely interconnected, therefore, it was not surprising to see them clustered together (cluster 6) in the present multivariate analyses. Previous studies suggest that area 8B may be called premotor ear-eye field (PEEF; Lanzilotto, Perciavalle and Lucchetti, 2015) as intracortical stimulation in this area evoked eye and ear movements (Mitz and Godschalk, 1989; Bon and Lucchetti, 1994; Schall *et al.*, 1995). Distinct neurons found in this area encode different auditory environmental stimuli (Lucchetti *et al.*, 2008; Lanzilotto *et al.*, 2013) and neuronal activation is modulated by eye movement, regardless of the presence of a visual target (Mitz and Godschalk, 1989; Schlag *et al.*, 1992), suggesting that 8B is involved in visual and acoustic processing for the control of orienting movements in space. Thus the subdivisions of area 8B (8Bd, 8Bs and 8Bm), defined in the present study, may imply different coordination mechanisms for this ear-eye orientation process.

Area 8A is subdivided into dorsal and ventral parts based on cytoarchitectonic studies (Petrides and Pandya, 1999; present study see *Results*) and previous electrostimulation experiments, i.e. frontal eye field (FEF; Bruce *et al.*, 1985). Differences in receptor architecture were identified as well, which not only confirm the location of the cytoarchitectonic border between areas 8Ad and 8Av, but also result in their differential clustering pattern: 8Ad clusters with 8Bm (cluster 6), whereas 8Av showed higher similarity posterior premotor areas F2 and F4 (cluster 7) as well as with primary motor area 4. The

dorsal part of FEF (8Ad) has been connected to areas involved in peripheral vision, i.e. areas MSTd and PO (Lanzilotto *et al.*, 2013). And compare to ventral portion of the FEF (8Av), neurons located in dorsal FEF have larger receptive fields (RF) (Suzuki and Azuma, 1983).

Similar to the visual system, the auditory cortical system is organized in two different streams, i.e. dorsal and ventral, projecting to the prefrontal cortex in non-human primates (Romanski *et al.*, 1999). The dorsal stream originates from caudal auditory belt and directly targets area 8A (Romanski *et al.*, 1999), bringing information about sound spatial localization. On the other hand, the ventral stream, that provides information about the nature of the auditory stimulus, originates from rostral auditory belt and rostral auditory parabelt, projecting indirectly to area 8A through the ventral prefrontal cortex (Romanski *et al.*, 1999; Gerbella *et al.*, 2010). Based on the present data, it is possible to speculate that the auditory dorsal stream rather influences area 8Ad than area 8Av (*Fig. 52* and *Fig. 56*) due to the similarity of 8Ad and areas 8B (PEEF), that have direct connection to the caudal auditory belt as well through the dorsal auditory stream (Romanski *et al.*, 1999).

Interestingly, the present receptorarchitectonic analysis revealed that subarea F4v is closely related to areas grouped in cluster 6 than to any other surrounding (*Fig. 52*). Although, this relationship has to be further investigated, previous electrostimulation data showed that the population of mirror neurons recorded in area F4v activates during an observation of communicative mouth movements (Ferrari *et al.*, 2003), thus, could play role in the evolution of speech functions in humans. Additionally, the majority of projections to the caudal ventral premotor cortex are nonvisual, somatosensory and memory-related signals (Gregoriou and Savaki, 2003), that are reciprocally exchanged between the rostrally neighboring area F5c (areas F5d and F5v identified here) (Gerbella *et al.*, 2011) and lateral subdivisions of F4, especially area F4v, as they share strong connections. Finally, it may be concluded that areas 8A and 8B play a crucial role in visual and auditory spatial localization, as well as, in the transforming those signals into motor commands, therefore, we can see in present hierarchical cluster analysis, a grouping with certain premotor areas (cluster 6).

Furthermore, area 46, together with area 9, is part of the prefrontal region that plays a major role in spatial working memory processes (Goldman-Rakic, 1996; Petrides, 1996; Fuster, 1997). However, lesion studies within 46 not only cause impaired performance in spatial working memory tasks, but also in non-spatial working memory ones, indicating that this region also plays role as complex module for the high-level tasks monitoring and

guidance of different cognitive representations (Petrides, 1991, 1995; Petrides and Pandya, 1999). In particular, the most caudal part of area 46 has also been associated with the modulation and control of visually-guided and memory-guided saccades (Funahashi *et al.*, 1993; Takeda and Funahashi, 2002; Kuwajima and Sawaguchi, 2007), as well as in controlling eye accommodation (Gamlin and Yoon, 2000). Therefore, it has been considered as a part of the oculomotor network and is referred as so-called prefrontal eye field (Lynch and Tian, 2006). Conversely, the rostral portion of area 46 is densely interconnected with the auditory association cortex that responds to complex auditory stimuli and is considered crucial for language functions (Medalla and Barbas, 2014).

The subdivisions of area 8 (i.e., microanatomical components of the FEF) were located in cluster 6 and subdivisions of area 46 built cluster 5 together with areas 44, 45, which are considered as homolog to the human Broca's language region (Petrides and Pandya, 1999, 2002; Petrides *et al.*, 2005), and the rostral part of ventral premotor area F5, which have been associated with audio-visual working memory (Romanski, 2012) and sequence processing (Wilson *et al.*, 2015). Thus, it may be speculated that although area 46 can be considered a multimodal association area, it is more strongly involved in the processing of complex auditory stimuli than in the control of saccades. Moreover, recent electrophysiological experiments have shown that this region plays a crucial role in cognitive control of vocalizations in the monkey (Hage and Nieder, 2013, 2015), indicating that in the primates it represents an evolutionary pre-modified region for language functions that later developed in humans (Gavrilov *et al.*, 2017).

The most dorsal subdivision of the area 46, i.e. p46dr, showed the strongest similarity to the area 45A (*Fig. 52* and *Fig. 56*). Area 45 is subdivided into 45A and 45B based on the development of the layer IV (Petrides and Pandya, 2001; present study see *Results*) and on differences in receptor architecture (present study see *Results*). Functional studies have revealed that area 45A is involved in the multisensory processing of vocal stimuli (Romanski and Averbek, 2009) and activates during action and face observation (Nelissen *et al.*, 2005; Tsao *et al.*, 2008; Kuraoka *et al.*, 2015) as well as during eye movement (Premereur *et al.*, 2015), whereas area 45B is connected with the lateral intraparietal area LIP associated with eye movements (Luppino *et al.*, 1999), and is activated during the execution of saccades (Premereur *et al.*, 2015) as well as in the observation of the objects and faces (Denys *et al.*, 2004; Tsao *et al.*, 2008). Therefore, area 45A is important for gaze direction in communication behavior and social interactions, and 45B represents a preoculomotor area

involved in guiding the survey of visual space for the perception of objects, actions, and faces (Gerbella *et al.*, 2010). Stimulation of neurons in area 44 triggered orofacial movements and, to lesser extent, hand movements, but not oculomotor movements (Petrides *et al.*, 2005).

Area F5a (Belmalih *et al.*, 2008) (located within area F5s identified here), which shares dense reciprocal connections with the adjacent prefrontal area 44 (Matelli *et al.*, 1986), and is also relatively similar from the neurochemical point of view, has been proposed to be an integration site for parietal sensory-motor inputs with projections from prefrontal and premotor areas (Gerbella *et al.*, 2011). Finally, several studies have confirmed the presence of afferents from orbitofrontal areas to premotor area F5 (Barbas and Pandya, 1987; Morecraft *et al.*, 1992; Carmichael and Price, 1995), which are also associated with a similarity in the neurochemical composition of areas in these two regions, as seen in the present hierarchical cluster analysis, in particular, within cluster 4 (*Fig. 52*), where areas F5d and F5v clustered with orbital area 12l, that belongs to the orbital neural network, and areas 14r and 9m, which are part of the medial neural network. In general, area F5 is related to hand and mouth movement. Hand movements are represented mostly in its dorsal parts, while mouth movements tend to be more ventral (Rizzolatti *et al.*, 1995), thus supporting the subdivision of area F5 into dorso-ventrally arranged areas as proposed in the present study. Area F5 is thought to use information from the prefrontal areas to coordinate distal arm movements and goal-related motor act based on motivationally meaningful visual stimuli (Gentilucci *et al.*, 1988; Rizzolatti *et al.*, 1988). Interestingly, area 14r is actually one of the intermediate areas in the orbital region and has direct connection with both networks, thus, providing communication between the sensory-receptive orbital and visceromotor medial network, serving as bridge for sensory-motor linkage (Carmichael and Price, 1996). Moreover, areas 12l and 14r receive a substantial projection from visual areas in the inferior temporal cortex (Carmichael and Price, 1995; Öngür and Price, 1996), whereas area 9m projects to lateral prefrontal area 46 and orbitofrontal areas 10, 11, and 12 (Eradath *et al.*, 2015), and plays role in the goal-based action selection and prediction of the error regarding action value (Eradath *et al.*, 2015).

Caudal cluster (group C; *Fig. 55*).

The caudal cluster encompasses the three subdivisions of the primary motor cortex (i.e., 4d, 4s, 4m) in one cluster (*cluster 8*), as well as the lateral premotor areas abutting the arcuate sulcus dorsally (F2v, F7i and F7v) and ventrally (F4s, F4d, and 8Av, i.e. the ventral part of

the FEF) in a second cluster (*cluster 7*) (*Fig. 52*). Lesion studies have shown that the most caudal region of the frontal lobe, which includes the primary motor cortex (areas 4) and caudal premotor areas, e.g. F2 and F4, is involved in fine motor control and direct transformation of sensory (mainly somatosensory and visual stimuli) inputs into goal-directed motor actions such as reaching, grasping or any manipulation of objects (He *et al.*, 1993; Rizzolatti and Luppino, 2001). The primary motor cortex (Brodmann's area 4, F1) is the only motor area whose projections are directly connected to the motor neurons in the spinal cord, allowing it to control and perform the finest movements, such as independent finger movements (Porter and Lemon, 1993).

The uniqueness of area 4 in regard to all other frontal areas is reflected in its molecular composition, since the fingerprints of the subdivisions of area 4 were the smallest of all examined areas. In particular, as also observed in humans (Zilles and Palomero-Gallagher, 2017), in macaques the densities of almost all examined receptor types were lower in the primary motor areas than in any other prefrontal area, resulting in an early segregation in the hierarchic cluster analysis. Indeed, areas 4d, 4s and 4m were found in a separate cluster from all other areas of the main caudal cluster (cluster C). However, the group of areas (cluster 7 in *Fig. 52*), closely clustered with the subdivisions of area 4, share a common functional profile related to visuo-motor coordination, especially to the hand orientation and movement.

Furthermore, the cluster analysis showed a clear segregation of the subdivisions within areas F2 and F7, since only the subdivisions ventral to the superior precentral dimple (i.e. F2v and F7i/F7s, respectively) were part of the caudal cluster (cluster C), whereas the most dorsal parts F2d and F7d were in the intermediate cluster (cluster B). Therefore, we here provide further results demonstrating that areas F2 and F7 each consist of at least two functionally distinct sectors, as suggested by Rizzolatti *et al.* (1998). Thus, only the ventral part of F7 (corresponding to areas F7i and F7s identified here) uses information from medial parietal area PGm to locate the object in space for orientation, as well as to coordinate arm-body movements (Matelli *et al.*, 1998; Luppino and Rizzolatti, 2000), whereas the ventral part of F2 (corresponding to area F2v identified here) is involved in planning and executing arm movements guided by somatosensory as well as visual stimuli (Luppino and Rizzolatti, 2000).

Premotor areas F4s and F4d clustered with 8Av. Neuronal activity recorded within and around arcuate sulcus, i.e., at a position occupied by areas 8Av (ventral part of the FEF), F4s,

F2v and F7s, showed that this region is visually responsive and represents eye movements, as well as eye position-related movements (Boussaoud *et al.*, 1993; Fujii *et al.*, 1998, 2000). The FEF has a strong reciprocal connection with the forelimb region in the area 4, indicating that the FEF not only plays an essential role in the control of eye movements per se, but also in the control of eye-hand coordinative behaviors (Miyachi *et al.*, 2005). Furthermore, area 8Av is the only part of the FEF which integrates information from both the dorsal and ventral visual streams (Passingham and Wise, 2012). Area F4d identified in the present study is comparable in location extent to the functionally defined area F4d by Maranesi *et al.* (2012), which represents forelimb and mouth movements (Maranesi *et al.*, 2012), and in particular is involved in reaching movements under visual guidance (Gregoriou and Savaki, 2003; Kurata and Tanji, 1986; di Pellegrino and Wise, 1993). In general, area F4 is the main target of intraparietal area VIP (Colby *et al.*, 1993; Luppino *et al.*, 1999) which has been suggested to be involved in defensive movements of the head and arm to protect the head (Cooke *et al.*, 2003). F4 and VIP share many functional properties and, together, play crucial role in transforming object locations into appropriate movements within peripersonal space. Visual neurons clustered in receptive fields in F4d are independent of eye position, which means that these neurons encode space using a body part-centered frame of reference (Graziano *et al.*, 1994; Fogassi *et al.*, 1996; Luppino and Rizzolatti, 2000; Rizzolatti *et al.*, 1998). Therefore, subarea F4d (also called F4d in the present study) is likely to be involved in the control of the hand, as well as eye movements (Kurata and Tanji, 1986; di Pellegrino and Wise, 1993).

5 Conclusion

The present work revealed a detailed parcellation of the macaque frontal lobe into 50 areas based on quantitative multimodal analysis integrating macrostructural, microstructural and neurochemical aspects of cortical organization in the macaque monkey. Receptor densities could be measured in 48 of these 50 areas, and hierarchical cluster and principal component analyses were conducted to reveal similarities and dissimilarities between them. As a result, an obvious segregation was found between the most caudal areas and all other cortical areas studied here, as well as a dorso-ventral trend of grouping within main cluster groups with sporadic similarities between areas that do not share borders and occupy different parts of the frontal lobe.

6 List of References

- Adhami, H. (1973). Die photometrische Bestimmung des Cortextzell- und Graugehalts auf der Grundlage des Nissl-Bildes. *Acta Anatomica*, 84:1-52.
- Amaral, D. G., & Price, J. L. (1984). Amygdalo-cortical projections in the monkey (*Macaca fascicularis*). *The Journal of Comparative Neurology*, 230(4):465-496.
- Amunts, K., & Zilles, K. (2001). Advances in cytoarchitectonic mapping of the human cerebral cortex. *Neuroimaging Clinics of North America*, 11(2):151-169.
- Andersen, R. A., Asanuma, C., Essick, G., & Siegel, R. M. (1990). Corticocortical connections of anatomically and physiologically defined subdivisions within the inferior parietal lobule. *The Journal of Comparative Neurology*, 296(1):65-113.
- Averbeck, B. B., & Seo, M. (2008). The statistical neuroanatomy of frontal networks in the macaque. *PLoS Computational Biology*, 4(4):e1000050.
- Barbas, H. (2007). Specialized elements of orbitofrontal cortex in primates. *Annals of the New York Academy of Science*, 1121:10-32.
- Barbas, H., & Mesulam, M. M. (1981). Organization of afferent input to subdivisions of area 8 in the rhesus monkey. *The Journal of Comparative Neurology*, 200(3):407-31.
- Barbas, H., & Mesulam, M. M. (1985). Cortical afferent input to the principalis region of the rhesus monkey. *Neuroscience*, 15(3):619-37.
- Barbas, H., & Pandya, D. N. (1987). Architecture and frontal cortical connections of the premotor cortex (area 6) in the rhesus monkey. *The Journal of Comparative Neurology*, 256:211-228.
- Barbas, H., & Pandya, D. N. (1989). Architecture and intrinsic connections of the prefrontal cortex in the rhesus monkey. *The Journal of Comparative Neurology*, 286:353-375.
- Bartels, P. H. (1981). Numerical evaluation of cytologic data. X. Introduction to multivariate analysis of variance. *Analytical and Quantitative Cytology*, 3(4):251-260.

- Belmalih, A., Borra, E., Contini, M., Gerbella, M., Rozzi, S., & Luppino, G. (2008). Multimodalarchitectonic subdivision of the rostral part (area F5) of the macaque ventral premotor cortex. *Research in Systems Neuroscience*, 512(2):183-217.
- Betz, W. (1874). Anatomischer Nachweis zweier Gehirncentra. *Centralblatt für die medizinische Wissenschaften*, 12:578-580, 595-599.
- Bon, L., & Lucchetti, C. (1994). Ear and eye representation in the frontal cortex, area 8B, of the macaque monkey: an electrophysiological study. *Experimental Brain Research*, 102(2):259-71.
- Borra, E., Ferroni, C. G., Gerbella, M., Giorgetti, V., Mangiaracina, C., Rozzi, S., & Luppino, G. (2019). Rostro-caudal connectional heterogeneity of the dorsal part of the macaque prefrontal area 46. *Cerebral Cortex*, 29(2):485-504.
- Bouret, S., & Richmond, B. J. (2010). Ventromedial and orbital prefrontal neurons differentially encode internally and externally driven motivational values in monkeys. *The Journal of Neuroscience*, 30(25):8591-8601.
- Boussaoud, D., Barth, T. M., & Wise, S. P. (1993). Effects of gaze on apparent visual responses of frontal cortex neurons. *Experimental Brain Research*, 93(3):423-434.
- Brodmann, K. (1905). Beiträge zur histologischen Lokalisation der Grosshirnrinde. III. Mitteilung: Die Rindenfelder der niederen Affen. *Journal of Neurology and Psychology*, 4:177-226.
- Brodmann, K. (1909). *Vergleichende Lokalisationslehre der Grosshirnrinde in ihren Prinzipien dargestellt auf Grund des Zellenbaues*. Leipzig: Barth JA.
- Bruce, C. J., & Goldberg, M. E. (1985). Primate frontal eye fields I: single neurons discharging before saccades. *Journal of Neurophysiology*, 53(3):603-635.

- Bruce, C. J., Goldberg, M. E., Bushnell, M. C., & Stanton, G. (1985). Primate frontal eye fields II: physiological and anatomical correlates of electrically evoked eye movements. *Journal of Neurophysiology*, 54(3):714-734.
- Bruni, S., Giorgetti, V., Bonini, L., & Fogassi, L. (2015). Processing and integration of contextual information in monkey ventrolateral prefrontal neurons during selection and execution of goal-directed manipulative actions. *The Journal of Neuroscience*, 35(34):11877–11890.
- Bruni, S., Giorgetti, V., Fogassi, L., & Bonini, L. (2015). Multimodal encoding of goal-directed actions in monkey ventral premotor grasping neurons. *Cerebral Cortex*, 27(1):522-533.
- Caminiti, R., Borra, E., Visco-Comandini, F., Battaglia-Mayer, A., Averbeck, B., & Luppino, G. (2017). Computational architecture of the parieto-frontal network underlying cognitive-motor control in monkeys. *eNEURO*, 4(1):e0306-16.
- Carmichael, T. S., & Price, J. L. (1994). Architectonic subdivision of the orbital and medial prefrontal cortex in the macaque monkey. *The Journal of Comparative Neurology*, 346:366-402.
- Carmichael, T. S., & Price, J. L. (1996). Connectional networks within the orbital and medial prefrontal cortex of macaque monkeys. *The Journal of Comparative Neurology*, 371:179-207.
- Caspers, J., Palomero-Gallagher, N., Caspers, S., Schleicher, A., Amunts, K., & Zilles, K. (2015). Receptor architecture of visual areas in the face and word-form recognition region of the posterior fusiform gyrus. *Brain Structure and Function*, 220(1):205-219.
- Castelman, K. R. (1979). *Digital image processing*. Prentice-Hall.

- Cavada, C., & Goldman-Rakic, P. S. (1989). Posterior parietal cortex in rhesus monkey: I. Parcellation of areas based on distinctive limbic and sensory corticocortical connections. *The Journal of Comparative Neurology*, 287(4):393-421.
- Cavada, C., & Goldman-Rakic, P. S. (1989). Posterior parietal cortex in rhesus monkey: II. Evidence for segregated corticocortical networks linking sensory and limbic areas with the frontal lobe. *The Journal of Comparative Neurology*, 287(4):422-45.
- Colby, C. L., Duhamel, J. R., & Goldberg, M. E. (1993). Ventral intraparietal area of the macaque: anatomic location and visual response properties. *Journal of Neurophysiology*, 69(3):902-14.
- Cooke, D. F., Taylor, C. S., Moore, T., & Graziano, M. S. (2003). Complex movements evoked by microstimulation of the ventral intraparietal area. *Proceedings of the National Academy of Sciences of the United States of America*, 100:6163–6168.
- Deacon, T. W. (1992). Cortical connections of the inferior arcuate sulcus cortex in the macaque brain. *Brain Research*, 573:8-26.
- DeFelipe, J. (2015). The anatomical problem posed by brain complexity and size: a potential solution. *Frontiers in Neuroanatomy*, 9:104.
- Denys, K., Vanduffel, W., Fize, D., Nelissen, K., Sawamura, H., Georgieva, S., . . . Orban, G. A. (2004). Visual activation in prefrontal cortex is stronger in monkeys than in humans. *Journal of Cognitive Neuroscience*, 16(9):1505-1516.
- di Pellegrino, G., & Wise, S. P. (1993). Effects of attention on visuomotor activity in the premotor and prefrontal cortex of a primate. *Somatosensory & Motor Research*, 10(3):245-62.
- di Pellegrino, G., & Wise, S. P. (1993). Visuospatial versus visuomotor activity in the premotor and prefrontal cortex of a primate. *The Journal of Neuroscience*, 13(3):1227-1243.

- Dixon, W. J., Brown, M. B., Engelman, L., Hill, M. A., & Jennrich, R. I. (1988). *BMDP Statistical Software Manual*. Berkley: University California Press.
- Dum, R. P., & Strick, P. L. (2002). Motor areas in the frontal lobe of the primate. *Physiology & Behavior*, 77(4-5):677-682.
- Eickhoff, S. B., Rottschy, C., Kujovic, M., Palomero-Gallagher, N., & Zilles, K. (2008). Organizational principles of human visual cortex revealed by receptor mapping. *Cerebral Cortex*, 18:2637-2645.
- Eradath, M. K., Abe, H., Matsumoto, M., Matsumoto, K., Tanaka, K., & Ichinohe, N. (2015). Anatomical inputs to sulcal portions of areas 9m and 8Bm in the macaque monkey. *Frontiers in Neuroanatomy*, 9:30.
- Ferrari, P. F., Gallese, V., Rizzolatti, G., & Fogassi, L. (2003). Mirror neurons responding to the observation of ingestive and communicative mouth actions in the monkey ventral premotor cortex. *European Journal of Neuroscience*, 17:1703-1714.
- Fogassi, L., Gallese, V., Fadiga, L., Luppino, G., Matelli, M., & Rizzolatti, G. (1996). Coding of peripersonal space in inferior premotor cortex (area F4). *Journal of Neurophysiology*, 76(1):141-57.
- Fujii, N., Mushiake, H., & Tanji, J. (1998). An oculomotor representation area within the ventral premotor cortex. *Proceedings of the National Academy of Sciences of the United States of America*, 95(20):12034-12037.
- Fujii, N., Mushiake, H., & Tanji, J. (2000). Rostrocaudal distinction of the dorsal premotor area based on oculomotor involvement. *Journal of Neurophysiology*, 83(3):1764-1769.
- Fulton, J. F., & Sheehan, D. (1935). The uncrossed lateral pyramidal tract in higher primates. *Journal of Anatomy*, 69(2):181-187.

- Funahashi, S., & Takeda, K. (2002). Information processes in the primate prefrontal cortex in relation to working memory processes. *Reviews in the Neurosciences*, 13(4):313-345.
- Funahashi, S., Chafee, M. V., & Goldman-Rakic, P. S. (1993). Prefrontal neuronal activity in rhesus monkeys performing a delayed anti-saccade task. *Nature*, 365(6448):753-756.
- Fuster, J. M. (1997). Network memory. *Trends in Neurosciences*, 20(10):451-459.
- Fuster, J. M. (2001). The prefrontal cortex - an update: time is of the essence. *Neuron*, 30:319-333.
- Fuster, J. M. (2002). Frontal lobe and cognitive development. *Journal of Neurocytology*, 31:373-385.
- Gamlin, P. D., & Yoon, K. (2000). An area for vergence eye movement in primate frontal cortex. *Nature*, 407(6807):1003-1007.
- Gavrilov, N., Hage, S. R., & Nieder, A. (2017). Functional Specialization of the Primate Frontal Lobe during Cognitive Control of Vocalizations. *Cell Reports*, 21(9):2393-2406.
- Gennari, F. (1782). De peculiari structura cerebri, nonnullisque ejus morbis. *Parmae: Ex Regio Typographico*.
- Gentilucca, M., Daprati, E., & Gangitano, M. (1998). Implicit visual analysis in handedness recognition. *Consciousness and Cognition*, 7(3):478-493.
- Gentilucci, M., Fogassi, L., Luppino, G., Matelli, M., Camarda, R., & Rizzolatti, G. (1988). Functional organization of inferior area 6 in the macaque monkey. I. Somatotopy and the control of proximal movements. *Experimental Brain Research*, 71(3):475-490.
- Gerbella, M., Belmalih, A., Borra, E., Rozzi, S., & Luppino, G. (2007). Multimodal architectonic subdivision of the caudal ventrolateral prefrontal cortex of the macaque monkey. *Brain Structure and Function*, 212(3-4):269-301.

- Gerbella, M., Belmalih, A., Borra, E., Rozzi, S., & Luppino, G. (2010). Cortical connections of the macaque caudal ventrolateral prefrontal areas 45A and 45B. *Cerebral Cortex*, 20(1):141-68.
- Gerbella, M., Belmalih, A., Borra, E., Rozzi, S., & Luppino, G. (2011). Cortical connections of the anterior (F5a) subdivision of the macaque ventral premotor area F5. *Brain Structure & Function*, 216(1):43-65.
- Gerbella, M., Borra, E., Tonelli, S., Rozzi, S., & Luppino, G. (2012). Connectional heterogeneity of the ventral part of the macaque area 46. *Cerebral Cortex*, 23(4):967-987.
- Geyer, S., Ledberg, A., Schleicher, A., Kinomura, S., Schormann, T., Bürgel, U., . . . Roland, P. E. (1996). Two different areas within the primary motor cortex of man. *Nature*, 382(6594):805-807.
- Geyer, S., Matelli, M., Luppino, G., & Zilles, K. (1998). A new microstructural map of the macaque monkey lateral premotor cortex based on neurofilament protein distribution. *European Journal of Neuroscience*, Suppl. 10:83.
- Geyer, S., Matelli, M., Luppino, G., & Zilles, K. (2000). Functional neuroanatomy of the primate isocortical motor system. *Anatomy and Embriology*, 202:443-474.
- Geyer, S., Matelli, M., Luppino, G., Schleicher, A., Jansen, Y., Palomero-Gallagher, N., & Zilles, K. (1998). Receptor autoradiographic mapping of the mesial motor and premotor cortex of the macaque monkey. *The Journal of Comparative Neurology*, 397(2):231-250.
- Ghashghaei, H. T., Hilgetag, C. C., & Barbas, H. (2007). Sequence of information processing for emotions based on the anatomic dialogue between prefrontal cortex and amygdala. *NeuroImage*, 34(3):905-23.

- Goldman-Rakic, P. (1996). Regional and cellular fraction of working memory. *Proceedings of the National Academy of Science of the United States of America*, 93(24):13473-13480.
- Goulas, A., Uylings, H. B., & Stiers, P. (2014). Mapping the hierarchical layout of the structural network of the macaque prefrontal cortex. *Cerebral Cortex*, 24(5):1178-94.
- Gould, H. J., Cusick, C. G., Pons, T. P., & Kaas, J. H. (1986). The relationship of corpus callosum connections to electrical stimulation maps of motor, supplementary motor and the frontal eye fields in owl monkeys. *The Journal of Comparative Neurobiology*, 247:297-325.
- Graziano, M. S., & Gandhi, S. (2000). Location of the polysensory zone in the precentral gyrus of anesthetized monkeys. *Experimental Brain Research*, 135(2):259-266.
- Graziano, M. S., Yap, G. S., & Gross, C. G. (1994). Coding of visual space by premotor neurons. *Science*, 266(5187):1054-1057.
- Gregoriou, G. G., & Savaki, H. E. (2003). When vision guides movement: a functional imaging study of the monkey brain. *NeuroImage*, 19(3):959-967.
- Hage, S. R., & Nieder, A. (2013). Single neurons in monkey prefrontal cortex encode volitional initiation of vocalizations. *Nature Communications*, 4:2409.
- Hage, S. R., & Nieder, A. (2017). Audio-vocal interaction in single neurons of the monkey ventrolateral prefrontal cortex. *The Journal of Neuroscience*, 35(18):7030-7040.
- Haug, H. (1956). Remarks on the determination and significance of the gray cell coefficient. *The Journal of Comparative Neurology*, 104(3):473-492.
- He, S. Q., Dum, R. P., & Strick, P. L. (1993). Topographic organization of corticospinal projections from the frontal lobe: motor areas on the lateral surface of the hemisphere. *The Journal of Neuroscience*, 13:952-980.

- Herkenham, M., Lynn, A. B., Little, M. D., Johnson, R. M., Melvin, L. S., DeCosta, B. R., & Rice, K. C. (1990). Cannabinoid receptor localization in brain. *Proceedings of the National Academy of Science of the United States of America*, 87:1932-1936.
- Hoshi, E., & Tanji, J. (2000). Integration of target and body-part information in the premotor cortex when planning action. *Nature*, 408(6811):466-70.
- Hoshi, E., & Tanji, J. (2004). Differential roles of neuronal activity in the supplementary and presupplementary motor areas: from information retrieval to motor planning and execution. *Journal of Neurophysiology*, 92(6):3482-3499.
- Huerta, M. F., & Kaas, J. H. (1990). Supplementary eye field as defined by intracortical microstimulation: connections in macaques. *The Journal of Comparative Neurology*, 293(2):299-330.
- Jones, S., Meddi, R., Lim, S. C., & Temple, A. R. (2000). Toward a digital neuromorphic pitch extraction system. *IEEE Transactions on Neural Networks*, 11(4):978-987.
- Koechlin, E. (2014). An evolutionary computational theory of prefrontal executive function indecision-making. *Philosophical Transactions of the Royal Society B*, 369:20130474.
- Koechlin, E., & Summerfield, C. (2007). An information theoretical approach to prefrontal executive function. *Trends in Cognitive Sciences*, 11(6):229-235.
- Koechlin, E., Ody, C., & Kouneiher, F. (2003). The architecture of cognitive control in the human prefrontal cortex. *Science*, 302(5648):1181-1185.
- Kötter, R., & Wanke, E. (2005). Mapping brains without coordinates. *Philosophical Transactions of the Royal Society B: Biological Sciences*, 360(1456):751-766.
- Kringelbach, M. L., & Rolls, E. T. (2004). The functional neuroanatomy of the human orbitofrontal cortex: evidence from neuroimaging and neuropsychology. *Progress in Neurobiology*, 72(5):341-72.

- Kuraoka, K., Konoike, N., & Nakamura, K. (2015). Functional differences in face processing between the amygdala and ventrolateral prefrontal cortex in monkeys. *Neuroscience*, 304:71-80.
- Kurata, K., & Tanji, J. (1986). Premotor cortex neurons in macaques: activity before distal and proximal forelimb movements. *The Journal of Neuroscience*, 6(2):403-11.
- Kuwajima, M., & Sawaguchi, T. (2007). Involvement of the lateral prefrontal cortex in conditional suppression of gaze shift. *Neuroscience Research*, 59(4):431-45.
- Lanzilotto, M., Perciavalle, V., & Lucchetti, C. (2013). Auditory and visual systems organization in Brodmann Area 8 for gaze-shift control: where we do not see, we can hear. *Frontiers in Behavioral Neuroscience*, 7:198.
- Lanzilotto, M., Perciavalle, V., & Lucchetti, C. (2015). Evidence for a functional subdivision of Premotor Ear-Eye Field (Area 8B). *Frontiers in Behavioral Neuroscience*, 8:454.
- Leichnetz, G. R., & Goldberg, M. E. (1988). Higher centers concerned with eye movement and visual attention: cerebral cortex and thalamus. *Reviews of Oculomotor Research*, 2:365-429.
- Lucchetti, C., Lanzilotto, M., & Bon, L. (2008). Auditory-motor and cognitive aspects in area 8B of macaque monkey's frontal cortex: a premotor ear-eye field (PEEF). *Experimental Brain Research*, 186(1):131-41.
- Luppino, G., & Rizzolatti, G. (2000). The organization of the frontal motor cortex. *News in Physiological Sciences*, 15:219-224.
- Luppino, G., Matelli, M., Camarda, R. M., & Rizzolatti, G. (1993). Corticocortical connections of area F3 (SMA-proper) and area F6 (pre-SMA) in the macaque monkey. *The Journal of Comparative Neurology*, 338(1):114-140.
- Luppino, G., Matelli, M., Camarda, R. M., Gallese, V., & Rizzolatti, G. (1991). Multiple representation of body movements in mesial area 6 and the adjacent cingulate cortex:

- an intracortical microstimulation study in the macaque monkey. *The Journal of Comparative Neurology*, 311(4):463-482.
- Luppino, G., Murata, A., Govoni, P., & Matelli, M. (1999). Largely segregated parietofrontal connections linking rostral intraparietal cortex (areas AIP and VIP) and the ventral premotor cortex (areas F5 and F4). *Experimental Brain Research*, 128(1-2):181-187.
- Lynch, J. C., & Tian, J. R. (2006). Cortico-cortical networks and cortico-subcortical loops for the higher control of eye movements. *Progress in Brain Research*, 151:461-501.
- Mahalanobis, P. C. (1937). Normalization of statistical variates and the use of rectangular coordinates in the theory of sampling distribution. *Sankhya: The Indian Journal of Statistics*, 3:1-40.
- Mahalanobis, P. C., Majumdar, D. N., & Rao, C. R. (1949). Antropometric survey of the United Provinces, 1941: a statistical study. *Sankhya: The Indian Journal of Statistics*, 9:89-324.
- Maranesi, M., Roda, F. B., Rozzi, S., & Ferrari, P. F. (2012). Anatomico-functional organization of the ventral primary motor and premotor cortex in the macaque monkey. *The European Journal of Neuroscience*, 36(10):3376-3387.
- Matelli, M., Camarda, R., Glickstein, M., & Rizzolatti, G. (1986). Afferent and efferent projections of the inferior area 6 in the macaque monkey. *The Journal of Comparative Neurology*, 251(3):281-298.
- Matelli, M., Govoni, P., Galletti, C., Kutz, D. F., & Luppino, G. (1998). Superior area 6 afferents from the superior parietal lobule in the macaque monkey. *The Journal of Comparative Neurology*, 402(3):327-352.
- Matelli, M., Luppino, G., & Rizzolatti, G. (1985). Patterns of cytochrome oxidase activity in the frontal agranular cortex of the macaque monkey. *Behavioural Brain Research*, 18:125-136.

- Matelli, M., Luppino, G., & Rizzolatti, G. (1991). Architecture of superior and mesial area 6 and the adjacent cingulate cortex in the macaque monkey. *The Journal of Comparative Neurology*, 311:445-462.
- Medalla, M., & Barbas, H. (2014). Specialized prefrontal "auditory fields": organization of primate prefrontal-temporal pathways. *Frontiers in Neuroscience*, 8:77.
- Merker, B. (1983). Silver staining of cell bodies by means of physical development. *Journal of Neuroscience Methods*, 9(3):235-241.
- Mitz, A. R., & Godschalk, M. (1989). Eye-movement representation in the frontal lobe of rhesus monkeys. *Neuroscience letters*, 106(1-2):157-62.
- Mitz, A. R., & Wise, S. P. (1987). The somatotopic organization of the supplementary motor area: intracortical microstimulation mapping. *The Journal of Neuroscience*, 7(4):1010-1021.
- Miyachi, S., Lu, X., Inoue, S., Iwasaki, T., Koike, S., Nambu, A., & Takada, M. (2005). Organization of multisynaptic inputs from prefrontal cortex to primary motor cortex as revealed by retrograde transneuronal transport of rabies virus. *The Journal of Neuroscience*, 25(10):2547-2556.
- Molnar, Z., Kaas, J. H., DeCarlos, J. A., Hevner, R. F., Lein, E., & Nemec, P. (2014). Evolution and development of the mammalian cerebral cortex. *Brain, Behavior and Evolution*, 83(2):126-139.
- Morecraft, R., Cipolloni, P. B., Stilwell-Morecraft, K. S., Gedney, M., & Pandya, D. N. (2004). Cytoarchitecture and cortical connections of the posterior cingulate and adjacent somatosensory fields in the rhesus monkey. *The Journal of Comparative Neurology*, 469(1):37-69.

- Morecraft, R., Geula, C., & Mesulam, M. M. (1992). Cytoarchitecture and neural afferents of orbitofrontal cortex in the brain of the monkey. *The Journal of Comparative Neurology*, 323:341-358.
- Morecraft, R., Stilwell-Morecraft, K. S., Cipolloni, B., Ge, J., McNeal, D., & Pandya, D. N. (2012). Cytoarchitecture and cortical connections of the anterior cingulate and adjacent somatomotor fields in the rhesus monkey. *Brain Research Bulletin*, 87:457-487.
- Murray, E. A., & Izquierdo, A. (2007). Orbitofrontal cortex and amygdala contributions to affect and action in primates. *Annals of the New York Academy of Sciences*, 1121:273-96.
- Nauta, W. J. (1971). The problem of the frontal lobe: a reinterpretation. *Journal of Psychiatric Research*, 8(3):167-87.
- Nelissen, K., Luppino, G., Vanduffel, W., Rizzolatti, G., & Orban, G. A. (2005). Observing others: multiple action representation in the frontal lobe. *Science*, 310(5746):332-336.
- Öngür, D., & Price, J. L. (2000). The Organization of Networks within the Orbital and Medial Prefrontal Cortex of Rats, Monkeys and Humans. *Cerebral cortex*, 10:206–219.
- Palomero-Gallagher, N., & Zilles, K. (2017). Cortical layers: cyto-, myelo-, receptor- and synaptic architecture in human cortical areas. *NeuroImage*, doi: 10.1016/j.neuroimage.2017.08.035.
- Palomero-Gallagher, N., Mohlberg, H., Zilles, K., & Vogt, B. A. (2008). Cytology and receptor architecture of human anterior cingulate cortex. *The Journal of Comparative Neurology*, 508(6):906-926.

- Palomero-Gallagher, N., Vogt, B. A., Schleicher, A., Mayberg, H. S., & Zilles, K. (2009). Receptor architecture of human cingulate cortex: evaluation of the four-region neurobiological model. *Human Brain Mapping*, 30:2336-2355.
- Park, M. C., Belhaj-Saif, A., Gordon, M., & Cheney, P. D. (2001). Consistent features in the forelimb representation of primary motor cortex in rhesus macaques. *The Journal of Neuroscience*, 21(8):2784-2792.
- Passingham, R. (1993). The frontal lobes and voluntary action. In R. E. Passingham, *The frontal lobes and voluntary action (Oxford Psychology Series)*. New York: Oxford University Press.
- Passingham, R., & Wise, S. W. (2012). *The Neurobiology of the Prefrontal Cortex: Anatomy, Evolution, and the Origin of Insight*. Oxford: Oxford University Press.
- Penfield, W., & Welch, K. (1951). The supplementary motor area of the cerebral cortex: a clinical and experimental study. *A.M.A. Archives of Neurology and Psychiatry*, 66(3):289-317.
- Petrides, M. (1991). Functional specialization within the dorsolateral frontal cortex for serial order memory. *Proceedings of the Royal Society B: Biological Sciences*, 246(1317):299-306.
- Petrides, M. (1995). Impairments on nonspatial self-ordered and externally ordered working memory tasks after lesions of the mid-dorsal part of the lateral frontal cortex in the monkey. *The Journal of Neuroscience*, 15(1):359-375.
- Petrides, M. (1996). Specialized systems for the processing of mnemonic information within the primate frontal cortex. *Philosophical Transactions of the Royal Society B*, 351(1346):1455-1461.

- Petrides, M. (2005). Lateral prefrontal cortex: architectonic and functional organization. *Philosophical Transactions of the Royal Society B Biological Sciences*, 360(1456): 781-795.
- Petrides, M., & Pandya, D. N. (1984). Projections to the frontal cortex from the posterior parietal region in the rhesus monkey. *The Journal of Comparative Neurology*, 228:105-116.
- Petrides, M., & Pandya, D. N. (1994). Comparative architectonic analysis of the human and macaque frontal cortex. In B. a. Grafman, *Handbook of Neuropsychology* (pp. 17-58). Amsterdam: Elsevier Science Publishers.
- Petrides, M., & Pandya, D. N. (1999). Dorsolateral prefrontal cortex: comparative cytoarchitectonic analysis in the human and the macaque brain and corticocortical connection patterns. *European Journal of Neuroscience*, 11:1011-1036.
- Petrides, M., & Pandya, D. N. (2002). Comparative cytoarchitectonic analysis of the human and the macaque ventrolateral prefrontal cortex and corticocortical connection patterns in the monkey. *European Journal of Neuroscience*, 16:291-310.
- Petrides, M., & Pandya, D. N. (2006). Efferent association pathways originating in the caudal prefrontal cortex in the macaque monkey. *The Journal of Comparative Neurology*, 498:227-251.
- Petrides, M., & Pandya, D. N. (2009). Distinct parietal and temporal pathways to the homologues of Broca's area in the monkey. *PLoS Biology*, 7(8):e1000170.
- Petrides, M., Cadoret, G., & Mackey, S. (2005). Orofacial somatomotor responses in the macaque monkey homologue of Broca's area. *Nature*, 435(7046):1235-1238.
- Petrides, M., Tomaiuolo, F., Yeterian, E. H., & Pandya, D. N. (2012). The prefrontal cortex: comparative architectonic organization in the human and the macaque monkey brains. *Cortex*, 48:46-57.

- Porter, R., & Lemon, R. (1993). *Corticospinal Function and Voluntary Movement*. Oxford : Oxford University Press.
- Premereur, E., Janssen, P., & Vanduffel, W. (2015). Effector specificity in macaque frontal and parietal cortex. *The Journal of Neuroscience*, 35(8):3446-3459.
- Preuss, T. M. (1995). Do rats have prefrontal cortex? The Rose-Woolsey-Akert program reconsider. *Journal of Cognitive Neuroscience*, 7:1-24.
- Preuss, T. M., & Goldman-Rakic, P. (1991). Myelo- and cytoarchitecture of the granular frontal cortex and surrounding regions in the strepsirrhine primate Galago and the anthropoid primate Macaca. *The Journal of Comparative Neurology*, 310:429-574.
- Preuss, T. M., Stepniewska, I., Jain, N., & Kaas, J. H. (1997). Multiple divisions of macaque precentral motor cortex identified with neurofilament antibody. *Brain Research*, 767(1):148-153.
- Quigley, M. (2007). Non-human primates: the appropriate subjects of biomedical research? *Journal of Medical Ethics*, 33(11):655-658.
- Rathelot, J. A., & Strick, P. L. (2009). Subdivisions of primary motor cortex based on cortico-motoneuronal cells. *Proceedings of the National Academy of Science of the United States of America*, 106(3):918-923.
- Reed, M. G., & Howard, C. V. (1998). Surface-weighted star volume: concept and estimation. *Journal of Microscopy*, 190(3):350-356.
- Rizzolatti, G., & Luppino, G. (2001). The cortical motor system. *Neuron*, 31(6):889-901.
- Rizzolatti, G., Camarda, R., Fogassi, L., Gentilucci, M., Luppino, G., & Matelli, M. (1988). Functional organization of inferior area 6 in the macaque monkey. II. Area F5 and the control of distal movements. *Experimental Brain Research*, 71(3):491-507.
- Rizzolatti, G., Fadiga, L., Gallese, V., & Fogassi, L. (1996). Premotor cortex and the recognition of motor actions. *Cognitive Brain Research*, 3:131-141.

- Rizzolatti, G., Gentilucci, M., Fogassi, L., Luppino, G., Matelli, M., & Ponzoni-Maggi, S. (1987). Neurons related to goal-directed motor acts in inferior area 6 of the macaque monkey. *Experimental Brain Research*, 67(1):220-224.
- Rizzolatti, G., Luppino, G., & Matelli, M. (1998). The organization of the cortical motor system: new concepts. *Electroencephalography and Clinical Neurophysiology*, 106(4):283-296.
- Romanski, L. M. (2007). Representation and integration of auditory and visual stimuli in the primate ventral lateral prefrontal cortex. *Cerebral Cortex*, 17(suppl 1):i61-i69.
- Romanski, L. M., & Averbeck, B. B. (2009). The primate cortical auditory system and neural representation of conspecific vocalizations. *Annual Review of Neuroscience*, 32:315-46.
- Romanski, L. M., Bates, J. F., & Goldman-Rakic, P. S. (1999). Auditory belt and parabelt projections to the prefrontal cortex in the rhesus monkey. *The Journal of Comparative Neurology*, 403(2):141-57.
- Romanski, L. M., Tian, B., Fritz, J., Mishkin, M., Goldman-Rakic, P. S., & Rauschecker, J. P. (1999). Dual streams of auditory afferents target multiple domains in the primate prefrontal cortex. *Nature Neuroscience*, 2(12):1131-6.
- Rozzi, S., & Fogassi, L. (2017). Neural Coding for Action Execution and Action Observation in the Prefrontal Cortex and Its Role in the Organization of Socially Driven Behavior. *Frontiers in Neuroscience*, 11:492.
- Rudebeck, P. H., & Murray, E. A. (2014). The orbitofrontal oracle: cortical mechanisms for the prediction and evaluation of specific behavioral outcomes. *Neuron*, 84(6):1143-56.

- Sakata, H., Shibutani, H., & Kawano, K. (1980). Spatial properties of visual fixation neurons in posterior parietal association cortex of the monkey. *Journal of Neurophysiology*, 43(6):1654-1672.
- Sallet, J., Mars, R. B., Noonan, M. P., Neubert, F. X., Jbabdi, S., O'Reilly, J. X., . . . Rushworth, M. F. (2013). The organization of dorsal frontal cortex in humans and macaques. *The Journal of Neuroscience*, 33(30):12255-12274.
- Schall, J. D., Hanes, D. P., Thompson, K. G., & King, D. J. (1995). Saccade target selection in frontal eye field of macaque. I. Visual and premovement activation. *The Journal of Neuroscience*, 15(10):6905-18.
- Schlag, J., & Schlag-Rey, M. (1987). Evidence for a supplementary eye field. *Journal of Neurophysiology*, 57(1):179-200.
- Schlag-Rey, M., Schlag, J., & Dassonville, P. (1992). How the frontal eye field can impose a saccade goal on superior colliculus neurons. *Journal of Neurophysiology*, 67(4):1003-1005.
- Schleicher, A. Z. (1986). A quantitative approach to cytoarchitectonics: software and hardware aspects of a system for the evaluation and analysis of structural inhomogeneities in nervous tissue. *Journal of Neuroscience Methods*, 18(1-2):221-235.
- Schleicher, A., & Zilles, K. (1988). The use of automated image analysis for quantitative receptor autoradiography. In F. Van Leeuwen, B. RM, P. CW, & P. O, *Molecular neuroanatomy* (pp. 147-157). Amsterdam: Elsevier.
- Schleicher, A., & Zilles, K. (1990). A quantitative approach to cytoarchitectonics: analysis of structural inhomogeneities in nervous tissue using an image analyser. *Journal of Microscopy*, 157:367-381.

- Schleicher, A., Amunts, K., Geyer, S., Kowalski, T., Schormann, T., Palomero-Gallagher, N., & Zilles, K. (2000). A stereological approach to human cortical architecture: identification and delineation of cortical areas. *Journal of Chemical Neuroanatomy*, 20(1):31-47.
- Schleicher, A., Amunts, K., Geyer, S., Morosan, P., & Zilles, K. (1999). Observer-independent method for microstructural parcellation of cerebral cortex: a quantitative approach to cytoarchitectonics. *NeuroImage*, 9(1):165-177.
- Schleicher, A., Palomero-Gallagher, N., Morosan, P., Eickhoff, S. B., Kowalski, T., DeVos, K., . . . Zilles, K. (2005). Quantitative architectural analysis: a new approach to cortical mapping. *Anatomy and Embryology*, 210(5-6):373-386.
- Selemon, L. D., & Goldman-Rakic, P. S. (1988). Common cortical and subcortical targets of the dorsolateral prefrontal and posterior parietal cortices in the rhesus monkey: evidence for a distributed neural network subserving spatially guided behavior. *The Journal of Neuroscience*, 8(11):4049-68.
- Simone, L., Bimbi, F., Rodà, F., Fogassi, L., & Rozzi, S. (2017). Action observation activates neurons of the monkey ventrolateral prefrontal cortex. *Scientific Reports*, doi:10.1038/srep44378.
- Snyder, L. H., Batista, A. P., & Andersen, R. A. (1997). Coding of intention in the posterior parietal cortex. *Nature*, 386(6621):167-170.
- Stanton, G. B., Deng, s. Y., Goldberg, M. E., & McMullen, N. T. (1989). Cytoarchitectural characteristics of the frontal eye field in macaque monkeys. *The Journal of Comparative Neurology*, 282:415-427.
- Stepniewska, I., Preuss, T. M., & Kaas, J. H. (1993). Architectonics, somatotopic organization and ipsilateral cortical connections of the primary motor area (M1) of owl monkey. *The Journal of Comparative Neurology*, 330(2):238-271.

- Strick, P. L., & Preston, J. B. (1982). Two representations of the hand in area 4 of primate I: motor output organization. *Journal of Neurophysiology*, 48(1):139-149.
- Strick, P. L., & Preston, J. B. (1982). Two representations of the hand in area 4 of primate II: somatosensory input organization. *Journal of Neurophysiology*, 48(1):150-159.
- Suzuki, H., & Azuma, M. (1983). Topographic studies on visual neurons in the dorsolateral prefrontal cortex of the monkey. *Experimental Brain Research*, 53(1):47-58.
- Tsao, D. Y., Schweers, N., Moeller, S., & Freiwald, W. A. (2008). Patches of face-selective cortex in the macaque frontal lobe. *Nature Neuroscience*, 11(8):877-879.
- Von Economo, C. F., & Koskinak, G. N. (1925). Die cytoarchitektonik der hirnrinde des erwachsenen menschen. In C. F. Von Economo, *Textband und Atlas mit 112 Mikrophotographischen Tafeln*. Vienna: Springer.
- Walker, E. A. (1940). A cytoarchitectural study of the prefrontal area of the macaque monkey. *Journal of Comparative Neurology*, 73:59-86.
- Walton, M. E., & Mars, R. B. (2007). Probing human and monkey anterior cingulate cortex in variable environments. *Cognitive, Affective & Behavioral Neuroscience*, 7(4):413-22.
- Weibel, E. R. (1979). Stereological methods. In E. R. Weibel, *Practical methods for biological morphometry*. London: Academic Press.
- Wilson, B., Kikuchi, Y., Sun, L., Hunter, D., Dick, F., Smith, K., . . . Petkov, C. I. (2015). Auditory sequence processing reveals evolutionarily conserved regions of frontal cortex in macaques and humans. *Nature Communications*, 6:8901.
- Wilson, F. A., Scallan, S. P., & Goldman-Rakic, P. S. (1993). Dissociation of object and spatial processing domains in primate prefrontal cortex. *Science*, 260(5116):1955-1958.

- Wise, S. P. (1985). The primate premotor cortex: past, present and preparatory. *Annual Review of Neuroscience*, 8:1-19.
- Woolsey, C. N., Settlage, P. H., Meyer, D. R., Sencer, W., Pinto Hamuy, T., & Travis, A. M. (1952). Patterns of localization in precentral and "supplementary" motor areas and their relation to the concept of a premotor area. *Research Publications-Association for Research in Nervous and Mental Disease*, 30:238-264.
- Wree, A., Zilles, K., & Schleicher, A. (1982). Estimation of volume fractions in nervous tissue with an image analyzer. *Journal of Neuroscience Methods*, 6:29-43.
- Zhang, X. L., Pang, W., Hu, X. T., Li, J. L., Yao, Y. G., & Zheng, Y. T. (2014). Experimental primates and non-human primate (NHP) models of human diseases in China: current status and progress. *Zoological Research*, 35:447-464.
- Zilles, K., & Amunts, K. (2009). Receptor mapping: architecture of the human cerebral cortex. *Current Opinion in Neurology*, 22:331-339.
- Zilles, K., & Palomero-Gallagher, N. (2017). Multiple transmitter receptors in regions and layers of the human cerebral cortex. *Frontiers in Neuroanatomy*, 11:78.
- Zilles, K., Bacha-Trams, M., Palomero-Gallagher, N., Amunts, K., & Friederici, A. D. (2015). Common molecular basis of the sentence comprehension network revealed by neurotransmitter receptor fingerprints. *Cortex*, 63:79-89.
- Zilles, K., Palomero-Gallagher, N., Grefkes, C., Scheperjans, F., Boy, C., Amunts, K., & Schleicher, A. (2002). Architectonics of the human cerebral cortex and transmitter receptor fingerprints: reconciling functional neuroanatomy and neurochemistry. *European Neuropsychopharmacology*, 12(6):587-599.
- Zilles, K., Schleicher, A., Rath, M., & Bauer, A. (1988). Quantitative receptor autoradiography in the human brain. Methodical aspect. *Histochemistry*, 90(2):129-137.

Zilles, K., Schleicher, A., Rath, M., Glaser, T., & Traber, J. (1986). Quantitative autoradiography of transmitter binding sites with an image analyzer. *Journal of Neuroscience Methods*, 18(1-2):207-220.

7 Abbreviations

2D	two dimensional
NMDA	N-methyl-D-aspartate
5HT _{1A}	5-hydroxytryptamine 1A, serotonin receptor
5HT ₂	5-hydroxytryptamine 2, serotonin receptor
AMPA	α -amino-3-hydroxy-5-methyl-4-isoxazolepropionic acid
arcs	spur of the arcuate sulcus
aspd	anterior superior principal dimple
cgs	cingulate sulcus
CM	cortico-motoneuronal neurons
cs	central sulcus
EEG	electroencephalogram
FEF	frontal eye field
fMRI	functional magnetic resonance imaging
GABA _A	γ -aminobutyric acid A
GABA _{A/BZ}	γ -aminobutyric acid A, associated benzodiazepine binding sites
GABA _B	γ -aminobutyric acid B
GLI	grey level index
ias	inferior arcuate branch
IC	inner contour
lf	lateral fissure
LIP	lateral intraparietal area
M ₁	muscarinic acetylcholine receptor M ₁
M ₂	muscarinic acetylcholine receptor M ₂
M ₃	muscarinic acetylcholine receptor M ₃

MC	motor cortex
MD	Mahalanobis distance
MEG	magnetoencephalography
OC	outer contour
PEc	parietal area PEc
PEEF	prefrontal eye-ear field
PEip	parietal area PEip
PET	positron emission tomography
PFC	prefrontal cortex
PG	parietal area PG
preMC	premotor cortex
preSMA	presupplementary motor area
ps	principal sulcus
pspd	posterior superior principal dimple
ROI	region of interest
sas	superior arcuate branch
SEF	supplementary eye field
SMA	supplementary motor area
spcd	superior precentral dimple
sts	superior temporal sulcus
α_1	α_1 adrenergic receptor
α_2	α_2 adrenergic receptor

Erklärung § 5 Abs. 1 zur Datenaufbewahrung

Hiermit erkläre ich, dass die dieser Dissertation zu Grunde liegenden Originaldaten

- bei meinem Betreuer, Prof. Dr. med. Dr. h.c. Karl Zilles, Institut für Neurowissenschaften und Medizin (INM-1) des Forschungszentrums Jülich GmbH,

hinterlegt sind.

Eidesstattliche Erklärung gemäß § 5 Abs. (1) und § 11 Abs. (3) 12. der Promotionsordnung

Hiermit erkläre ich, Lucija Janković-Rapan an Eides statt, dass ich folgende in der von mir selbstständig erstellten Dissertation „Multimodal analysis of the macaque monkey frontal lobe“ dargestellten Ergebnisse erhoben habe:

Bei der Durchführung der Arbeit hatte ich folgende Hilfestellungen:

Bitte Namen angeben ----->	Doktorandin Lucija Janković- Rapan	Secondary supervisor, PD Dr. Nicola Palomero-Gallagher	Labormitarbeiter U. Blohm, R. Dohm, B. Machus	Doktorvater, Prof. Karl Zilles	Summe (%)
Studienüberwachung		60		40	100
Studiendesign/Konzeption		40		60	100
Bereitstellung von Materialien				100	100
Durchführung der Experimente Zytoarchitektur	25		75		100
Auswertung Zytoarchitektur	70	30			100
Durchführung der Experimente Rezeptorarchitektur	20		80		100
Auswertung Rezeptorarchitektur	80	20			100
Statistische Auswertung	70	30			100
Interpretation der Datenauswertung	70	20		10	100

Hier ggf. auch Experimente oder statistische Auswertungen aufführen, die nicht selbstständig gemacht, sondern von den entsprechenden Personen übernommen wurden.

Unterschrift der Doktorandin/des Doktoranden

Als Betreuer der obigen Dissertation bestätige ich die Angaben von Lucija Janković-Rapan

Unterschrift des Doktorvaters

Curriculum vitae

Lucija Janković-Rapan

03.01.1987, Zabok, Republic of Croatia

Bismarckstraße 51, 50672 Köln

0176 22 333 914

lucijarapan@gmail.com

Education

August 2013 - present	Doctoral student at the RWTH Aachen University, Department of Psychiatry, Psychotherapy and Psychosomatics and Research Centre Jülich (Institute of Neuroscience and Medicine, INM-1), Germany Prof. Dr. Dr. h.c. Karl Zilles (k.zilles@fzj-juelich.de)
2009 – 2012	Master of Experimental Biology, Faculty of Science, University of Zagreb, Croatia
2006 – 2009	Bachelor of Biology, Faculty of Science, University of Zagreb, Croatia
2001 – 2005	Gymnasium „Vladimir Nazor“ in Zadra, Croatia

Laboratory experience

August 2013 – present	Research Centre Jülich (Institute of Neuroscience and Medicine, INM-1), Germany Prof. Dr. Dr. h.c. Karl Zilles (k.zilles@fzj-juelich.de) - quantitative <i>in vitro</i> receptor autoradiography - classical histological stainings
April 2015 – July 2015	Visiting Doctoral Fellow at University of Pennsylvania, School of Medicine, Department of Psychiatry, Dr. Steven Siegel (siegels@usc.edu) - immunohistochemistry

- behavioral tests on mice
- June 2012 - February 2013 Postgraduate Associate in Neurobiology,
 Yale University School of Medicine, USA
 Dr. Nenad Sestan (nenad.sestan@yale.edu)
- maintainig several lines of KO mice (cre/loxP technology)
 - immunohistochemistry
 - confocal microscopy
 - Western blotting
 - extracted RNA from post-mortem human brain tissue
- March 2011 - July 2012 Master student in the laboratory of Animal Neurophysiolgy,
 Faculty of Science, University of Zagreb, Croatia
 Prof.dr.sc. Dubravka Hranilović (dubravka@zg.biol.pmf.hr)
- Master thesis: „Effects of increased serotonin levels on social behavior of young rats”
- neuropharmacology
 - behavioral tests on rats
 - recorded USV of rats and analyzed it in the BatSound

Publication

Olmos-Serrano JL, Kang HJ, Tyler WA, Silbereis JC, Cheng F, Zhu Y, Pletikos M, **Jankovic-Rapan L**, Cramer NP, Galdzicki Z, Goodliffe J, Peters A, Sethares C, Delalle I, Golden JA, Haydar TF, Sestan N (2016): Down Syndrome Developmental Brain Transcriptome Reveals Defective Oligodendrocyte Differentiation and Myelination. *Neuron*, 89(6):1208-22.

Poster presentations

Jankovic-Rapan L, Zilles K, Palomero-Gallagher N. Multimodal analysis of the macaque monkey frontal lobe. *24th Annual Meeting of the Organization for Human Brain Mapping*. Rome, Italy. 2019

Froudust-Walsh S, Palomero-Gallagher N, **Jankovic-Rapan L**, Niu M, Zilles K, Wang X-J. Emergence of working memory in macaque cortical areas with high neurotransmitter receptor density. *BNA2019 Festival of Neuroscience*. Dublin, Ireland. 2019

Impieri D, Zilles K, Niu M, **Jankovic-Rapan L**, Schubert N, Gamberini M, Galletti C, Palomero-Gallagher N. Receptor architecture of the macaque monkey superior parietal

lobule. *Joint Meeting of the Federation of European Physiological Societies and the Italian Physiological Society*. Bologna, Italy. 2019

Impieri D, Zilles K, Niu M, **Jankovic-Rapan L**, Galletti C, Palomero-Gallagher N. Receptor architecture of the macaque monkey superior parietal lobule. *48th Annual Meeting of the Society for Neuroscience*. San Diego, USA

Additional skills

Languages	Croatian - native
	English - fluent (TOEFL)
	German – basic
	Python (beginner level)
Computational skills	MS Office (Word, Excel, PowerPoint)
	Internet and e-mail for everyday use
	GraphPad Prism 5, BatSound,
	Adobe Illustrator 6, MatLab (basic)